In situ gelling bioadhesive hydrogel for topical and mucosal applications

In situ gelling bioadhesive hydrogel for topical and mucosal applications

By

Juhina Elmajdoub

A Thesis Submitted to the School of Graduate Studies in Partial Fulfillment of the Requirements for the Degree Master of Applies Science

MASTER OF APPLIED SCIENCE (2015) McMaster University

(Biomedical Engineering) Hamilton, Ontario

TITLE: *In situ* gelling bioadhesive hydrogel for topical and mucosal applications

AUTHOR: Juhina Elmajdoub

SUPERVISOR: Dr. Todd Hoare

NUMBER OF PAGES: xii, 121

Abstract

Hydrogel networks have attracted considerable research interest due to their potential in multiple biomedical applications, including drug delivery, wound healing, tissue engineering, and biomedical equipment coatings. In particular, multi-functional hydrogels that are injectable, non-cytotoxic, anti-bacterial, and bioadhesive offer potential applications in wound management, surgical barrier materials, and mucosal or skin-based drug delivery. In this thesis, an *in situ* injectable hydrogel network based on chitosan and poly(oligoethylene glycol methacrylate (POEGMA) was prepared using covalent aldehyde-hydrazide chemistry to form a stable hydrazone bond that is biodegradable, biocompatible, and adaptable to form networks with varying mechanical properties. Chitosan, a cationic polymer, has inherent adhesive and antibacterial properties, while POEGMA is innately protein-repellent and non cytotoxic. Therefore, by combining these materials, a non-cytotoxic and degradable hydrogel with both adhesive and antibacterial properties can be produced, with potential applications in drug delivery and wound healing.

The focus of this thesis is to functionalize chitosan to possess hydrazide groups without losing its inherent adhesive and antibacterial characteristics. This was be confirmed through titration and FT-IR to confirm and quantify the degree hydrazide functionalization followed by typical hydrogel characterization such as gelation time, degradation kinetics at different pH, transparency, and mechanics to ensure the required criteria for potential use in vaginal and skin applications are all met. The adhesive properties of the hydrogel with biological tissue (porcine skin) were assessed using peel and tack testing strategies, while mucoadhesion potential was screened using tack tests relative to a model mucosal membrane. Antibacterial properties of the

functionalized chitosan polymer and chitosan-POEGMA hydrogel were characterized using minimum inhibitory concentration measurements, zone of inhibition assays, macro broth dilution, and LIVE/DEAD bacterial assay using *E.coli* as the bacterial model. Different chitosan weight percentage incorporations in the hydrogel matrix were investigated and compared, both internally as well as with a cationic POEGMA-POEGMA hydrogel to identify the role of chitosan in controlling the gel properties.

Acknowledgment

I would first like to thank Dr. Todd Hoare for his constant support and guidance during my graduate studies.

I would also like to thank Asmaa Mannan for her endless encouragement and guidance; the outcome would have been different without your friendship.

Special thanks to my lab mates who turned this two-year experience into a memorable one, especially the summer of 2015. Tarushika Vasanthan, Rabia Mateen, Maryam Badv, and Sahar Mokhtari, you were always there whenever I needed help in the lab or to talk, I'll always cherish those talks. Thanks to Emilia Bakaic and Ivan Urosev for their help in cell culture and Rahul Sadavarte for bacterial culturing.

I would also like to thank my summer student, Angus Lam, for the time and effort he put into tying up the loose ends for this project.

Last and most importantly, thank you to my family; for their constant encouragement, for their love, and for always pushing me to try harder and supporting me in whatever I do. To my dad whose priority has always been my education, to my mom who motivated me to never settle, to my brother for his care and brotherly support, and to my sister for always being there when I needed her and providing her artistic skills for my schematics.

Table of contents

List of Figures

List of Tables

Nomenclature

AA	Acrylic acid
ADH	Adipic acid dihydrazide
AIBME	2,2-azobisisobutryic acid dimethyl ester
$CDCl_3$	Deuterated chloroform
CFU	Colony forming units
CMC	Carboxymethyl cellulose
DD	Degree of deacetylation
DMAEAm	N-(2,2-dimethoxyethyl)methacrylamide
DMAEMA	2-(dimethylamino)ethyl methacrylate
DMSO	Dimethyl sulfoxide
DS	Degree of substitution
ECM	Extracellular matrix
E.Coli	*Escherichia coli*
EDC	N'-ethyl-N-(3-dimethylaminopropyl)-carbodiimide
EO	Ethylene oxide
FTIR	Fourier transform infrared spectroscopy
G'	Storage modulus
G''	Loss modulus
KCl	Potassium chloride
MCAA	Monochloroacetic acid
MIC	Minimum inhibitory concentration
MEO_2MA	Di(ethylene glycol) methyl ether methacrylate
OEGMA	Oligo(ethylene glycol) methyl ether methacrylate
PBS	Phosphate buffer saline
PDI	Polydispersity index
PEG	Poly (ethylene glycol)
PEO	Poly (ethylene oxide)
POEGMA	Poly[oligo(ethylene glycol) methyl ether methacrylate]
TGA	Thioglycolic acid
UV-VIS	Ultraviolet visible spectrophotometry
3T3	*Mus musculus* mouse cells

1. Literature review

1.1. Bioadhesion

Bioadhesion, also named tissue adhesion, is a process by which any substrate (biological or not) adheres to a biological substrate through different mechanisms [1]. Bioadhesive materials, particularly bioadhesive polymers, are of current interest in both research and clinical fields for their potential application for hemostasis, non-invasive tissue sealing, and local transdermal and topical drug delivery [2].

To better understand how to design a bioadhesive polymer, the mechanism of bioadhesion must be understood. The exact mechanism, however, remains unclear, with several theories proposed to explain observed phenomena. Indeed, the bioadhesion mechanisms should be thought of as supplementary processes that occur at different stages in the overall polymer and biological substrate interaction and/or at different intensities for different polymer-tissue interfaces [3], [4].

1.1.1. Bioadhesion mechanisms

There are five main theories explaining bioadhesion, four of which are primarily chemical and two of which are primarily physical [5]. Other theories are also available that may be relevant to specific cases of adhesion [6], [7].

1) Electrostatic interaction: The electronic theory focuses on the difference in charge between the biological substrate and the polymer driving an adsorption event. Different charges promote electrostatic interactions between the two interacting double layers at the interface, resulting in adhesion due to the attractive forces developed. For example, given that most biological interfaces (skin, mucin, hair, etc.) are negatively charged, positively charged polymers typically exhibit higher bioadhesion than neutral or anionic polymers [8]. However, cationic polymers may

cause cell aggregation and other toxic reactions, indicating that charge density must be balanced to achieve both adhesion and biocompatibility [9].

2) Adsorption: Adsorption theory attributes bioadhesion to the formation of van der Waals interactions, hydrophobic interactions, or hydrogen bonding and represents one of the most universal and significant contributions to bioadhesion [1], [5].

3) Wetting: Wetting theory attributes bioadhesion events to the polymer's ability to spread and develop intimate contact with the biological surface. Typically used with regards to liquids and low viscosity polymers, the wettability of the interface allows the polymer to penetrate the biological surface's irregularities and subsequently anchor itself to the surface. This theory is also relevant to injectable or phase transition polymers that are initially liquid but gel over time while in the presence of the biological surface [10], [11].

4) Mechanical interlocking: Mechanical interlocking describes a polymer's ability to penetrate and infiltrate into the pores and irregularities of a rough surface, leading to surface binding due to a Velcro-like effect. This theory's significance is generally downplayed in most cases since smooth surfaces have also been known to possess good adherence [11], [12], but may be relevant particularly in the case of nanostructured surfaces.

5) Diffusion: Diffusion theory describes the penetration and subsequent physical entanglement of the chains of the polymer and the biological surface and/or interpenetration of the biological strands into the polymer's porous structure. The degree of chain entanglement and interpenetration determines the bioadhesion strength between the biological substrate and the polymer [5], [13]. Structurally, the more

similar the polymer is relative to the biological substrate, the greater the bioadhesion. The chain length and the concentration of the polymer both have strong effects on this process, since a 0.2-0.5 μm interpenetration layer is typically cited as required for an effective bond to form [14]; generally, this would suggest that a critical polymer molecular weight of 100kDa is needed to obtain sufficient interpenetration of the polymer chains within the mucin [15]. Figure 1-1 further shows that diffusion at the polymer:mucin interface is a function of the initial contact time. The more contact time, the higher the interpenetration between the polymer and mucin.

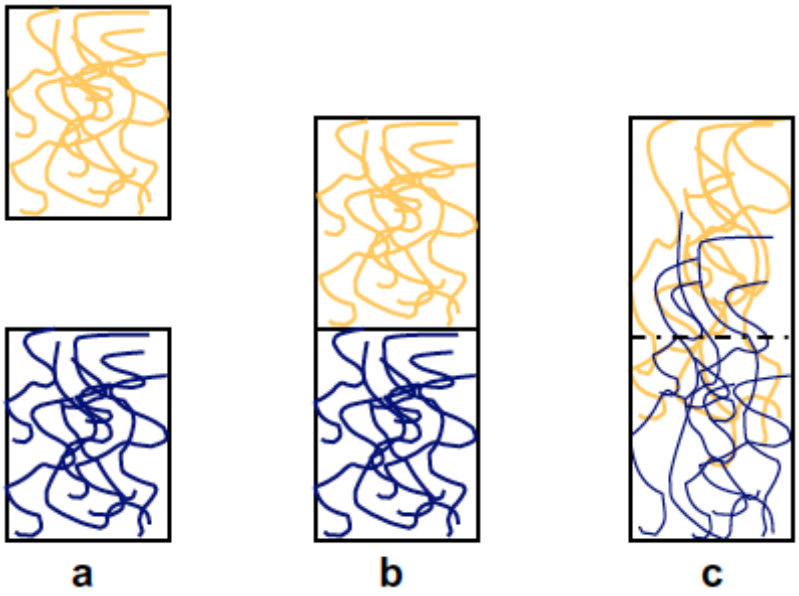

Figure 1-1: Mechanism of the diffusion theory (yellow = polymer; blue = mucin): (a) before contact; (b) at the moment of contact; (c) after an initial contact time [13]

6) Ligand-receptor interactions: Ligands are ions or molecules, such as functional groups, that bind to a receptor atom to form a coordination complex. Typical biological ligands used are enzyme-substrate pairs [16], streptavidin-biotin (the strongest non-covalent interaction known) [17], aptamer-target pairs [18], antigen-antibody interactions [19] and protein-protein interactions [20], all of which

can drive bioadhesive interactions with biomaterials when ligands (or receptors) are functionalized onto the free ends of the polymer chain. When a receptor surface is in close contact with a complementary ligand functionalized polymer surface, the ligands bind to the receptors, forming a bond that can be considered bioadhesive if the receptor surface is biological [21].

1.1.2. Polymeric factors affecting bioadhesion

There are many factors that are taken into account when selecting a strong bioadhesive polymer. Flexibility of the polymer chains, hydrogen bonding capacity, molecular weight, concentration, cross linking density, and the charge of the polymer are among some of the most important factors affecting a polymer's bioadhesiveness [3], [4], [5], [14]. As polymer chains cross-link, their mobility and thus diffusion coefficient for transport into the biological layer decreases; therefore, flexible polymer chains are ideally needed for sufficient penetration of the polymer chains into the biological layer to achieve a strong bioadhesion, particularly in the case of hydrogel bioadhesion [13]. Polymers with functional groups such as carboxyls (-COOH), hydroxyls (-OH), amines ($-NH_2$), and sulphates ($-SO_4H$) can exhibit enhanced hydrogen bonding with a biointerfaces and thus higher bioadhesion [3], [6]. Molecular weight of the polymer affects both the degree of physical entanglement and interpenetration of the chains, with a lower molecular weight favorably promoting interpenetration while a higher molecular weight favorably promoting physical entanglement. Typically, higher molecular weight polymers possess superior bioadhesive properties [10], although a ceiling effect is observed in which the bioadhesion drops after an optimum molecular weight is exceeded, at the same concentration for each different MW polymer. This is due to increased coiling of the

polymer chains because of their increased length, (particularly in cases in which intramolecular bond formation is possible) resulting in less free movable polymer chains for entanglement and subsequently weaker bioadhesion [4]. This effect also applies to the polymer concentration; a concentration higher than the optimum will result in a drastic drop in the bioadhesion due to steric crowding and subsequent unavailability of the chains for interpenetration. However if the polymer concentration is too low, the available polymer chains per surface area of the biological substrate decreases, weakening the bioadhesion strength between the polymer and biological tissue [4], [14].

Charge attraction also promotes bioadhesion, although charge is not a pre-requisite for adhesive materials; for example, chitosan (cationic, attractive), poly(ethylene oxide) (neutral), and poly(acrylic acid) (anionic, repulsive) have all been reported to adhere to biointerfaces in certain contexts [3]. However, in the context of charge promotion of bioadhesion, since the biological surfaces are negatively charged they typically interact most strongly with cationic polymers. However, some neutral polymers, such as PEO, are also highly bioadhesive due to their strong hydrogen bonding and flexibility (and thus ability to interpenetrate) [9]. That said, most neutral polymers possess little to no bioadhesion, while cationic polymers' positive surface charge consistently promotes electrostatic interaction and the formation of surface bonds between the anionic tissues [13].

Different types of polymers primarily adhere via different mechanisms. Adhesion of anionic polymers to tissue is typically attributed to hydrogen bonding between tissue and carboxyl groups on the polymeric chain, while cationic polymer bioadhesion is primarily electrostatic and non-ionic polymer adhesion is primarily

driven by a combination of hydrogen bonding and chain interpenetration. While these principle mechanisms primarily drive bioadhesion in each polymer group, they are not the sole contributing factors to bioadhesion of such materials [9].

1.1.3. Environmental and physiological factors affecting bioadhesion

Environmental and physiological factors are also taken into account when choosing a bioadhesive polymer, including the nature of the biological substrate on which the polymer will be applied, the initial contact and application strength of the polymer and tissue, and the environmental pH. Different biological substrates have different surface charge densities as well as functional groups types and concentrations [13]; for example, mucosal layers, possess unique functional groups from usual skin tissue that favour different polymers for adhesion. Therefore mucosal and topical applications, while both under the bioadhesion umbrella, can be promoted via different functional groups and surface charge densities. The adhesion force increases as the force at which the adhesive is applied and the duration of that force is increased, both of which drive increased interpenetration of the polymer within the biological substrate [22]. Local pH determines the degree of ionization of both polymer and biointerface functional groups according to the dissociation constant (pK_a) of the functional groups. If the pK_a is not in the working range of the system, the functional group will remain uncharged and hydrogen bonding will be the only interaction between the polymer and the biological substrate, with no charge contribution. However, in the ionized state, the expanded polymer chains promote polymer chain mobility, diffusion, and physical entanglement. Chitosan is insoluble at

pH > 6.5 and the amine group is protonated at pH <6.5; therefore its bioadhesive strength is only present at a lower pH, where chitosan is then soluble and its cationic charge will promote bioadhesion [15]. The water content of the system also can strongly affect adhesion. For example, greater adherence to the skin layer is witnessed with increased skin hydration due to the unfolding of the keratin exposing more functional groups to interact with the adhered material [8].

1.1.4. Mucoadhesion

Mucosal membranes line the walls of various parts of the human body and are comprised of connective tissue oriented below a layer of epithelial cells. This layer is found in the stomach, the small and large intestines, the bronchi, the esophagus, vagina, and cornea. Mucus is a glycoprotein that is present as either an adhering gel layer to the mucosal surface or in a soluble form adjacent to that layer [23]. Figure 1-2 shows the typical structure of mucus glycoproteins, coupled with the various types of interactions such as glycoprotein structures that can support and promote adhesive interactions.

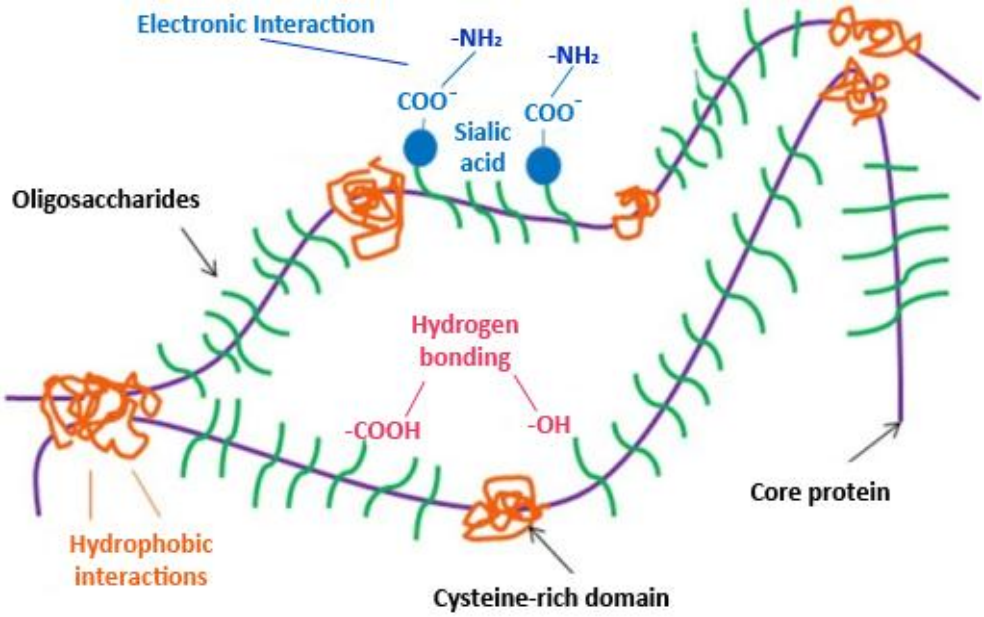

Figure 1-2: Mucin glycoprotein structure and its mucoadhesive interactions [24]

Electronic (Electrostatic) interactions as well as hydrogen bonding are the two predominant adhesion mechanisms supporting polymer: mucin interaction. Polymers that possess functional groups such as carboxyls, hydroxyls, sulphates, and amines tend to have superior adhesion strength to the mucosal layer. Also, mucin's overall negative charge, due to the presence of the sialic acid on its backbone, results in electrostatic interactions between its negative charge and a cationic polymer's positive charge [23].

1.1.5. Applications for bioadhesive polymers

Tissue adhesive and/or mucoadhesive polymers can be employed in various clinical and medical applications, particularly those in which immobilization of a material to a biointerface may offer significant performance advantages [12].

1.1.5.1. Wound Healing

Wound healing is a complex and cellular process with overlapping stages that requires proper progression to ensure complete healing of the wound. Would healing proceeds through four stages: hemostasis, inflammation, proliferation, and maturation (remodeling). Figure 1-3 shows the approximate timeline of this sequence of events in wound healing.

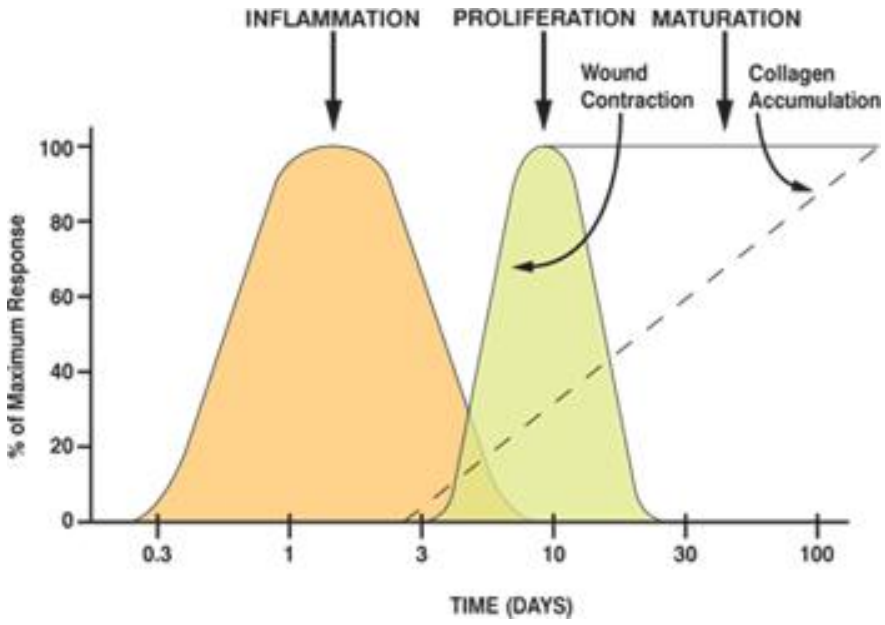

Figure 1-3: The stages of wound healing [25]

Once a blood vessel is injured, the wound healing process begins. The body activates a series of actions to initiate biological hemostasis, including constriction of the local vasculature and triggering of a clotting response via platelets. Subsequently, once a clot is formed, the blood vessels dilate to allow antibodies, white blood cells, growth factors, enzymes, and nutrients to the wound area, leading to the production of exudate that marks the inflammation stage. At the proliferation stage, new granulation tissue made up of collagen (mostly type III) and other extracellular matrix (ECM)

proteins fill the wound and new blood vessels develop. Macrophages degrade the epithelial membrane of the native vessels and release growth factors to stimulate growth of new vessels at the site of inflammation, a process known as angiogenesis. Epithelial cells then resurface the wound via a process known as epithelialization [26, 27]. Lastly, at the maturation stage, collagen type III is remodeled to collagen type I and cellular activity and blood vessels are reduced [25].

The presence of infection during this wound healing process can significantly disrupt the normal cascade of events, resulting in chronic wounds that fail to heal in a timely and orderly manner. Wounds are more susceptible to infection since the host bacteria equilibrium in a traumatized tissue shifts in favor of the bacteria, enabling the bacteria to inhibit the process of normal wound healing and also cause sepsis, a systemic response to this disturbance. Serious complications such as keloids, ulcers, limb amputation, and even fatality can result. This impaired healing is usually attributed to how the presence of bacteria alter components of the healing process, including growth factors, cytokines, or enzymes. Therefore, in order to ensure a smooth and undisturbed wound healing process, preventative as well as combative measures are taken through the use of different wound healing agents [12], [28], [29].

Wound healing agents are defined as materials that aid in the stoppage of wound bleeding and promote healthy wound healing by eliminating infection and tissue necrosis [30]. There are three main classes of wound healing agents: hemostat agents, sealants, and tissue adhesives. A clear definition and distinction between the three types of materials is needed before proceeding. A hemostat actively aids in blood clotting and is only effective in the presence of blood, a sealant creates a physical barrier that prevents any gas or liquid leaking from the wound, and an adhesive glues

biological tissue together. Both sealants and adhesives are most effective in dry fields and can also possess hemostatic capabilities by blocking blood flow but do not necessarily aid in blood clotting [12], [31], [32].

1.1.5.1.1. Hemostatic agents

Hemostatic agents promote primary hemostasis by initiating fibrin formation and inhibiting fibrinolysis [26]. While hemostatic agents are themselves not bioadhesive, they may be embedded inside bioadhesive dressings. Hemostatic materials are available as granular powders applied directly to the wound or powders embedded in dressings, and are classified as either mechanical agents or active agents [12]. Mechanical hemostatic material prevent blood loss by forming a mechanical barrier and are usually in the form of powder, sponges, sheets, or micro particles, while active agents such as thrombin to enhance the effectiveness of wound healing by directly participating in the process of fibrin clot formation. However, major safety concerns are associated with using thrombin-based agents based on the potential off-target effects which may induce thrombosis, hypotension, and death; as such, thrombin must not be injected intravascularly. *Floseal* (a combination of thrombin with a gelatin matrix), porcine gelatin (*Gelfoam, Surgifoam*), bovine collagen (*Helitene, Avitine, Instat*), and oxidized regenerated cellulose (*Surgicel*) are among some of the current commercialized hemostats available [12], [31].

1.1.5.1.2. Tissue adhesives and sealants

The emergence of tissue adhesives and sealants as an alternative to sutures that can double as hemostatic and mechanical agents has been of significant interest in recent clinical research. Tissue adhesives offer the ability to mechanically block bleeding, actively participate in the blood clotting process, and even serve as

antibacterial agents. This branch of materials could potentially decrease post-surgery infection rates and enhance wound healing while causing minimal pain for patients, typically a problem with conventional wound dressings [12]. They are generally made up of natural or synthetic polymers that undergo polymerization or cross-linking to form an insoluble adhesive matrix.

Commercially available bioadhesives can be divided into five categories based on their chemical makeup: fibrin-based, albumin-based, cyanoacrylate-based, collagen based, and hydrogel-based [2,33]. Fibrin glue consists of a combination of thrombin and fibrinogen and is the most widely used adhesive in medical and clinical applications. It mimics the chemistry of the last stage of blood clotting by creating a deliverable clot for use as a hemostat and sealant. Fibrin glue has been used for sealing air leaks from lung procedures, controlling burn bleeding, and treating spleen and liver lacerations, among other functions. Of particular interest, given that the chemistry directly mimics native clotting, fibrin glues are biodegradable via normal fibrinolysis and directly integrate to support the native wound healing process. However, thrombin's susceptibility to cross-react with human clotting factors pose a risk of hemorrhaging, a major safety concern [12], [31]. Albumin-based compounds are made up of a combination of albumin and adhesion/cross-linking compounds including gelatin, resorcinol, formaldehyde, and glutaraldehyde. Currently, they have proven difficult to commercialize due to the toxicity of the formaldehyde present in the adhesive. Cyanoacrylates are stronger than fibrin sealants but are not biodegradable so can only be used topically because they may lead to internal inflammation, tissue necrosis, and infection risks. They have also been associated with carcinogenesis [12], [33]. Collagen-based adhesives are comprised of a combination of bovine collagen

and bovine thrombin, providing a matrix for clotting and assisting native fibrinogen to clot. Hydrogels, typically based on photocross-linked poly(ethylene glycol), offer the advantages of controlled degradation times and mechanical properties suited to the particular tissue. However, current generations of hydrogel tissue adhesives require time to apply and set, and the required photoactivation for polymerization makes the application more complex (indeed, impossible in the case of hemorrhaging) and potentially toxic to surrounding cells. However current advances in hydrogel synthesis eliminate the activation step, leading to the development of hydrogels able to accelerate wound healing as well as offering antibacterial properties as an alternative to antibiotics [33], [34].

1.1.5.1.3. Desired polymer bioadhesive properties in wound healing

For practical use, bioadhesive materials must be safe, non-toxic (both in terms of the actual material and its degradation products), sterilizable, and easy to prepare and apply. The adhesive should be flexible and possess flow characteristics that enable it to easily and precisely be applied to the desired area without losing its integrity during the application or during any body movement. The material should be able to rapidly solidify once in contact with the targeted site at physiological conditions in order to minimize bleeding and surgery time. In addition to adhesion, other desirable material properties include hemostatic properties, wound healing and regeneration characteristics, and infection control. Lastly, the material must be biodegradable on an appropriate time scale. Combining all of these properties in one material has not yet been accomplished; however, advances in research have led to materials that possess many desirable properties for applications as bioadhesive and sealant products [12].

1.1.5.2. Drug Delivery

Mucoadhesive drug delivery systems offer potential in providing localized drug release to desired regions, increasing the residence time of the drug (thus reducing dosage frequency), and enhancing the intimate contact of the drug with membranes of the biological system for better drug absorption at the site of application [3], [35].

Drug delivery systems are engineered technologies for enabling the targeted and controlled delivery of a therapeutic drug by addressing the physiological barriers that decrease a drug's efficacy. Figure 1-4 shows the conventional (pill-based) versus desired controlled drug delivery release profiles, with controlled release both minimizing the risk of overdose and maximizing the duration of time over which the local drug concentration lies within the therapeutic range.. Depending on the medication and how the medication is delivered, undesirable side effects may also be avoided or minimized with controlled delivery vehicles [36]; in particular, for medications intended to have local effects (e.g. chemotherapy agents), controlled local release minimizes the systemic toxicity of the drug.

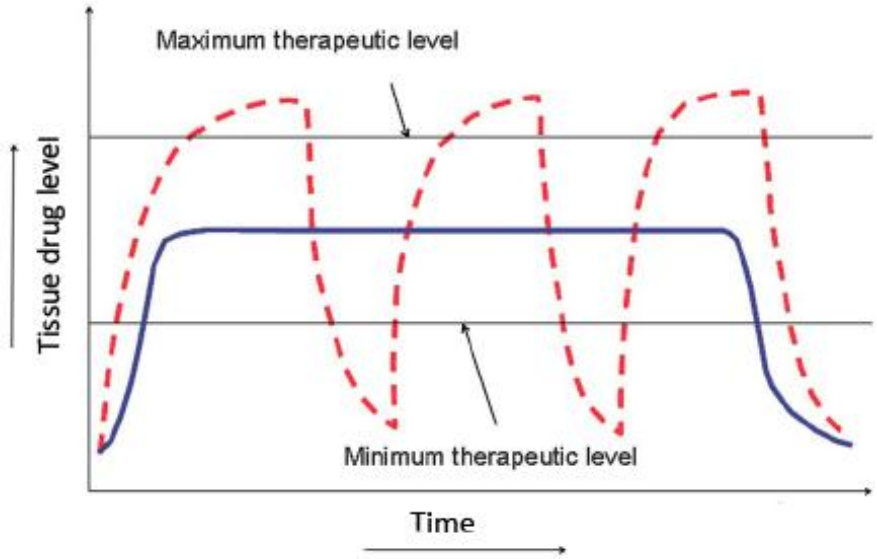

Figure 1-4: Conventional vs. controlled drug delivery release profiles [37]

1.1.5.2.1. Bioadhesive polymers as drug delivery matrixes

Bioadhesive drug delivery systems have several advantages in the context of drug delivery. Bioadhesive polymers have the potential to prolong residence time at the site of drug absorption and enhance the absorption of usually poor absorbable drugs such as peptides and proteins, increasing the bioavailability of the delivered drug as well as decreasing the required dosage frequency and amount [5]. These polymers come in the form of tablets, hydrogels, microspheres, beads, nanoparticles, films, or patches and can deliver the drug locally or systemically [6]. Some of the application sites explored in the literature include oral, nasal, ocular, rectal, vaginal, and gastrointestinal [1]. Carboxymethyl cellulose (CMC), carbopol 934p, chitosan, and polyethylene oxide (PEO) have in particular been studied as buccal mucoadhesive delivery systems [23].

Nasal delivery is another important delivery route, representing a mucoadhesive site with a surface area between 150 to 200 cm^2 [38]. The residence

time of the drug has been proven to increase when delivered using the nasal route [39]. Sodium carboxymethyl cellulose and carbopol 934p have in particular been explored as potential nasal drug delivery systems [23].

Ocular drug delivery is also an emerging popular route of drug administration to treat eye disorders. The strong bioavailability limitation observed based on current ocular drug delivery approaches has shifted research toward the investigation of mucoadhesive polymeric systems. The anatomy of the eye coupled with the protective mechanisms of the eye cause most of the drug administered via eyedrops to be lost before reaching its targeted area; use of a mucoadhesive delivery system offers potential to prolong residence time and thus increase drug efficacy. Polyvinyl pyrrolidone (PVP), thiolated poly(acrylic acid) (PAA), polyamidoamine, and methyl and hydroxyl ethyl cellulose are among some of the researched and tested mucoadhesive polymers for ophthalmic drug delivery [40].

Mucoadhesive polymers can also greatly reduce the migration of the drug and thus increase therapeutic efficacy in the context of vaginal and rectal drug delivery. The polymers most typically used include gelatin, polycarbophil, and sodium alginate [23].

1.1.5.2.2. Desired polymer bioadhesive properties in drug delivery

As in wound healing, bioadhesive material must have strong adherence to the biological substrate to enable strong interpenetration and thus effective and long-term topical drug delivery efficacy, mandating the use of polymers with high enough molecular weights and chain flexibilities for strong interpenetration and chemistries containing appropriate functional groups for adhesion. In addition, the polymers

should be unreactive towards the loaded drug, facilitate easy incorporation of various drug doses within its matrix, biodegrade at an appropriate rate for the targeted application, and facilitate controlled release with kinetics appropriate to the clinical need [5], [6].

1.1.5.3. Tissue engineering

Bioadhesive polymers are currently being researched as a potential scaffold materials in the context of tissue engineering and regenerative medicine. Scaffolds are three dimensional porous solid biomaterials designed to 1) promote extra cellular matrix (ECM) deposition, cell adhesion, and cell-biomaterial interaction, 2) allow sufficient transfer of gas, nutrients, and regulatory factors for cell survival, proliferation, and differentiation, 3) biodegrade at the same rate as tissue regeneration, and 4) have minimal inflammation and toxicity effects [41], [42]. Appropriate scaffolds for particular tissue engineering challenges ideally offer properties that mimic natural tissue, including strength, rate of degradation, porosity, size, and microstructure [41], [43]. Figure 1-5 shows the typical process for growing cells using a polymeric scaffold.

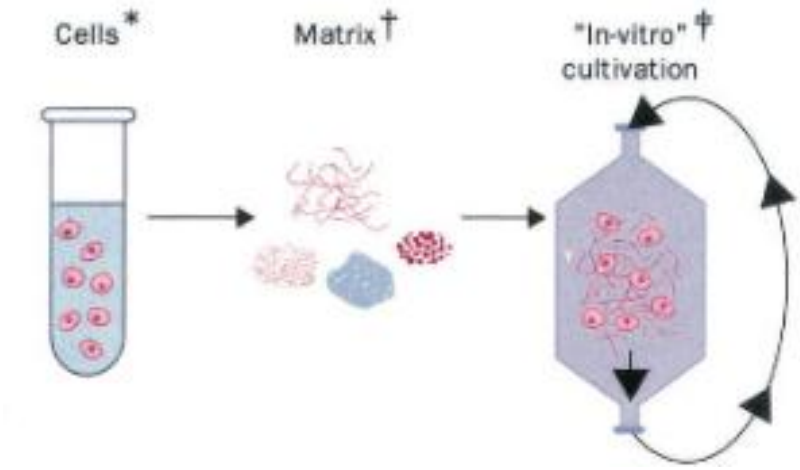

Figure 1-5: Tissue engineering process using polymeric scaffolds [43]

Polymers can be tuned to meet desired characteristics based on the material and reaction chemistry used, the type and degree of functionalization, and the polymer molecular weight [44]. Porous polymer or hydrogel scaffolds have been used for the regeneration of skin, bone, and cartilage, organs such as the liver, bladder, or pancreas, heart valves, arteries, corneas, and other soft tissues [41], [45].

1.2. Hydrogels

Hydrogels are three-dimensional systems composed of water-soluble polymers that are formed by crosslinking polymer chains through physical or covalent interactions [46], [47], [48]. Hydrogels are known for their ability to absorb and retain water, and have thus attracted interest in various biomedical fields such as drug delivery, wound healing, tissue regeneration, cell immobilization, and biocompatible coatings [46], [49]. A hydrogel's ability to absorb water is attributable to the hydrophilic functional groups attached to the polymer backbone while its resistance to dissolution comes from the cross-links present between the network chains [47], [50].

Hydrogels have also typically exhibited good biocompatibility due to their high water content and thus low interfacial tension within the aqueous biological environment [48]. Hydrogels can be used in the form of slabs, films, micro particles, nanoparticles, and coatings [49].

Hydrogels can be created by using any modified natural or synthetic water soluble polymer that can facilitate cross-linking and hence hydrogel formation to occur. Different mechanisms of network formation have been extensively studied; the main two methods are chemical and physical cross-linking [48]. Physical cross-linking is a reversible mechanism that has the advantage of not using any chemical cross-linking agents. Physical cross-links can be achieved through different environmental factors such as temperature, pH, and ionic interaction, as well as physiochemical interactions such as hydrophobic, charge condensation, and hydrogen bonding [48], [49]. Chemical cross-linking mechanisms use cross-linking agents or polymer-polymer crosslinking to form covalent bonded hydrogels. Glutaraldehyde and genipin are two widely used cross-linking agents that promote fast gelation between carbohydrates and other natural polymers [51]. However, the use of small molecule cross-linking agents can cause cytotoxic side effects that result in a non-biocompatible hydrogel [48], [49]. Polymer-polymer cross-linking, facilitated by the reactivity of the side chains of the polymer backbone chains, usually offers a more non-cytotoxic alternative. In particular, our group has extensively studied the cross-linking of hydrazide and aldehyde-functionalized polymers that, when in contact, form a (hydrolytically reversible) hydrazone bond without the use of external promoters such as UV photopolymerization or radiation. This approach to use macromolecular cross-

linking agents typically promotes the formation of a more non-toxic, biocompatible hydrogel that has the potential to be used in clinical *in vivo* settings [48].

Hydrogels can effectively be tuned according to their cross-linking density, which determines important parameters such as pore size, swelling, degradation, and mechanical strength [48]. Controlling the cross linking density can be achieved through using different chain length monomers, amounts of cross-linking functional groups, concentrations of product polymer in the hydrogel network, and the reaction temperature [50].

1.3. *In situ* gelling chemistries

The effective application of most conventional hydrogels for internal medicine remains difficult due to the difficulty in delivering hydrogels in a minimally invasive method through a syringe. Pre-formed hydrogels are highly elastic and thus difficult to inject, while other established synthetic routes to *in situ*-formed hydrogels are incompatible with *in vivo* requirements (e.g. glutaraldehyde crosslinking). Enabling injection significantly decreases the damage incurred at the targeted and surrounding tissue during the delivery, which reduces the risk of infection, inflammation, patient pain and healing time. Furthermore, their ability to gel at the site of injection allows the hydrogel to take the form of the tissue surrounding it, filling any cavities and undesired voids in a way particularly essential for barrier applications of the hydrogels [52], [53].

Some chemical cross-linking hydrogels can be used non-invasively (e.g. photopolymerized hydrogels cross-linked under UV radiation [54]; however, such hydrogels require a photoinitiator and UV radiation at the *in vivo* site of application,

which poses safety concerns associated with the use of high-intensity UV, potential heating effects, and subsequent cell death [52]. These factors limit the potential *in vivo* application of *in situ*-gelling hydrogels [54].

Injectable, or *in situ* gelling, hydrogels fabricated through physical cross-linking have attracted interest due to their ability to avoid some of the limitations mentioned above. Their shear-responsive nature enables injection and thus avoidance of surgery, as well as (often) rapid gelation once injected into the physiological environment. Physical cross-links can be formed in a stimulus-responsive nature using a physical trigger (e.g. pH and/or temperature) or by the physical interaction of the prepolymer gel components through a number of interactions such as electrostatic and hydrophobic [52], [55]. However, these physically cross-linked hydrogels typically offer minimal control over the degradation mechanism, with some formulations, such as poloxamer 407 [49], being highly dilution-sensitive *in vivo* (and thus rapidly cleared) and others bonding so strongly to the point the material is not functionally degradable (leading to bioaccumulation and potential inflammation) such as PINPAAm-grafted-collagen [56]. Physically cross-linked hydrogels in the aqueous *in vivo* environment also typically show poor mechanical properties that can be disrupted by low magnitudes of shear [52], [54], beneficial in some applications, such as the eye [57], but undesirable for long-term immobility at the site of injection in other applications.

In response to the native disadvantages of both physical and conventional covalent chemistries for gelation, a series of reactive functional group pairs (typically tethered to polymers to minimize the toxicity of functionalized small molecules) have

been developed [52], with the most common such chemistries being the Michael reaction [44], disulfide formation [58], and Schiff base/hydrazone bond formation [52].

A Michael reaction, also known as Michael addition, is the nucleophilic addition of a nucleophile to a β-unsaturated carbonyl compound such as an aldehyde or ketone. Amines, alcohols, and thiol groups are generally employed as the nucleophile(s), with ketone and aldehydes used as the electrophile(s) [52]. Michael addition chemistry can occur spontaneously under physiological conditions [59]. However, the basic conditions of a Michael reaction, its often slower gelation rate, and the functional irreversibility of most Michael adducts might be undesirable for *in vivo* use [52], [60].

Disulfide formation can be achieved through the reaction of two thiol groups, forming a S-S bond in an oxidizing environment [52]. While this method produces hydrogels that are easily reversible (via disulfide exchange) and generally non-cytotoxic *in vivo* and *in vitro* in the absence of catalysts, the low gelation rate poses a disadvantage; in addition, since this chemistry is routinely used biologically, proteins are highly reactive with this chemistry as well, leading to (in some cases) protein denaturation that limits its practical use [52].

Hydrazone bonds are formed through the reaction between nitrogen from a hydrazine or hydrazide group, a functional group containing nitrogen-nitrogen bond, and a carbonyl-containing functional group such as aldehydes or ketones, with the oxygen in the carbonyl group eliminated via reaction [52], [61]. The main advantage of hydrazone bond formation (hydrazide-aldehyde) is the fast gelation time upon injection, with highly functionalized polymers gelling in mere seconds. The degradation time can be tuned due to the hydrolytic lability of the hydrazone bond and

the amount of cross-links present (based on the number of functional groups on the precursor polymers) in the hydrogel matrix; such control offers the potential to develop a controlled release drug delivery system as well as other degradable biomedical products [36], [52].

1.3.1. *In situ* Gelation chemistry used

The gelation chemistry used for this project is hydrazide-aldehyde chemistry, shown schematically in Figure 1-6.

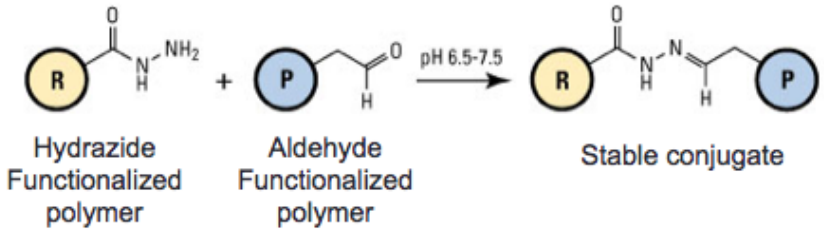

Figure 1-6: Aldehyde-hydrazide gelation chemistry used in the project [62]

When one or more hydrazide-functionalized polymer is mixed with one or more aldehyde-functionalized polymer, a stable hydrazone cross-linked conjugate is formed, enabling the (rapid) formation of a hydrogel from low-viscosity precursor polymers that are easily injected or sprayed. This polymer-polymer cross-linking chemistry allows for tunable degradation of the hydrogel depending on the number of functional groups present on the polymers, the chemistry adjacent to the functional group, and the degree of swelling (related to the accessibility of water to penetrate into the gel to hydrolyze the hydrazone bond) [49], [63].

1.4. Polymers used

The hydrogel matrix synthesized for this project consists of both a natural and synthetic polymer. The natural polymer is chitosan, while the synthetic polymer is poly(oligoethylene glycol methacrylate), functionalized with appropriate functional groups (hydrazides and aldehydes respectively) to induce *in situ* covalent polymer-polymer cross-linking once the polymers are mixed.

1.4.1. Chitosan

Chitosan is linear cationic aminopolysaccharide biopolymer made up of N-acetyl-D-glucosamine repeat units bound to each other by beta-1,4 linkages (Figure 1-7) [64], [65], [66]. It is derived from chitin, which is one of the most abundant natural polymers found in nature (second only to cellulose) [67]. Chitin is composed of β-(1→4)-poly-N-acetyl D-glucosamine and is a high molecular linear polysaccharide (Figure 1-7). Chitin is found mainly in the exoskeletons of crustaceans such as shrimp, crabs, and lobsters, and in mushrooms [64], [68]. Due to the lack of charge in its functional groups, it is considered a charge neutral polysaccharide; furthermore, it possesses a rigid crystalline structure due to inter-molecular hydrogen bonding. Hence, chitin is insoluble in water and common solvents, limiting its applicability in research and industries [69].

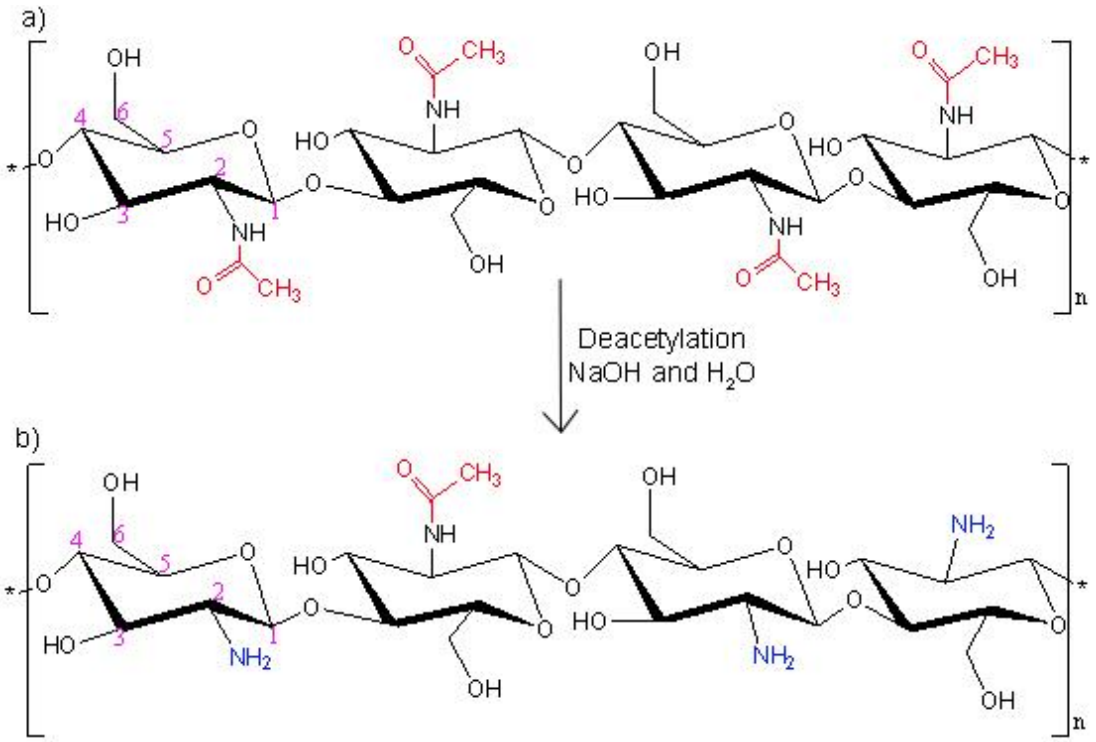

Figure 1-7: The chemical structures of a) chitin and b) chitosan [70]

Chitosan is derived from the partial deacetylation of chitin, producing d-glucosamine units that improve its solubility due to their charged state at pH< 6.5 [64]. While chitin's degree of deacetylation (DD) ranges from 5-10%, chitosan's DD typically ranges from 60-95% [69], [71]. This partial deacetylation is carried out through chemical hydrolysis under severe alkali conditions using sodium hydroxide or enzymatic hydrolysis in the presence of particular enzymes such as lysozyme, lipase, protease, carbohydrase, and tannase [70], [72], [73]. The molecular weight of chitosan typically varies from 10kDa to 1000kDa depending on its source and preparation [70], [74].

The presence of primary amino groups in chitosan's structure differentiates it from chitin. Chitosan is soluble in dilute acidic aqueous solutions due to the

protonation of these amino groups; chitosan is the only naturally occurring cationic polysaccharide [70]. The three reactive functional groups at the C2, C3, and C6 positions of chitosan (corresponding to the primary amine and two hydroxyl groups) offer possibility of a vast variety of chemical modification to tune biological properties [64]. However, the higher the molecular weight of chitosan, the more compact its structure is due to the enhanced intramolecular interactions present (particularly hydrogen bonding). This reduces the reactivity of the hydroxyl and amine groups, making them more difficult to modify and functionalize [67].

Chitosan is an attractive biopolymer for its demonstrated biocompatibility, biodegradability, and low toxicity in multiple applications [75], [76], [77]. In addition, chitosan's cationic nature gives rise to several useful properties, including antibacterial [78], antifungal [68], and antiviral [79] characteristics as well as film, fiber, and hydrogel forming capabilities [70, 80]. On the other hand, chitosan, at a higher charge density, has been known to have cytotoxic effect [81], leading to a need for an optimum charge density that is both toxic to bacterial cells but nontoxic to mammalian cells.

Chitosan's role in wound healing has been extensively studied, with studies indicating up to 30% acceleration of the wound healing process when chitosan scaffolds are used [82]. It has been shown to possess bacterial cell-binding activity due to its positive charge interacting with the negatively charged bacterial cell surface. The exact mechanism of bacterial lysis is thought to be chitosan's role in interrupting the bacterial membrane and thus disrupting mass transport across the bacterial wall [83]. Indeed, a suggested reason for chitosan's wound healing and hemostatic

capabilities is its ability to accelerate the permeation of inflammatory cells during the inflammation stage, as triggered by the lysis of bacteria and thus local cytokine release. Another study showed that scar tissue (resulting from an imbalance between collagen I and III fibers) was reduced when a wound was treated with chitosan [29], [72]. Its ability to form a film directly on the wound allows for excellent oxygen permeability, and its carbohydrate backbone can degrade over time via enzymatic processes (with lysozyme representing the most common *in vivo* degradation enzyme), without the need to remove it at the injury site [82], [84].

Chitosan has also been demonstrated to possess bioadhesive and mucoadhesive properties, again attributed primarily to electrostatic interactions between (cationic) chitosan and (anionic) tissues, including keratin (skin) and sialic acid (mucous); hydrogen bonding may also contribute to these adhesive responses [79], [85].

Many chemical derivatizations of chitosan have been pursued, depending on the end application. Specific interest has been paid to chemically modifying chitosan to create a more soluble polymer over a wider pH range. The introduction of bulky side groups, including the introduction of small functional groups such as alkyl and carboxymethyl groups, has been demonstrated to improve the solubility of chitosan without affecting its cationic properties [69], [86]. The improved solubility of carboxymethyl chitosan is attributed to the side group's ability to disrupt the intrachain hydrogen bonding of chitosan [69]. The most widely used soluble chitosan derivatives include carboxylated chitosan (using monochloroacetic acid as the reagent and isopropanol as the solvent) [64], N-O-acetylchitosan (using acetyl chloride as the reagent and methanesulfonic acid as the solvent) [87], and N-phthaloylated chitosan

(using phthalic anhydride as the reagent and N,N-dimethylformamide as the solvent) [88], although a variety of other graft water soluble chitosans have been produced [86].

1.4.1.1. Carboxymethyl chitosan

Carboxylating chitosan is one of the most well known methods to produce a hydrophilic chitosan derivative [69]. Carboxymethyl chitosan is an amphoteric polymer that contains hydroxyl, carboxyl, and amine groups. It is usually synthesized by the reaction of chitosan (pre-treated with sodium hydroxide) with monochloroacetic acid (MCAA), using 2-propanol as the solvent [64], [67]. Different carboxymethyl derivatives can be achieved by varying the reaction conditions and pretreatment conditions, including time, temperature, and the ratios of sodium hydroxide and monochloroacetic acid to chitosan [67]. Due to the multiple nucleophiles present on chitosan, O-carboxymethyl chitosan, N,O-carboxymethyl, and N,N-carboxymethyl chitosan derivatives may all be produced, depending on the reaction conditions and solvents used. A low NaOH concentration (< 50%) is not enough to break chitosan's rigid crystalline structure during the pre-treatment, lowering the penetration ability of MCAA into the polymer chain. Also, a lower NaOH:MCAA ratio results in insolubility over a wider pH range. Therefore, higher NaOH concentrations and NaOH:MCAA ratios are favourable for more complete carboxylation. Also, as the MCAA:chitosan ratio increases, the degree of carboxyl group substitution on the polymer chain increases until a point where a higher ratio of feed MCAA will not exhibit any further substitution increase [67], likely due to steric effects. Further functionalization can occur using the carboxyl groups for substitution, provided that those functional groups do not compromise the solubility benefits of the original carboxylation reaction.

1.4.2. Poly(oligoethylene glycol methacrylate)

Poly(oligoethylene glycol methacrylate) (POEGMA) is a free radical polymerizable analogue of poly(ethylene glycol) (PEG) (Figure 1-8). Unlike natural polymers, which have high batch-to-batch variation and a limited scope of properties based on their source, synthetic polymers like POEGMA are easily tunable to exhibit different hydrophilicities, cross-link densities, charges, mechanical strengths, and molecular weights by varying the copolymerization conditions as well as the number of ethylene oxide groups in the side chain [89], [90]. Shorter side chains (n=2 repeat units) exhibit thermoresponsive properties similar to poly(N-isopropyacrylamide), while longer side chains (n=7-8 repeat units) exhibit highly hydrophilic and cell/protein-repellent properties similar to PEG [91].

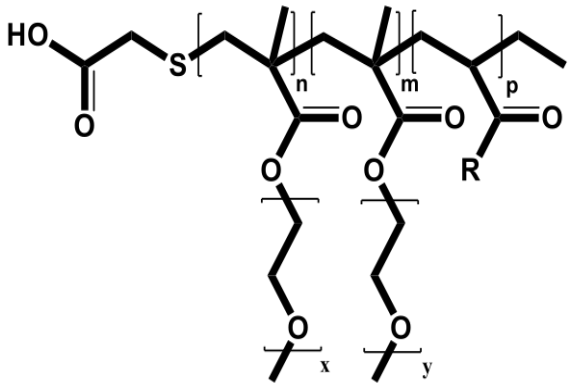

Figure 1-8: Chemical structure of POEGMA

POEGMA also offers considerable advantages in terms of being highly protein-repellent, non-cytotoxic, non-immunogenic, as well as easily prepared from low-cost monomeric precursors in a highly reproducible fashion. In addition, unlike PEG, POEGMA polymers can be easily functionalized by simple free radical copolymerization with functional (meth)acrylate comonomers [89], [90].

1.5. Objectives

The central objective of this thesis is to design an *in situ* gelling hydrogel that combines the tissue and mucous adhesion properties of chitosan with the tunability, non-cytotoxicity, and non-immunogenicity of POEGMA to create an injectable or sprayable bioadhesive material. Specifically, we aim to apply hydrazone bond chemistry to make an *in situ*-gelling, injectable matrix of hydrazide-functionalized chitosan and aldehyde-functionalized POEGMA polymer, where the incorporation of chitosan will give the hydrogel its bioadhesive and potential antibacterial properties and the chemical versatility of the POEGMA polymer will give rise to a tunable gelation times, swelling responses, and degradation kinetics as well as anticipated non-cytotoxicity. To achieve this goal, different paths of chitosan functionalization will first be investigated to enable chitosan solubilization and functionalization with carboxymethyl groups followed by hydrazide groups. Different concentrations of chitosan will be incorporated in the hydrogel to investigate the effect of chitosan on the hydrogel properties, including swelling and degradation kinetics, gelation time, rheology, bioadhesion, and mucoadhesion (using skin and processed mucin as the model substrates). The antibacterial properties of the chitosan-POEGMA hydrogel will be assessed through several antibacterial experiments including minimum inhibitory concentration and LIVE/DEAD bacterial assays, using *E.coli.* as the model bacterium.

2. *In situ* gelling bioadhesive hydrogel for topical and mucosal applications

2.1. Introduction

The development of bioadhesive hydrogels for biomedical applications such as wound healing and drug delivery offer significant potential to address existing clinical challenges. In the former application, infection of wounds post-surgery poses a significant problem for hospitals due to the tedious aftercare of surgical infections which lead to discomfort for the patient, longer hospital stays, and higher expenses [12]. In 2011, it was estimated that between 500,000 to 750,000 patients per year suffer from surgical site infections (SSIs) in the U.S. alone [92], [93]. If infection occurs, a patient is 60% more likely to stay in the ICU post-surgery and will remain in hospital for a median of two additional weeks; furthermore, even after release, such a patient is 5 times more likely to be readmitted to the hospital [93]. The relative cost of treating these patients is thus, on average, 1.43 times greater for patients with SSIs than patients without, increasing the economic burden on the health care system [94]. In the latter application, existing drug delivery systems, particularly those targeted to local areas such as the eye or the vagina, largely lack a high enough residence time at the biointerface to deliver a drug with adequate clinical efficacy over extended periods [37].

Bioadhesive polymers, specifically hydrogels, have gained interest in both of these fields of research for multiple reasons. Hydrogels are generally advantageous in biomedical applications due to their typically high biocompatibility and tunable biodegradability [7]. Bioadhesive polymers offer particular advantages in that their adhesive properties and high water contents and have demonstrated to be beneficial for wound healing applications while their mucoadhesive properties, specific affinities

to different drugs, and their ability to control the release of the drug is beneficial for targeted local drug delivery through mucosal membranes [7], [12], [14].

In situ gelation is a favorable technique for its ability to be an injectable system which eliminates the need for invasive surgery, decreasing the probability of any complications such as inflammation and infection, as well as the ability to localize the site of application, and once injected, the hydrogel's ability for gelation to occur in the presence of the tissue, taking its form and filling any undesired cavities. Achieving in situ gelation through hydrazone chemistry creates an *in vivo* compatible network due to the elimination of any crosslinking agents or UV radiation, as well as decreasing the gelation time, which posed as a limitation for other *in situ* gelation chemistries [52], [53].

In this work, we report the design of an *in situ* gelling bioadhesive hydrogel that can be both injected and sprayed based on reversible covalent bond formation between hydrazide-functionalized chitosan and aldehyde-functionalized poly(oligoethylene glycol methacrylate) (POEGMA). Chitosan was selected in this application to exploit its biodegradable, bioadhesive and antibacterial properties, while POEGMA provides an inert and highly tunable gelling pair that provides the biomedical advantages of PEG while promoting facile design of hydrogels with desirable mechanical, cell/protein adhesive, and smart properties.

Two main targeted applications were tackled: preparing a mucoadhesive *in situ*-gelling hydrogel for vaginal applications and a skin adhesive *in situ*-gelling hydrogel for topical applications. The end goal of this project is to design a hydrogel library with various properties (tunable based on the POEGMA gelling agent) that are suitable for various bioadhesive biomedical applications. While wound healing, which

requires the hydrogel to be bioadhesive and antibacterial, and mucosal drug delivery, which requires the hydrogel to be mucoadhesive as well as control the release kinetics of a drug, were the main target applications, the generation of the hydrogel library outlined may also yield a hydrogel with properties more suitable to another application.

2.2. Materials

All chemicals were received from Sigma-Aldrich Inc. (Oakville, Ontario) unless otherwise indicated. Medium molecular weight chitosan (75-85% deacetylated, 200-800 cP) and low molecular weight chitosan (75-85% deacetylated, 20-300 cP), monochloroacetic acid (≥99%), sodium hydroxide pellets (≥97%), 2-propanol (99.5%), and anhydrous ethyl alcohol (Commercial Alcohols, Ontario, Canada) were all used as received for carboxymethyl chitosan synthesis. N-(2,2-dimethoxyethyl)methacrylamide aldehyde monomer (DMAEAm, 98%) was synthesized in our lab via the addition of methacryloyl chloride to a concentrated sodium hydroxide solution in the presence of aminoacetaldehyde dimethylacetal and TEMPO [89]. Oligo(ethylene glycol) methyl ether methacrylate (OEGMA, M_n ~ 475, 95%) and di(ethylene glycol) methyl ether methacrylate (MEO_2MA, 95%) were both purified prior to use by passing through a column of basic aluminum oxide (Type CG-20) to remove methyl ether hydroquinone (MEHQ) and butylated hydroxytoluene (BHT) inhibitors. 2,2-azobisisobutryic acid dimethyl ester (AIBMe, 98.5%, Wako Chemicals), acrylic acid (AA, 99%), and thioglycolic acid (TGA, 98%) were used as received. Adipic acid dihydrazyde (ADH, 98%, Alfa Aesar), 1-Ethyl-3-(3-dimethylaminopropyl)carbodiimide (EDC, commercial grade, Carbosynth, Crompton

CA), 2-(dimethylamino)ethyl methacrylate (DMAEMA, 98%), and thioglycolic acid (TGA, 98%) were used for POEGMA and chitosan aldehyde and hydrazide functionalization respectively and were also used as received.

Luria-Bertani broth (EMD Chemicals), agar (Bioshop, Burlington, Canada), *E. coli* bacteria donated by Dr.Gerry Wright at McMaster University (strain: BL21 (DE3) containing the antibiotic resistant gene (ampR) against ampicillin), ampicillin (anhydrous, 96.0-100%), and LIVE/DEAD backlight bacterial viability kit (kit L-7012, Life Technologies) were used for antibacterial work. Mucin from porcine stomach (Type III, bound sialic acid 0.5-1.5%) was used for mucoadhesion work. Porcine hairless stomach skin was acquired from an abattoir. HCl and NaOH solutions for titration were prepared from Acculute standards. Resazurin sodium salt (80% dye content) was used for the cytotoxicity assay. LIVE/DEAD viability/cytotoxicity kit, for mammalian cells (kit L-3224, Life Technologies) was used for cell adhesion work. All water was Milli-Q grade with a resistivity of >18 MΩ-cm.

2.3. Synthesis

2.3.1. Synthesizing Chitosan

Due to the presence of three reactive groups on chitosan, different paths can be taken to generate a water-soluble chitosan. After extensive research on the different pathways, carboxymethylation of chitosan followed by conversion of the carboxyl groups to hydrazide groups was selected as the optimal pathway [64]. Due to the three possible reactive sites (amine, primary –OH, and secondary –OH groups), different carboxylation routes could be carried out depending on which reactive groups is targeted for substitution, as shown in Figure 2-1. Due to the amine (-NH_2) group being

the main source of chitosan's bioadhesive as well as antibacterial properties, O-carboxylation (on the primary hydroxyl group) was targeted as the carboxylation pathway to minimize amine substitution [95], [96]. Hydrazide functionalization was then carried out to produce the final functionalized polymer.

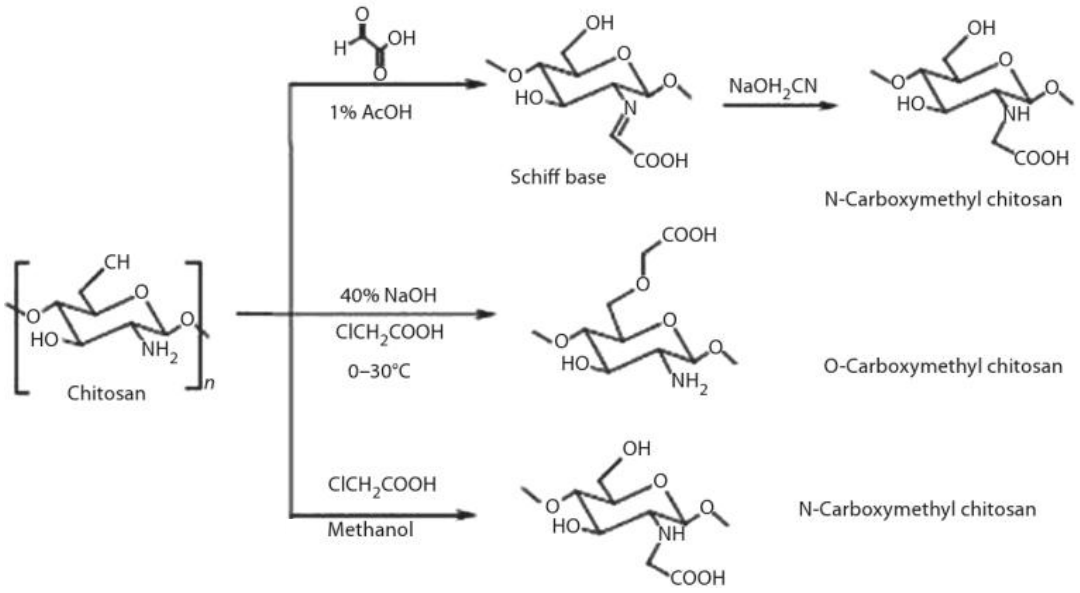

Figure 2-1: Different carboxylation pathways for chitosan [97]

2.3.1.1 Carboxymethyl chitosan:

O-carboxymethyl chitosan was prepared by the selective substitution of the hydroxyl (-OH) group in favor of a carboxyl (-COOH) group. Initially, in a 250mL flask, 1.75g of sodium hydroxide was dissolved in 2mL of Milli-Q water by constant stirring. Once the sodium hydroxide was fully dissolved, 1g of chitosan was weighed and gradually added under manual mixing, to ensure all the chitosan powder is at least swollen in the sodium hydroxide solution. Due to the reaction proceeding when chitosan is in its solid state, alkalization of the chitosan molecules was needed to ensure the penetration of the monochloroacetic acid within the chitosan structure. 8mL of 2-propanol was then added, and the whole mixture was left stirring (at ~300 rpm) for one hour. After one hour, all the liquid was soaked up by the chitosan powder,

indicating that the chitosan molecules have swollen and hence alkalized. 1g of monochloroacetic acid was next weighed and dissolved separately in 2mL of 2-propanol. Using a glass pipette, the monochloroacetic acid solution was gradually added to the chitosan mixture under stirring. Once the monochloroacetic acid solution was completely added, the reaction was left stirring at room temperature for four more hours to ensure that the carboxylation occurs uniformly throughout the whole mixture. Running the reaction at room temperature favors O-substitution while at higher temperatures, N-carboxylation is favoured [95]. After four hours, 50mL of 70% ethanol was added to the mixture to stop the reaction. The polymer was purified through several washings with 70% ethanol using vacuum filtration. The precipitate was left in a humidity chamber at 30 ℃ and 30% humidity overnight to evaporate the residual 70% ethanol. Potentiometric titration (Mantech Inc.) indicated a carboxymethyl substitution % ~ 40 overall based on primary hydroxyl groups as well as minimal amine groups, (carboxylic groups weight % ~ 13),

2.3.1.2. Hydrazide functionalized chitosan

The two-step functionalization, as shown in Figure 2-2, ends with attaching hydrazide groups on the chitosan backbone. Carboxymethyl chitosan (~1g) was dissolved in 150mL of Milli-Q water in a 500mL round-bottom flask and the pH was brought down to 4.75 (the reaction pH). Note that the solution was filtered using a vacuum filter to get rid of any undissolved carboxymethyl chitosan prior to initiating the reaction. Once the solution was purified, an ADH/EDC reaction was conducted using a 5-fold excess of ADH (2.1g) and a 2.5-fold excess of EDC (1g), with masses calculated based on the measured degree of carboxylation of the chitosan. The pH was maintained at 4.75 over the four hour time course of the reaction, after which the

product was dialyzed against Milli-Q water (MWCO 13k-14k) for six cycles (6 hours each) for purification and lyophilized for storage.

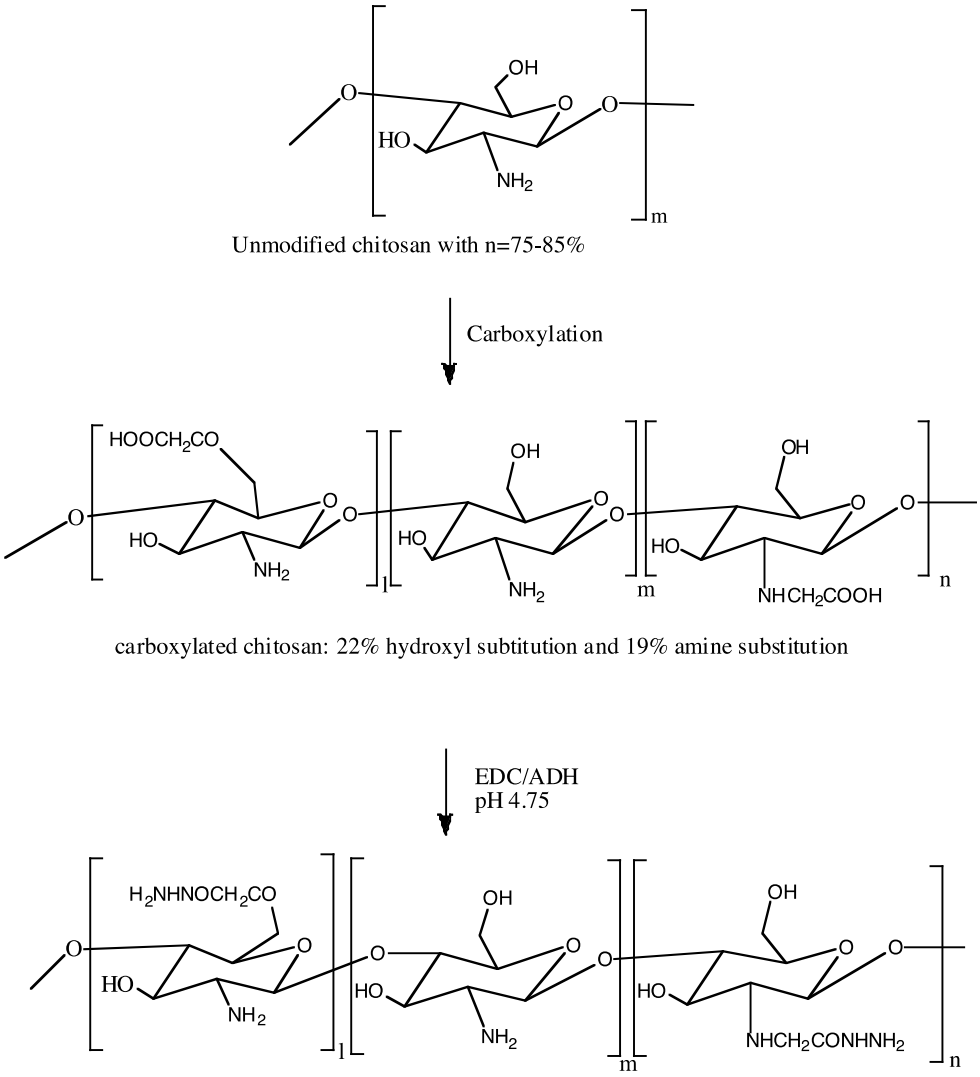

Figure 2-2: Full synthesis route from the raw material (75-85% deacetylated chitosan) to chitosan-hzd through carboxylation and ED/ADH reaction. (l) denotes the percentage of hydroxyl substituted chitosan units, (n) denotes the percentage of deacetylated chitosan units, and (m) denotes the percentage of amine substituted chitosan units.

2.3.2. Synthesis of POEGMA

Free radical polymerization was carried out to synthesize the POEGMA polymers. 2,2-azobisisobutryic acid dimethyl ester (AIBME) was used as the free

radical initiator and thioglycolic acid (TGA) was used as the chain transfer agent to reduce the molecular weight of the resulting polymers below the renal cut-off (<32kDa) [98]. $OEGMA_{475}$ (n=8-9 EO repeat units) was used as the long chain OEGMA monomer, while MEO_2MA (n=2 EO repeat units) was used as the short chain OEGMA monomer. Different ratios of short to long chain result in different hydrophilicities and phase transition temperatures, according to the needs of the application [98].

2.3.2.1 Aldehyde functionalized POEGMA

Free radical polymerization was carried out by copolymerizing $OEGMA_{475}$ and MEO_2MA with the functional acetal monomer N-(2,2-dimethoxyethyl)methacrylamide (DMAEAm). $OEGMA_{475}$ (0.9 g), MEO_2MA (3.1 g), DMAEAm (1.3 g), TGA chain transfer agent (7.5 μL), AIBMe initiator (50 mg), and dioxane (20 mL) were added to a 250mL flask, purged with nitrogen for ~ 30 minutes, and reacted at 70 ℃ under 250 RPM stirring for four hours. After evaporating the dioxane, acid catalyzed hydrolysis was performed over 24 hours to convert the acetal groups to aldehyde groups using 1M hydrochloric acid, after which the polymer was purified by 6x6 hour dialysis runs (MWCO ~3500), lyophilized, and then dissolved in PBS at a desired %wt/v and stored at 4 ℃ for further use. This polymer is denoted throughout the thesis as $PO_{10}A_{30}$, with '10' referring to the percentage of short chain monomer incorporated in the system, and the '30' referring to the aldehyde (A) functionalization percentage in the system.

2.3.2.2 Charged hydrazide functionalized POEGMA

Cationically-charged, hydrazide-functionalized POEGMA polymers were produced using the same method outlined above but including acrylic acid (AA) as a

grafting comonomer enabling subsequent hydrazide functionalization and 2-(dimethylamino)ethyl methacrylate (DMAEMA) as the cationic monomer. In this case, $OEGMA_{475}$ (0.9 g), MEO_2MA (3.1 g), DMAEMA (6.142 mL), TGA chain transfer agent (7.5 μL), AA (714 μL), AIBMe initiator (37 mg), and dioxane (20 mL) were added to a 250mL flask, purged with nitrogen for ~ 30 minutes, and reacted at 70 ℃ under 250 RPM stirring for four hours. After evaporating the dioxane, the product was re-dissolved in 100 mL of water to which was added a 5-fold excess of ADH (6.85 g) and a 2.5-fold excess of EDC (2.44 g) relative to the acrylic acid loading in the polymer. The reaction was carried out at pH 4.75 and room temperature overnight, dialyzed (MWCO ~3500), lyophilized, and then dissolved in PBS to the required wt/v%. This polymer is denoted as $+PO_{10}H_{29}$, where the positive denotes its cationic charge, the '10' represents the percentage of short chain versus long chain OEGMA monomer used to prepare the polymer, and the '29' represents the incorporation of hydrazide groups in the polymer chain.

2.4. Polymer and gel characterization methods

2.4.1. Potentiometric-conductometric titration

Potentiometric-conductometric titration was used to confirm and quantify 1) the carboxymethyl (-COOH) content of the chitosan polymer after the carboxylation step 2) the consumption of the carboxyl groups after hydrazide functionalization of the polymer, and 3) the content of free amines in order to confirm the minimum substitution of the amine groups throughout the two reaction steps.

To perform the titrations, the polymer was dissolved in Milli-Q water (1mg/mL) and the pH was lowered 2.3 using 1M HCl. Potassium chloride (KCl crystals 99.5-100.5%, EMD chemicals, USA) was added to increase the conductivity

of the polymer solution to 5mS/m. The polymer solution was titrated using the Mandel PC titrator by the automatic gradual addition of 0.1M NaOH, where the pH and conductivity were recorded as a function of the base volume addition. Data analysis was carried out using the derivative of the pH vs. base volume curve to quantify the degree of substitution, weight percentage of carboxylic groups, the content of free amine, degree of hydrazide functionalization, and hydrazide groups per polymer chain, depending on the polymer titrated.

2.4.2. Nuclear magnetic resonance

POEGMA polymer composition was analyzed by ^{1}H-NMR (Bruker 600 MHz spectrometer). The cationic hydrazide POEGMA was dissolved in dimethyl sulfoxide and aldehyde POEGMA in deuterated chloroform.

2.4.3. Gel permeation chromatography

The number average molecular weight (Mn) and poly dispersity (PDI) of the POEGMA polymers were determined using DMF gel permeation chromatography. This was done using a Waters 590 HPLC pump with three Waters Ultrastyragel Linear columns operating in series and a Waters 410 refractive index detector.

2.4.4. Double barrel syringe device

For all hydrogel characterization, the hydrogel was injected into a silicone mold of determined shape and size, depending on the experiment, using a double barrel syringe. This device is able to store the aldehyde-functionalized POEGMA polymer and hydrazide-functionalized chitosan polymer in separate compartments in preparation for mixing. A helical mixer attached to the double barrel enables intimate mechanical mixing when the two polymers enter the helical interior of the mixer and leave through the nozzle, as shown in Figure 2-3. A 20-½ gauge needle can be

attached to the end of the mixer to deliver the precursor polymers to the desired site, particularly important when creating thin films for the bioadhesion experiments, as shown in Figure 2-4.

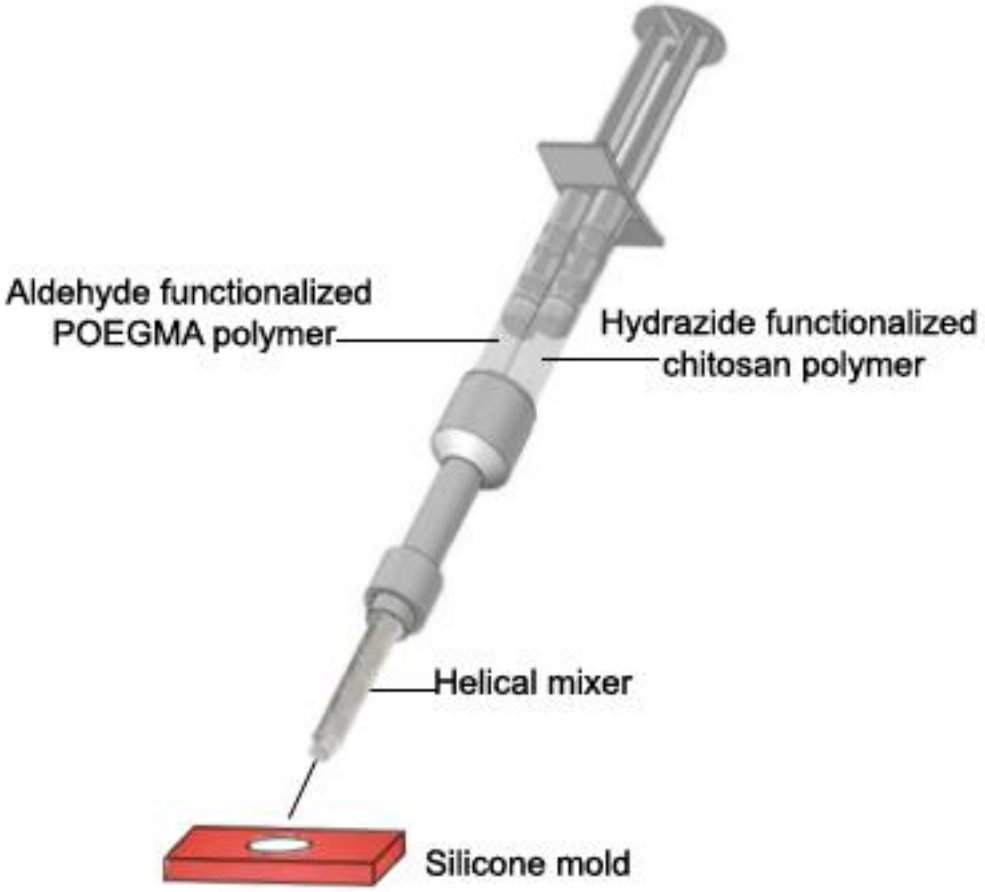

Figure 2-3: Hydrogel injection using a double barrel syringe

2.4.5. Gelation Kinetics

Chitosan and POEGMA precursor solutions were loaded into a double barrel syringe (1:1 volume ratio), co-extruded into a microcentrifuge tube, and mixed using a vortex shaker. A vial inversion test was conducted at various times after extrusion (t=0), with gelation considered to have occurred when no visible flow was recorded 30 seconds after vial inversion.

2.4.6. Transparency

A UV plate reader (1420 Victor 3 multi-label plate reader, Perkin Elmer Life Sciences) was used to measure the absorbance of the hydrogels over the full visible light wavelength range (400-650 nm). Using a double barrel syringe, 1.5mL of polymer solution was deposited in each well of polystyrene 12-well plate, resulting in a film thickness of ~ 4.4 mm. The trials were run three times consecutively, with results averaged. The absorbance of each well was subtracted by the absorbance of the blank to isolate the absorbance of the sample itself based on the equation:

$$\text{Transmittance (\%)} = \left(\frac{1}{10^{(Abs\ of\ sample - Abs\ of\ blank)}}\right) \text{x100\%} \qquad \text{Equation 2-1}$$

Note that POEGMA concentrations of 10 wt/v% instead of 20 wt/v%, for $PO_{10}A_{30}$ and $+PO_{10}H_{29}$ were used for this study only, as the gels with the POEGMA at 20 wt/v% concentration gelled too quickly to be spread evenly across the plate in order to acquire accurate measurements.

2.4.7. Swelling and degradation

Gel swelling and degradation was tracked gravimetrically as a function of time in an acidic media adjusted to relevant pH values using 0.1M HCl (pH 4 for vaginal application and pH 5.5 for topical/skin applications) as well as in phosphate buffered saline (pH 7.4 for other physiological environments). After gelling the precursor polymers into disks (diameter=0.9cm, height=0.35cm), the hydrogel samples were placed inside transwell plate inserts and then into separate wells of a polystyrene 12-well plate. Each sample was fully submerged in 4mL of the test solution and kept at 37 ℃ inside a shaking incubator. The residual mass of the gel sample was measured at

pre-determined times to assess the rate of gel degradation, with all swelling/degradation normalized using the equation:

$$\text{Swelling/degradation ratio (\%)} = \frac{W_t}{W_o} \text{ x } 100 \qquad \text{Equation 2-2}$$

where W_o is the initial weight of the hydrogel and W_t is the weight after each time interval. All data was normalized to the initial mass of each gel in order to correctly compare data using different gels. Four replicates per sample were used, with the error bars representing the standard deviation of the replicates of each sample.

2.4.8. Gel drying

A similar gravimetric analysis to that used for swelling experiments was conducted on the gels at different humidities using a controlled humidity chamber to track the time scales of gel drying. The three relative humidity settings used were 30%, 50%, and 75%, with all samples tested at 25 ℃. Precursor polymers were gelled in the same circular molds (d=0.9cm, h=0.35cm) as used for degradation and swelling tests, placed in inserts, and weighed at predefined intervals. A benchtop drying experiment was also performed for comparison at typical room temperature and humidity to assess any impact of the convection inside the humidity chamber on the evaporation times.

2.4.9. Rheological measurement

Rheological characterization was performed on all the hydrogels using the Mach-1 micromechanical tester to determine the elastic modulus (G') of each hydrogel. A series of oscillatory strain sweep runs were first performed to determine the linear viscoelastic region, followed by oscillatory stress sweep runs at an

amplitude in that viscoelastic region to obtain the modulus values that are ultimately plotted in a G' vs. frequency graph for comparison.

Initially, the hydrogels were prepared through usual double barrel syringe injection into silicone molds (diameter = 0.9cm, depth = 0.2cm), capped with a thin silicone layer, and left for several hours to ensure complete gelation. A gel was then mounted on the base of the instrument and a find contact function (critical force F=0.054N, speed 0.1mm/s) was run between the indenter and the hydrogel. Once the contact was found, 30% compression was applied to the gel to ensure complete contact between the hydrogel and the indenter, followed by oscillatory strain sweeps and then stress sweeps to determine the elastic modulus over a frequency range. Four replicates per sample were used, with the error bars representing the standard deviation of the replicates of each sample.

2.4.10. Mechanics and adhesion

The adhesive strength of a hydrogel was assessed using different geometries as well as different biointerfaces to determine the appropriateness of the hydrogels formed for the targeted applications. Initially, a conventional tack test was conducted (metal on hydrogel) to characterize the tackiness, or stickiness, of the hydrogel, which must be minimized for topical applications in particular. For assessing adhesion via topical application, animal skin was used to test the bioadhesive properties of the hydrogel via both peel and tensile testing to simulate the different typical shearing forces experienced by a topically-applied hydrogel film. For mucosal applications, a mucin mimic was used as the substrate, with the adhesive interactions assessed via both viscometry and tensile mechanical testing.

The bioadhesive strength of the polymer to porcine skin was assessed using two different testing modalities: the peel strength between the hydrogel and the skin and the compression and subsequent decompression of the hydrogel while in contact with the skin. Both of these cases represent typical applied force geometries expected to occur during the application of the hydrogel when used on skin. The work of adhesion was determined for each experiment by calculating the area under the curve (AUC) using the trapezoidal rule:

$$\text{AUC} = \int_a^b f(x)dx \cong (b-a)\frac{f(a)+f(b)}{2} \quad \text{Equation 2-3}$$

$$\text{Work of adhesion} = \frac{\text{AUC}}{\text{AUC}_{\text{blank}}} \quad \text{Equation 2-4}$$

Two different methods were used to characterize the hydrogel mucoadhesive properties. Rheological testing was used to measure the molecular adhesion properties of the functionalized chitosan prepolymer to soluble mucin, while a mechanical tack test using a mucosal layer mimic was used to characterize the mucoadhesive property of the chitosan-POEGMA hydrogel.

2.4.10.1. Tack measurement of chitosan-POEGMA hydrogel

Sample preparation for tack testing involved first layering a microscope glass slide with epoxy glue and placing a silicone rubber mold immediately on top. Using a double barrel syringe, hydrogel precursors were injected in the mold and left to cure within 5 minutes of layering the epoxy. After allowing one hour for the hydrogel to fully crosslink, the rubber mold was peeled off the glass slide, leaving the hydrogel glued to the glass slide via the epoxy. The mechanical test was then conducted using the Mach-1™ micromechanical tester (Biomomentum Inc.). The sequence created for this tack test used the following ordered configuration:

- Find contact (1mm/s with a contact load of 0.0034N)
- Move relative (+0.1mm at 1mm/s)
- Zero load and position
- Wait 120 seconds
- Move relative (-10mm at 0.1mm/s)

2.4.10.2. Peel adhesion test

In order to mimic the external force application of peeling, a tensile tester (4411, Instron, USA) was used in conjunction with a movable flat base and a downward facing vertical clamp, together defining a 90 degree peel configuration that mimics a typical peeling process of a thin flat polymer on a substrate (i.e. the hydrogel on the skin). The biological substrate used was porcine skin. The hydrogel in this test was allowed to crosslink and cure in the presence of the biological substrate (skin) on both sides, creating a 'sandwich' geometry that ensures that the weakest bond in the system is the hydrogel-skin bond and not the hydrogel-substrate bond (key to improving the consistency of the peel testing results). The peel sample was prepared according to the geometry and assembly shown in Figure 2-4.

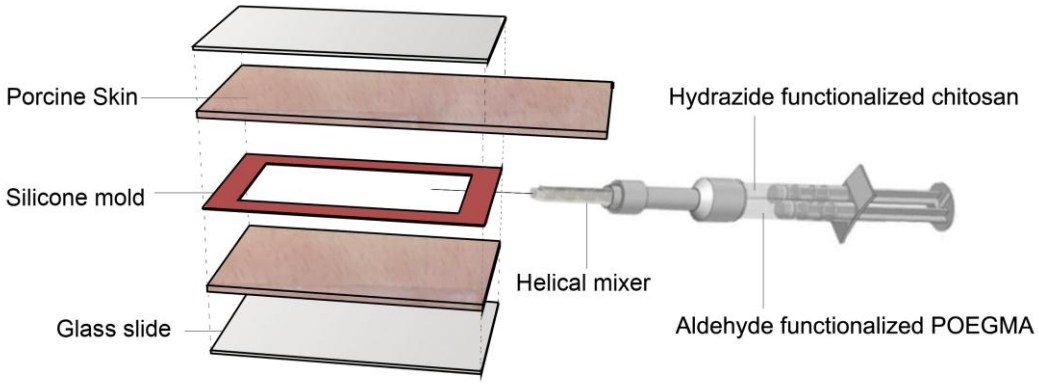

Figure 2-4: Sample preparation for peel testing

A silicone rubber mold with dimensions of LxWxH = 3.2x1.6x0.02 cm was used as the mold, and a 20½-gauge needle was inserted through the silicone mold to act as a port to inject the hydrogel. The silicone mold was placed between two pieces of porcine skin with larger dimensions, with one piece of skin having a significantly longer length in order to clamp the end and keep the sample at a 90-degree angle. A glass slide was placed on the other side of the porcine skin, and the whole sandwich was secured using two small clamps in order to ensure that the hydrogel would cover the whole interface without leaking out of the assembly. Once injected, the needle was immediately pulled out and a load (0.45kg) was added for two minutes during the gelation process to ensure intimate contact between the skin and hydrogel layers. The sandwich (after the load, clamps, and glass slides were removed) was then mounted on the Instron instrument according to the setup shown schematically in Figure 2-5, with a peel speed of 1mm/s used for testing. The maximum load, average load, and average load (per width) values following the point at which the two substrates were fully detached were reported. Four replicates per sample were used, with the error bars representing the standard deviation of the replicates of each sample.

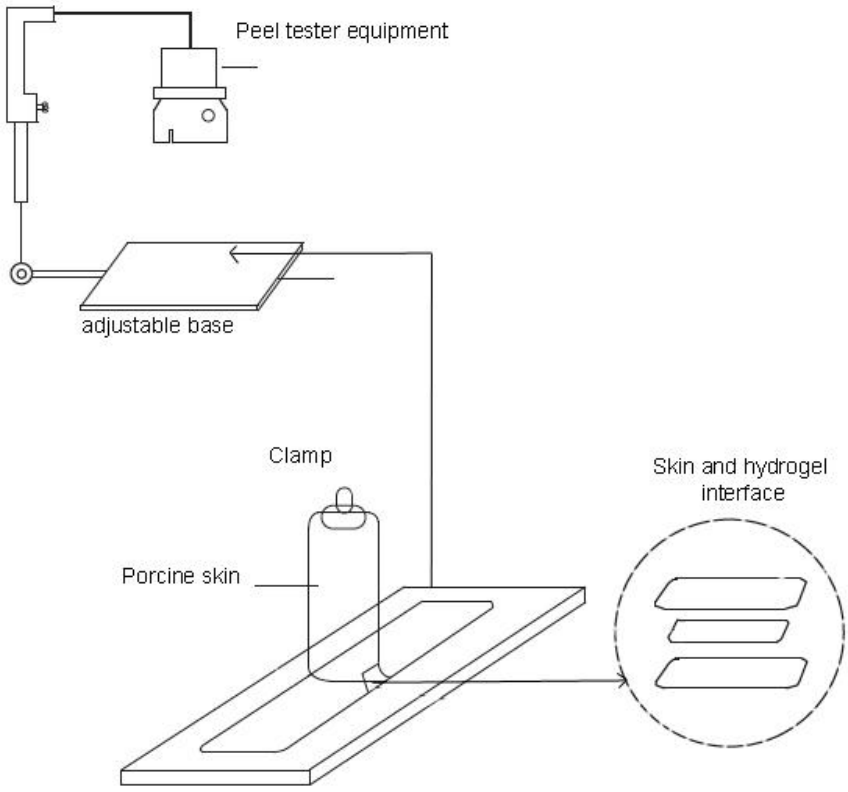

Figure 2-5: Peel testing experimental schematic

2.4.10.3. Tensile adhesion measurement of chitosan-POEGMA hydrogel

Pressure-responsive adhesion to skin was assessed using a compression/decompression experiment. The experiment used is similar to the tack experiment except that a biological substrate (porcine skin) was used as the substrate as opposed to the metal probe. In addition, the hydrogel was also allowed to cross-link in the presence of the biological substrate to better mimic the biological situation in which the hydrogel would be sprayed on to skin.

Test samples were prepared using the same procedure used in the peel adhesion experiment. The size of the biological substrate (3x3 cm) and the silicone mold (1.27 cm in diameter, 0.2cm depth) was chosen to match the diameter of the equipment's

indenter. A sequence tailored for compression and decompression testing was then applied using the Mach-1™ micromechanical tester (Biomomentum Inc., Canada), as follows:

- Find Contact: contact criteria of 0.0501 N at a velocity of 0.1 mm/s
- Move relative: amplitude of +0.3mm at a velocity of 0.1 mm/s (15% compression)
- Wait: 10 seconds
- Zero Load and Zero Position
- Move Relative: amplitude of -10mm at a velocity of 0.1 mm/s

* Negative is for upwards direction and positive is for downwards direction

2.4.10.4. Rheological measurement of chitosan precursor

Rheological measurement was performed in order to measure the magnitude of the mucoadhesive bond formation between different hydrazide-functionalized chitosan precursor polymer concentrations and mucin. A cone/plate oscillatory rheometer (ATS RheoSystems, USA) with a cone diameter and angle of 4cm and 20 degrees respectively was used for testing. Measurements were performed on chitosan 1wt/v%, 1.5wt/v%, and 2wt/v% solutions along with mucin 4wt/v% and the 1:1 volume combination of the chitosan and mucin pre-made solutions, all of which were prepared in PBS. The solutions were stored overnight at 4 ℃ to ensure complete hydration and equilibration before testing. Initially, in order to find the linear viscoelastic region of each polymer, an oscillation stress sweep was performed; a stress value in the linear viscoelastic region was subsequently selected and a frequency sweep was performed in which the frequency was changed from 0.01 Hz to 100 Hz in 30 intervals. These tests were performed for both the single polymer solutions (chitosan and mucin) and the mixture. The extent of mucoadhesion observed was assessed by calculating the excess modulus of the mixture, defined as the difference between the measured

modulus of the mixture and the modulus values of the two individual polymer solutions tested individually. This relationship, based on the concept of rheological synergism, is expressed mathematically in Eq. 3-5 (storage modulus) and Eq. 3-6 (loss modulus):

$$\Delta G' = G'_{mixture} - [G'_{polymer} + G'_{mucin}] \quad \text{Equation 2-5}$$

$$\Delta G'' = G''_{mixture} - [G''_{polymer} + G''_{mucin}] \quad \text{Equation 2-6}$$

When the modulus of the mixture is greater than the sum of the moduli of each individual solution comprising the mixture (the chitosan and mucin in this experiment), there is a specific interaction between the two mixed components, here a mucoadhesive interaction given the presence of mucous. The higher the value of $\Delta G'$, which signifies a higher $G'_{mixture}$ compared to the summation value of G'_{mucin} and $G'_{polymer}$, the stronger the mucoadhesion between the mucin and the polymer. Note that fresh samples of the polymers were used for each duplicate to avoid the presence of any residual stress in the sample after a run.

2.4.10.5. Mechanical measurement of chitosan-POEGMA hydrogel

The mucoadhesion of the chitosan-POEGMA hydrogel was measured relative to a mucosal layer mimic prepared by the immersion of a piece of filter paper (2.5cm, Whatman 1, GE Healthcare, UK) in a premade mucin solution (Type III, bound sialic acid 0.5-1.5%, Sigma-Aldrich) at either 75 mg/mL or 100 mg/mL in DIW half an hour before the start of the experiment [79]. These two different concentrations were chosen to cover a range of typical mucosal layer concentrations. The mucin-coated filter paper was then removed, rinsed to remove excess mucin, and mounted on the

base of the Mach-1 mechanical tester (Biomomentum Inc.), while the hydrogel was attached to the indenter. The sequence applied during the bioadhesion tensile testing (section 3.8.2.2) was also employed for this experiment.

2.4.11. Sterilization

For both bacterial and cell work, all equipment and polymers were sterilized. Pre-polymers, dissolved in PBS, were initially filtered using 0.45μm pre-sterilized filters, after which they were exposed to UV irradiation inside a biological safety cabinet (BK2-4 Class 2 Type A2 Biological Safety Cabinet, Micozone Corporation, Canada) for ~4 hours in clear scintillation vials. All equipment was sterilized by first sealing the equipment inside an autoclave pouch and then autoclaving using high pressure saturated steam at 121 ℃ for 15 minutes. All work was done in biosafety cabinets to ensure no contamination.

2.4.12. Characterization of antibacterial properties

Chitosan inherently possess antibacterial properties that are attributed to the amine functional groups present on its backbone chain [99]. Due to the functionalization of chitosan with first carboxymethyl groups and then hydrazide groups, some amine groups are lost to the functionalization, even with the selective hydroxyl group reaction path chosen. Therefore, characterizing and confirming the antibacterial property of the hydrazide functionalized chitosan precursor as well as the gel as a topical antibacterial polymer is necessary.

2.4.12.1. UV-vis spectrophotometry

UV-vis spectrophotometry was used to measure the optical density of the bacterial solution at a wavelength of 600nm after growing the *E.coli* bacteria. The

OD_{600} value of an *E.coli* suspension has been demonstrated to relate to the number of colony-forming units (CFU) per mL of that solution [7], [95], allowing for accurate quantification of the amount of bacteria present in the solution when performing any future antibacterial experiments.

2.4.12.2. Bacterial growth

E. coli (strain: BL21 (DE3) with ampR) was used as the bacterial model for all the experiments. An Eppendorf tube containing *E. coli* bacteria stored in a liquid nitrogen freezer was stored in a -20 ℃ freezer overnight. One hour before growing the bacteria, the Eppendorf tube was removed to thaw at room temperature. This gradual increase in temperature was necessary in order to avoid death by quick temperature change shock. *E. coli* was subsequently grown overnight in 10mL of LB broth in a 37 ℃ incubator while shaking at 270rpm. The rigorous shaking is needed so the bacteria does not clump together, cutting off the source of nutrients of bacteria inside the mass and leading to loss of cell viability. The next day, an aliquot (1:100 dilution) of the grown bacteria was removed, dispersed in 10mL of broth, and grown to the required optical density (as measured at 600nm). This was done in order to minimize the number of dead bacteria present in the final bacterial suspension used in the experiment.

2.4.12.3. Minimum Inhibitory Concentration

In order to measure the minimum concentration of the hydrazide-functionalized chitosan precursor polymer that is effective in inhibiting the growth of bacteria, a minimum inhibitory concentration (MIC) qualitative test was employed. Initially, *E.coli* was grown to an OD_{600} of 0.6 ($4.8x10^8$ CFU/mL), with serial dilutions

used to reach a final dilution of 10^4 CFU/mL. The hydrazide functionalized chitosan precursor polymer was diluted from 20mg/mL (2 wt/v%) to 0.05 mg/L (0.005%), again using serial dilutions, after which 100μL of each dilution concentration solution was loaded (three repeats per concentration) in a polystyrene 96-well plate. 50μL of the 10^4 CFU/mL bacterial suspension was subsequently added to each well plate and mixed with the polymer solutions. Controls of bacteria only, broth only, and hydrogel only were also added. The multiwell plate was shaken for one hour and then left in the incubator for 24 hours at 37 ℃. The MIC was reported as the lowest concentration where no bacterial growth was seen (i.e. at which the solutions remained clear).

2.4.12.4. LIVE/DEAD assay

The interfacial antibacterial properties of the chitosan-POEGMA hydrogels were assessed using a LIVE/DEAD assay. *E. coli* bacteria was grown overnight, after which a 1:100 dilution was performed up to a total volume of 5mL. This suspension was grown to OD_{600}=0.6 and centrifuged at 14,000 rpm for 5 minutes at 4 ℃. The supernatant was removed, and the pellet was then dispersed in sterilized Milli-Q water. The centrifugation step was repeated to ensure complete removal of the LB broth, as it interferes with the fluorescence imaging. The pellet was then suspended in 10mL PBS, and the OD_{600} was adjusted to a total concentration of ~10^9 CFU/mL by dilution according to the calibrated OD_{600} values.

Trial and error experimentation with different CFU/mL concentrations was used to optimize the concentration that gave the best images; bacterial concentrations ranging from 10^9 to 10^4 CFU/mL were imaged in both Milli-Q water and ethanol after adding the dye (green and red fluorescence) for this purpose. The hydrogels (0.9cm diameter, 0.2cm depth) were cross-linked and placed in a polystyrene 12-well plate,

after which 40μL of the bacterial suspension was added to fully cover the hydrogel surface and give a total count of $4x10^7$ CFUs per well. The gels were incubated for one hour before adding the dye. The dye solution was prepared by adding 1.5μL of both SYTO9 and propidium iodide to 1mL of sterilized Milli-Q water. A 1:1 volumetric ratio was used when adding the dye. After one hour of incubation, the hydrogels were washed off and the dye was added to both the wash solution and the surface of the hydrogel. Both samples were kept in the dark at room temperature for 30 minutes before imaging via confocal spectroscopy (LSM 510, Zeiss, Germany), using a x20 objective with ~645nm (for the SYTO9 green stained bacteria) and ~528nm (for propidium iodide red stained bacteria) measurement wavelengths.

2.4.12.5. Macro dilution method

In order to identify the presence of any leachates from the hydrogel (particularly degraded or uncross-linked chitosan), a macro dilution method was employed. The hydrogels were submerged inside the bacterial suspension and the OD_{600} of the bacterial suspension was measured (using UV-VIS at 600nm wavelength) before and after 24 hours of incubation. The hydrogels were first presoaked after gelation in sterilized PBS for an hour, wicked off, and added to 2mL of 10^4 CFU/mL of bacterial suspension in scintillation vials, the standard seed concentration that enables differentiation of results after 24 hours of subsequent incubation (over which time the bacterial concentration typically increases by 4-5 orders of magnitude). Vials with only bacterial suspension, broth, and hydrogels in broth only were used as controls.

2.4.12.6. Zone of inhibition

The leaching capability of the hydrogels was also assessed using a zone of inhibition experiment. A pre-formed hydrogel disk (1.27cm diameter, 0.2cm depth) was added to the center of an agar plate inoculated with 20μL of a 10^8 *E.coli* suspension, inverted, sealed, and left in the incubator at 37 ℃ for 24 hours. If the gel leaches anti-bacterial components, a circular zone around the gel can be observed where no bacteria is grown on the agar. The diameter of this zone (if present) was measured using a ruler or a caliper. Note that this method is not necessarily quantitative, as the measured diameter also depends on the diffusion rate of the antibacterial polymer into the agar; as such, the presence of an inhibition zone merely indicates polymer release from the hydrogel.

2.4.13. Cell viability

2.4.13.1. *In vitro* polymer cytotoxicity

The cytotoxicity of the chitosan and POEGMA precursor solutions to mammalian cells was assessed using a colorimetric resazurin (7-hydroxy-3H-phenoxazin-3-one 10-oxide) assay and 3T3 mouse fibroblasts as the test cells. Resazurin is an oxidation-reduction indicator, relating the fluorescence intensity to the aerobic respiration of viable cells present in the sample. The uptake of oxygen irreversibly reduces its colour from blue-purple to pink [100].

3T3 fibroblast cells were plated in a polystyrene 96-well plate at a density of 10,000 cells per well, with an appropriate volume of media added (depending on initial cell concentration) to each well to achieve a total volume of 150 μL. Cells were left to adhere for 24 hours, after which a 17μL aliquot of polymer solution, prepared

from a 10mg/mL stock polymer solution (in PBS) diluted appropriately such that the final concentration of the polymer inside the wells was 200, 400, 600, 800, or 1000 μg/mL, was added. After a 24-hour incubation period, 30 μL of a 40mg/mL resazurin sodium salt solution in PBS was added to each well, covered to prevent photobleaching, and left for four hours in an incubator. Immediately afterward, the fluorescence of each well was measured at a wavelength of 530nm using the multilabel plate reader (1420 Victor 3, Perkin Elmer Life Sciences, USA). The percentage cell viabilities are reported relative to the cell-only control as well as a media-only control as per Equation 2-7:

$$\%\ \text{cell viability} = \frac{\text{Absorbance}_{\text{normalized polymer solution}}}{\text{Absorbance}_{\text{normalized positive control}}} \qquad \text{Equation 2-7}$$

Four replicates for each polymer concentration were performed, with the error bars representing the standard deviation of the replicates of each sample concentration.

2.4.13.2. Hydrogel cell adhesion

Cell adhesion on the hydrogel surfaces was characterized using 3T3 fibroblast cells. Initially, the hydrogels were formed by injected in silicone molds matching the dimensions of the wells of a 24-well plate. The hydrogels were removed from the molds and placed in a 24 well plate with 1 mL of PBS and allowed to equilibrate in an incubator at 37 ℃ for 24 hours. Cells with a density of 10,000 cells/well were added to the surface of the hydrogels and incubated for 24 hours, after which the wells were washed several times to remove any non-adhered cells. The surface of each hydrogel was then stained with 30 μL of LIVE/DEAD assay solution (mammalian cells, L-

3224) that was prepared by adding 20μL of ethidium homodimer-1 and 5μL of calcein-AM to 10mL of sterilized PBS. The measurement wavelengths used were ~645nm (for the calcein-AM green stained cells) and ~528nm (for ethidium homodimer-1 red stained cells). Four replicates for each polymer concentration were performed, with the error bars representing the standard deviation of the replicates of each sample concentration.

3. Results

3.1. Quantification of the substitution and functionalization reactions

3.1.1. Chitosan

Potentiometric-conductometric titration was carried out in order to characterize the polymers after both carboxylation and hydrazide functionalization reactions. Titration was conducted for each new batch of chitosan polymer to ensure no significant batch-to-batch variation, particularly problematic for natural polymers such as chitosan; the titration results shown below are for one specific batch that is representative of polymer used for each experiment reported.

For comparison and calculations of the degree of substitution as well as degree of deacetylation and any other relevant calculations, a titration on unmodified chitosan was carried out. Two maxima appear in the dpH/dV result, a representative graph of which is given in Figure 3-1.

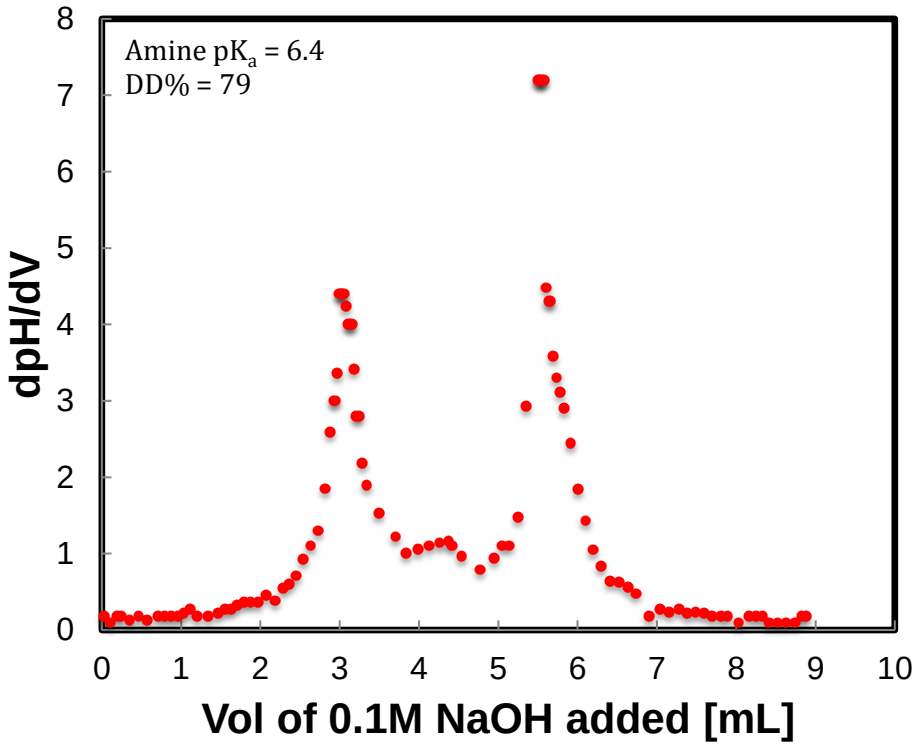

Figure 3-1: Unmodified chitosan potentiometric titration

3.1.1.1. Degree of carboxyl substitution

After performing a titration on the carboxylated chitosan solution, three maxima appear in the dpH/dV result, a representative graph of which is given in Figure 3-2.

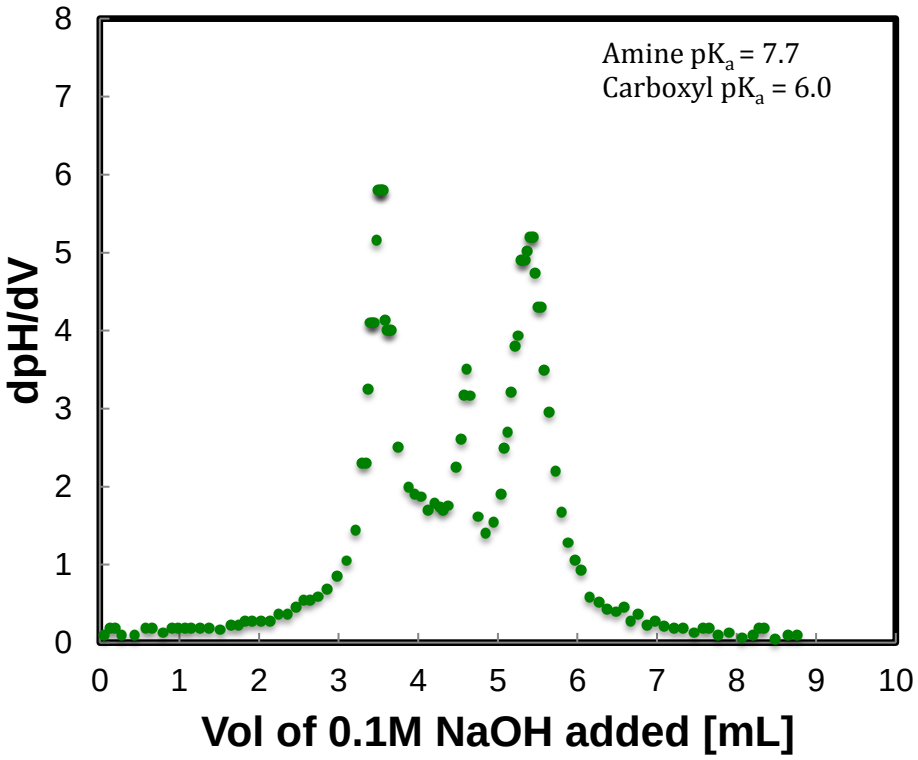

Figure 3-2: Carboxymethyl chitosan potentiometric titration

The degree of substitution of carboxyl groups is calculated based on partial substitution of both hydroxyl and amine groups to carboxyl groups. It does not infer any conclusions in regards to the specificity of the carboxylation, which will be addressed in the content of free amine section. This result is indicative of the presence of two different functional groups in the carboxymethylated chitosan product: -COOH from the carboxylation reaction at lower NaOH amounts (corresponding to lower pK_a values and quantified by the volume between the first and second maxima [64]) and $–NH_2$ from native chitosan at higher NaOH amounts (corresponding to higher pK_a values and quantified by the volume between the second and third maxima). The pK_a values of each functional group (-COOH and $–NH_2$) were calculated using the

potentiometric curves (Appendix A1) as well as the ionization vs. pH curves (Appendix A2).

The first, second, and third peaks in the first derivative plots are attributed to the endpoints associated with titration of excess hydrochloric acid, the carboxyl groups, and the amine groups, respectively, in the solution. These curves were analyzed as follows to extract the functionalization data:

1. The difference in volume between the second and first peaks was calculated.
2. The degree of substitution (DS) was calculated via the equation

$$DS_{\text{carboxyl goups}} = \frac{161 \times A}{W_{\text{carboxyl groups}} - 58 \times A}$$

Equation 3-1

where $A = V_{NaOH} \times C_{NaOH}$

V[=]L and C[=] mol/L of 0.1 M NaOH used as the titrant

W = mass of carboxmethylated chitosan sample in grams
161 = MW of glucosamine repeat unit
58 = MW of carboxymethyl group added as a result of derivatization

Based on this analysis, the degree of carboxyl substitution of the carboxymethylated chitosan is equal to 0.41.

3.1.1.2. Weight percentage of carboxylic groups

The number of moles of sodium hydroxide used to neutralize the carboxymethyl groups during titration (difference between second and first peaks) was used to estimate the mass of carboxymethyl groups titrated and thus the wt% of –COOH in the modified chitosan. This calculation was pursued since it is the standard metric used in the literature for quantifying the effectiveness of a carboxymethylation of chitosan [64], thus allowing for benchmarking of this result with previous work.

Wt% carboxylic group = mass of carboxymethyl groups titrated (g)/ mass of polymer (g) = 12.9%

3.1.1.3. Content of free amine

Following hydrazide modification of the available –COOH groups, only two maxima appear in the titration curve, as indicated in Figure 3-3.

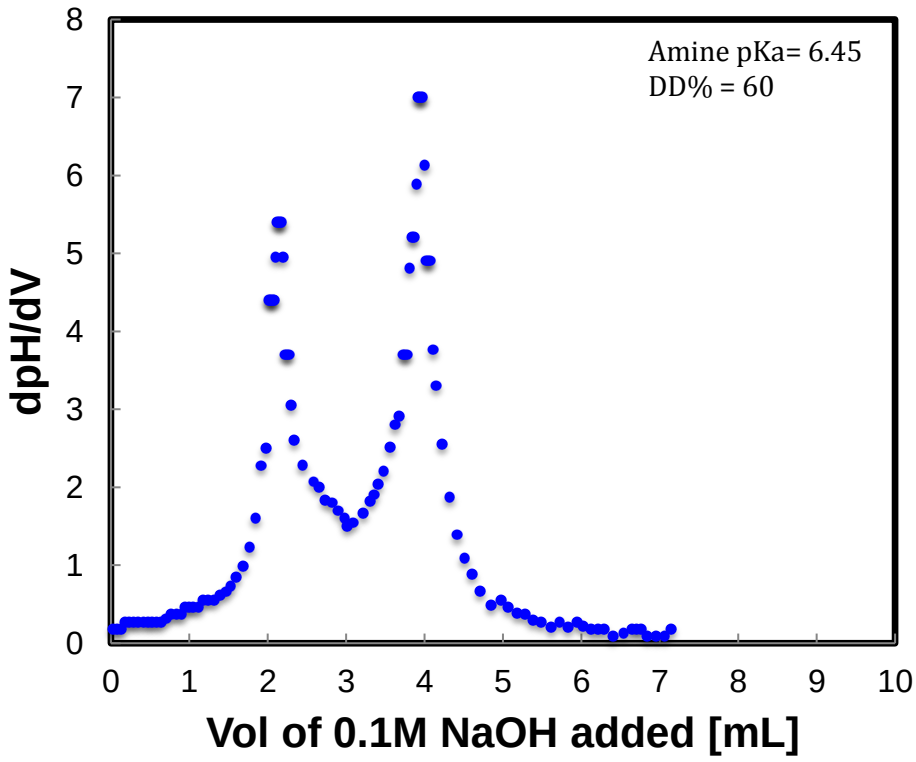

Figure 3-3: Hydrazide chitosan potentiometric titration

Given that our previous work has indicated nearly quantitative conversion of free carboxyl groups to hydrazide groups using this adipic acid dihydrazide/carbodiimide chemistry [54], and the titratable functional groups have a higher pK_a indicative of a base instead of an acid, this result suggests that free –COOH groups have been quantitatively converted to hydrazide groups and the signal from this titration result is attributable to residual amine groups (note that hydrazide groups

have a low pK_a in the 2.5-3.5 range and thus are not detected in this titration result) [101]. The free amine content, more commonly referred to as the degree of deacytelation (DD%) of chitosan, can thus be estimated, enabling comparison with the amount of amine prior to reaction to confirm the type of substitution that was conducted.

The slight difference in the pK_a of the amine groups could be due to the presence of extra functional groups (carboxyl or hydrazide groups) that might inductively shift the pK_a to slightly higher or lower values based on their respective electron withdrawing and electron donating properties.

On this basis, the number of moles of amine groups in a known mass of chitosan is:

$$A = V_{NaOH} \times C_{NaOH} = (V_2 - V_1) \times C_{NaOH}$$

where (V_2 - V_1) is the volume difference between peaks 1 and 2 for the unmodified and hydrazide functionalized chitosan titrations.

$$DD\% = \frac{161 \times A}{W} \text{ x } 100$$

Equation 3-2

$A = V_{NaOH} \times C_{NaOH}$ where V[=]L and C[=] mol/L (0.1 M NaOH used for titration)
$W =$ mass of sample in grams

Based on this analysis, the content of free amine of the hydrazide functionalized chitosan was equal to 60% while that of the unmodified chitosan was 79% (see the unmodified chitosan potentiometric curve in Appendix A1). Therefore, based on this result, 21% of primary hydroxyls and 19% of amines in the original chitosan are functionalized with carboxylmethyl groups. This leaves 81% of the original amines on

chitosan free, essential to promote the bioadhesive and antibacterial properties desired in the later results.

3.1.1.4. Hydrazide groups per chain of polymer

The number of hydrazide groups per chitosan chain was calculated based on the difference of the total titration signal between the carboxylated polymer and the hydrazide-functionalized polymer (loss of 1 mol –COOH = gain of 1 mol hydrazide, assuming no cross-linking with the adipic acid dihydrazide functionalization). The degree of hydrazide functionalization, based on the complete carboxyl conversion to hydrazide groups indicated by the titration result (Fig. 3-3), can thus be estimated using Equation 3-3:

$$\text{Hydrazide groups/chain} = \frac{\mathrm{DS}_{\mathrm{carboxylated}} \times 120{,}000}{161}$$

Equation 3-3

161 = MW of glucosamine
120kDa = average MW of chitosan polymer

On this basis, 305 hydrazide groups per chain of chitosan (assuming a molecular weight value of 120 kDa) are present, corresponding to 1 hydrazide group per 2.5 repeat units.

Overall, the titration of the three chitosan forms (unmodified, carboxylated, and hydrazide functionalized) can give information on the degree of functionalization, the location of functional group substitution, and the overall number of functional groups per chain of chitosan. The carboxylation reaction resulted an overall carboxylic acid weight percentage within chitosan of 12.9%, consistent with the typical 10-15% range previously reported in the literature [102]. In addition, results indicate that,

despite the amine being the stronger nucleophile, more of the carboxymethylation occurs on the hydroxyl groups, desirable to maintain the beneficial bioadhesive properties introduced via the amine groups. Furthermore, the degree of hydrazide functionalization achieved overall (1 hydrazide group per 2.5 repeat units in the chitosan backbone) is within the range previously identified in our lab for effective gelation of carbohydrates of similar molecular weights using hydrazone chemistry with lower molecular weight synthetic polymers such as POEGMA [101].

3.1.1.5. Chitosan batch-to-batch variation

As previously mentioned, natural polymers like chitosan tend to have high batch-to-batch variations that may lead to inconsistencies in the end product synthesized. This problem was faced during the synthesis stage of the experimentations, mandating the screening (through titration as well as solubility assays) of each synthesized chitosan batch to to achieve reproducible hydrogel properties and minimize any batch-to-batch variation. Batches were selected for further functionalization (hydrazide substitution) if the carboxyl attachment is between 40 and 50% with a maximum amine substitution of 20% and if the polymer does not dissolve completely in PBS at the concentrations of 1, 1.5, and 2w/v%. The key differentiation between batches appears to be the degree of substitution of the amines with carboxyl groups; too much substitution affects chitosan's inherent properties but too little results in a polymer that is not fully soluble at physiological pH. Table 3-1 shows the overall properties of the three main chitosan batch types usually synthesized, the first two of which were always discarded and the last of which was used for all other experiments conducted.

Table 3-1: Example of three different batches of carboxylated chitosan synthesized

Chitosan	Carboxyl substitution on polymer chain (mol%)	Substitution of amine (mol%)	Remarks
Batch 1	28	25	Not enough for functional group attachment, amine % too high
Batch 2	49	25	Amine substitution too high
Batch 3	41	19	Targeted substitution

3.1.2. POEGMA characterization

The properties of the aldehyde-functionalized POEGMA polymer used for all hydrogels reported as well as the cationic POEGMA polymer used to evaluate the effect of chitosan specifically on the gel properties are given in Table 3-2.

Table 3-2: Characterization of POEGMA precursor polymers: (a) M_n and PDI based on gel permeation chromatography in DMF; (b) mol% functionalization based on ^1H NMR; (c) percentage of charged monomer based on potentiometric titration

Polymer	M_n (kg/mol)[a]	PDI[a]	Functionalization (mol%)[b]	Charge (mol%)[c]
$PO_{10}A_{30}$	21.6	2.1	30	NA
$+PO_{10}H_{29}$	41.3	2.4	29	25

DMF gel permeation chromatography indicated that the M_n of the aldehyde polymer ($PO_{10}A_{30}$) is 21.6 kg/mol (PDI 2.1) while that of the cationic hydrazide polymer is 41.3 kg/mol (PDI 2.4). The high polydispersity is attributed to the free radical polymerization technique (performed using a chain transfer agent as opposed to a living polymerization to control molecular weight) and is a typical polydispersity of the POEGMA polymers synthesized this way in our lab. The cationic charge density

of $+PO_{10}H_{29}$ was quantified as 25 mol% via potentiometric titration, comparable to the theoretical mol% of 28.5.

^{1}H NMR was run on $PO_{10}A_{30}$ in chloroform (Figure 3-4) and $+PO_{10}H_{29}$ in dimethyl sulfoxide (Figure 3.5) before and after functionalization of the aldehyde and hydrazide groups, respectively, to characterize the composition of the polymers.

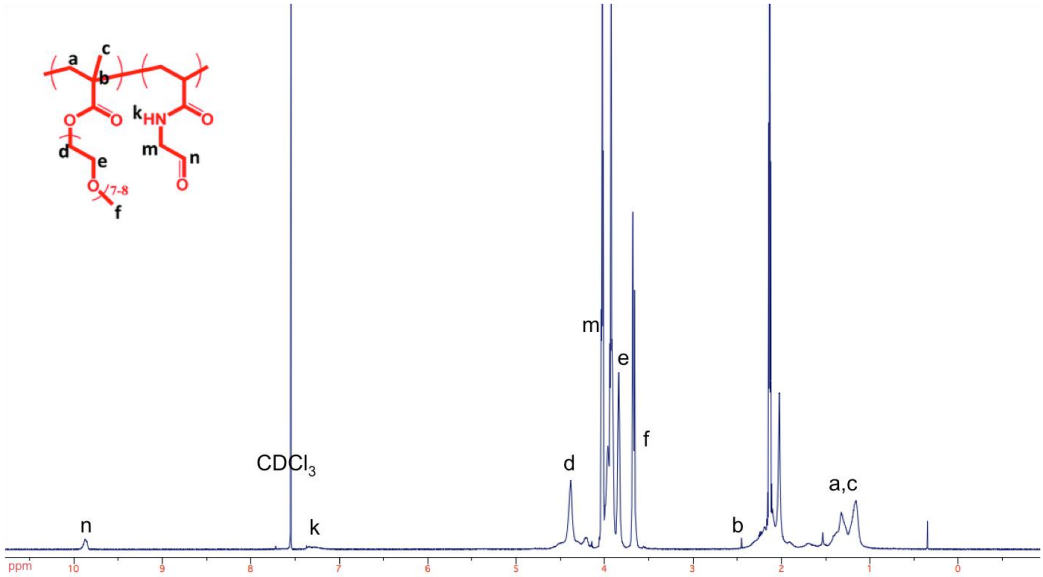

Figure 3-4: ^{1}H-NMR (600 MHz) analysis on $PO_{10}A_{30}$ using $CDCl_3$ as the solvent

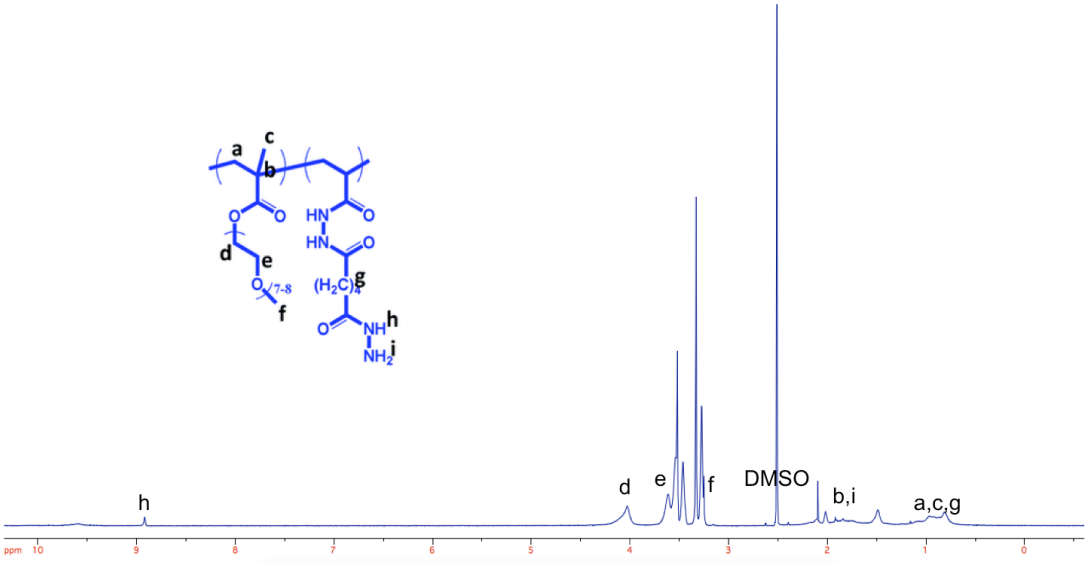

Figure 3-5: ^{1}H-NMR (600 MHz) analysis on $+PO_{10}H_{29}$ using DMSO as the solvent

Characteristic POEGMA signals are found in the spectra of both aldehyde and hydrazide functionalized POEGMA (δ = 0.9-1 ppm (a,c), 2 ppm (b), 4 ppm (d), 3.5 ppm (e), and 3.2 ppm (f), see peak assignments in Figures 3-4 and 3-5). Aldehyde groups are found at δ = 9.6 ppm (n) in Figure 3-4, while hydrazide groups are found at δ = 8.9 and 2 ppm (h, i) in Figure 3-5. Based on the integration of these peaks, Table 3-2 shows the mol% functionalization of each POEGMA polymer. The degree of aldehyde functionalization was calculated based on the integrals of the signals at δ = 9.6 ppm (CHO) and δ = 3.2 (O-CH_3 in the OEGMA repeat unit) in Figure 3-4; the degree of hydrazide functionalization was calculated based on the integrals of the signals at δ = 8.9 (NH-NH_2) and δ = 3.2 (O-CH_3 in the OEGMA repeat unit) in Figure 3-5.

3.2. Hydrogel design

A matrix of different combinations of the precursor polymers developed was constructed for property testing. Chitosan is a highly cationic polymer that is viscous, and increasing the hydrazide functionalized chitosan concentration to above 2wt/v% resulted in a significant increase in viscosity that would render the solution not easily injectable or sprayable. Also, higher chitosan concentrations promote inter- and intra-molecular interactions between the functional groups on chitosan and subsequent self-crosslinking of the polymer. As a result, studies were conducted on hydrogels prepared with chitosan concentrations of 1%, 1.5%, and 2% (all on a weight by volume basis), with the lower end selected based on the requirement for sufficient

cross-linking for hydrogel formation and the upper end based on rheological limitations. PBS was used to prepare all polymer solutions.

Initially, medium molecular weight (MMW, ~240kDa) non-modified chitosan was used to synthesize the hydrazide-functionalized chitosan; however it posed challenges in terms of viscosity, even at 2wt%, as well as ease of use during synthesis. In addition, hydrazide functionalized MMW chitosan precipitated out of PBS after approximately one month, indicating poor storage ability. Instead, low molecular weight (LMW, ~120kDa) chitosan was used given that it was easier to handle, resulted in lesser variation between batches, had a lower viscosity at any concentration, and (following hydrazide functionalization) remained stable in solution over at least three months. Note that the molecular weight of even the LMW chitosan is still high enough to impart the desired properties of the gel, bioadhesion in particular.

POEGMA polymers were used primarily at concentrations of 20wt%, due to the significantly lower molecular weights (<20 kDa) and thus lower viscosities of the starting polymers. A cationic hydrazide-functionalized POEGMA polymer with superior cationic charge density compared to hydrazide functionalized chitosan at 2wt% ($+PO_{10}H_{29}$) was alternately used to form a gelling pair with aldehyde-POEGMA to better understand the effect of the chitosan itself, without its charge contribution, on the gel properties.

All these hydrogels were easily extruded through the double barrel syringe assembly with minimal injection force, ideal for practical use. Furthermore, the ability to spray the hydrogels to form a thin homogenous layer was investigated by connecting an intranasal mucosal atomization device (Wolfe Tory Medical, USA) to

the end of a double barrel syringe. Figure 3-6 shows the resulting spray distribution, with food coloring added to enable visualization of the sprayed hydrogel.

Figure 3-6: A sprayed thin layer of hydrogel using the double barrel syringe and atomizing spray device

This result confirms the ability to not only inject these hydrogels but also facilitating the ability for this system to be sprayed, highly advantageous for topical applications (particularly wound healing applications).

3.2.1. Aldehyde to hydrazide ratio

The number of hydrazide and aldehyde functional groups per 1mL of chitosan and POEGMA prepolymer solution was calculated using Equation 3-4 to determine the ratio between the hydrazide and aldehyde groups in the hydrogel following mixing of the two precursor polymers (the latter calculated using Equation 3-5):

$$\frac{\text{func groups}}{1\text{mL}} = \frac{\text{mass of polymer per 1 ml} \times \#\text{ functional groups per chain}}{\text{Avg MW of polymer (Da)}} \quad \text{Equation 3-4}$$

$$\text{Ratio} = \frac{\text{Aldehyde functional groups}}{\text{Hydrazide functional groups}} \quad \text{Equation 3-5}$$

The recipes used for the key hydrogels to be studied and the resulting aldehyde to hydrazide ratio of those recipes is provided in Table 3-3.

Table 3-3: Hydrogel design matrix including functional group ratio, mass and wt% of polymer in hydrogel network

Hydrogel (wt/v)%	**Aldehyde to Hydrazide ratio**	**Overall dry polymer mass per mL of hydrogel (mg)**	**Wt% of each polymer in hydrogel**
Chit-Hzd 1 %/$PO_{10}A_{30}$ 20%	9.0	210	5% Chit-Hzd, 95% $PO_{10}A_{30}$
Chit-Hzd 1.5%/$PO_{10}A_{30}$ 20%	6.0	215	7% Chit-Hzd, 93% $PO_{10}A_{30}$
Chit-Hzd 2%/$PO_{10}A_{30}$ 20%	4.5	220	9% Chit-Hzd, 91% $PO_{10}A_{30}$
$PO_{10}A_{30}$ 20%/+$PO_{10}H_{29}$ 20%	1.2	400	50% +$PO_{10}H_{29}$, 50% $PO_{10}A_{30}$

Of note, considering the potential for excess aldehydes present following gelation to form Schiff bases with amines in native tissue, higher aldehyde contents may lead to higher bioadhesion but also potentially higher inflammation; the range of hydrogels produced here would enable optimization of gel composition on this basis. Note that these ratios can also be adjusted to any desired number by mixing the viscous chitosan-hydrazide with the non-viscous cationic POEGMA polymers (or neutral hydrazide-POEGMA polymers) to increase the concentration of hydrazide groups in the final gel as desired using the idea of modularity developed in previous work from our lab [101]; however, for first-pass screening, the compositions above were used.

3.2.2. Charge density

Quantifying the charge density is important when making comparison between the measured polymers and the reference. Table 3-4 shows the lineal (moles charge/gram of dry polymer) and volumetric (moles charge/volume of precursor polymer solution) associated with the hydrazide polymer used to prepare each of the studied hydrogels, as determined via titration.

Table 3-4: Charge density values in each dry polymer and polymer precursor solution

Polymer (w/v)%	Charge density per g of dry polymer (mmol/g)	Charge density per mL of polymer solution (mmol/mL)
Chit-Hzd 1.0%	3.6	0.036
Chit-Hzd 1.5%	3.6	0.054
Chit-Hzd 2.0%	3.6	0.072
$+PO_{10}H_{29}$ 20%	1.6	0.320

Hydrogels prepared with different chitosan contents have systematically increasing volumetric charge densities, but the lineal spacing between those charges is the same since the same precursor Chit-Hzd polymer is used. In comparison, the $+PO_{10}H_{29}$ POEGMA polymer used as a reference has a lineal charge density of only roughly half of the Chit-Hzd polymer (since only ~25% of repeat units carry a cationic charge versus ~80% in chitosan); however, given that significantly higher concentrations of $+PO_{10}H_{29}$ were used for gelation (20 wt% compared to a maximum of 2 wt% for chitosan), the net volumetric charge in the $+PO_{10}H_{29}$ control hydrogel is significantly (~4-fold) higher than even the most charged chitosan-based gel used. Thus, if only charge is important in driving bioadhesion, the $+PO_{10}H_{29}$ hydrogel should exhibit significantly stronger bioadhesion; this control thus allows for identification of the

role of chitosan itself on regulating the bioadhesive properties of the hydrogels. However, it should be noted that the cationic charge on chitosan and POEGMA is achieved using different types of amine groups; chitosan features a primary amine while POEGMA features a tertiary amine. The different nature of these two cationic groups may affect the actual cationic role in the bioadhesive/anti-microbial behaviour of the hydrogels. Primary amines have been shown to more effectively bind to bacterial cell membranes and disturb their abilities due to the complexation of the primary amines to the lipid's phosphate groups in the phospholipid bilayer through electrostatic forces and hydrogen bonding [103].

3.3. Gelation Kinetics

Hydrazide-functionalized chitosan was subsequently gelled with aldehyde-functionalized POEGMA using a double-barrel syringe to deliver and mix the precursor polymers. Table 3-5 shows the measured gelation times for all polymer pairs using the vial inversion test. All the polymer pairs gelled in <5 seconds, with gelation faster as the concentration of the polymers was increased and (a) the concentration of reactive functional groups and (b) the number of polymer chains available for cross-linking per unit volume are both increased.

Table 3-5: Gelation time of hydrogels

Hydrogel (wt/v)%	**Gelation time (s)**
Chit-Hzd 1.0%/$PO_{10}A_{30}$ 20%	< 5 seconds
Chit-Hzd 1.5%/$PO_{10}A_{30}$ 20%	< 5 seconds
Chit-Hzd 2.0%/$PO_{10}A_{30}$ 20%	< 5 seconds
+$PO_{10}H_{29}$ 20%/$PO_{10}A_{30}$ 20%	< 5 seconds

3.4. Transparency

Figure 3-6 shows the transmittances of the hydrogels over a wavelength range of 400-600 nm (visible range). All measured transmittance values for the chitosan-POEGMA hydrogels were >88% for the 2.5mm thick samples studied over the full visible range. For the cationic POEGMA-POEGMA gel, the transmittance measured was higher than 95% over the whole visible light range. Note that this thickness is much higher than what is required for a topical application, such that these results are significantly underestimating the actual transmittance values for a typical topical application thickness of <0.5mm (since absorbance is directly proportional to sample thickness according to Beer's law).

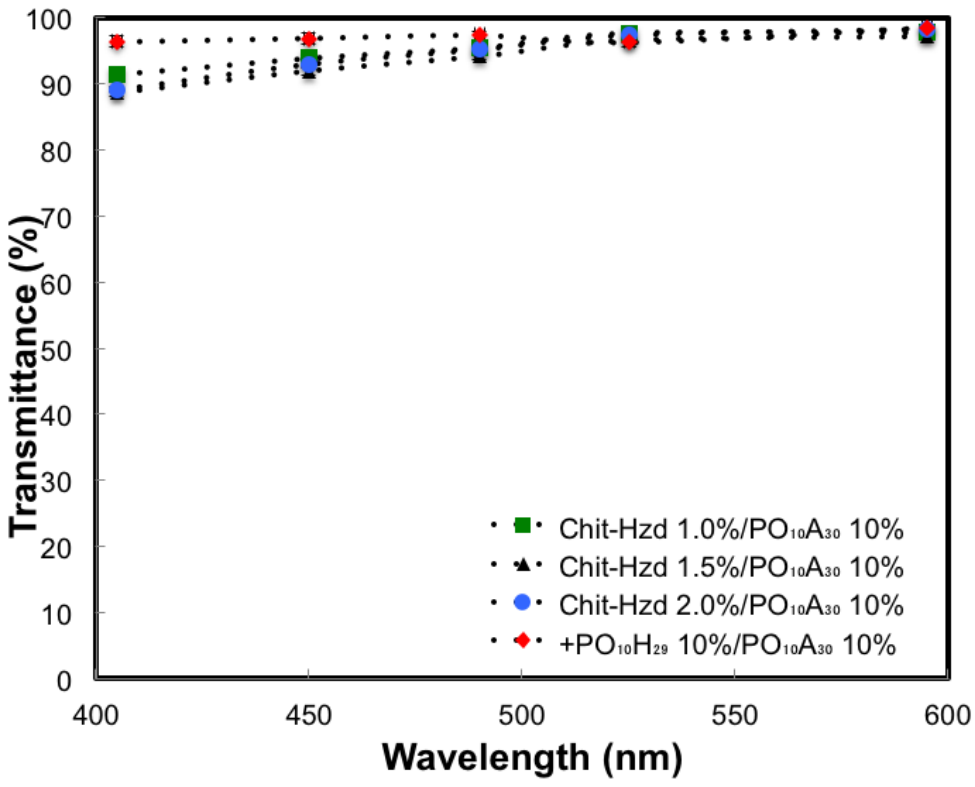

Figure 3-7: Transparency of hydrogels tested over the visible range (n=4)

3.5. Swelling and degradation kinetics

The swelling and degradation kinetics were characterized gravimetrically by measuring the change in mass over a time period where the hydrogel is submerged at a buffer of specific pH. Changes in hydrogel weight (representing a combination of swelling and degradation as a function of time) versus time were measured for hydrogels incubated at pH 4, 5.5, and 7.4 (using acetic acid-sodium acetate buffer for the lower pH values and phosphate buffered saline for pH 7.4), with all results normalized to the initial weight of each hydrogel. Figure 3-8 shows the swelling response of the hydrogels at pH 5.5, mimicking the pH of skin.

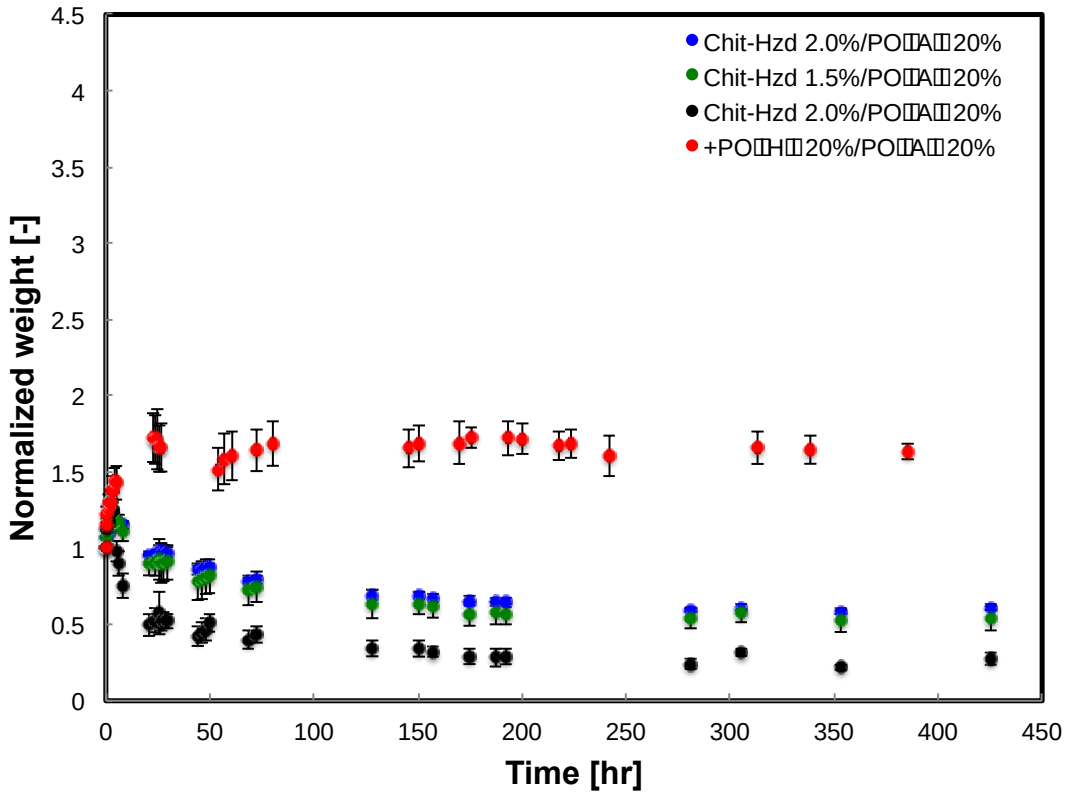

Figure 3-8: Swelling and degradation of POEGMA-POEGMA and chitosan-POEGMA hydrogels at pH 5.5 (n=4)

POEGMA-POEGMA hydrogels initially swell to ~1.7 times their initial mass then maintain their weight throughout the test period, indicative of slow degradation. In comparison, the chitosan hydrogels initially swelled but after relatively short times (<2 hours depending on the chitosan concentration) began to lose mass, indicative of gel degradation. Chit-Hzd 1.0%/$PO_{10}A_{30}$ 20% degraded the fastest, reaching a normalized weight of 0.5 within the first 21 hours, while Chit-Hzd 1.5%/$PO_{10}A_{30}$ 20% and Chit-Hzd 2.0%/$PO_{10}A_{30}$ 20% maintained a normalized weight of 0.89 and 0.95 respectively within the first 21 hours. This is attributed to the decrease in crosslinking density as the chitosan wt% decreases, as lower number of hydrazide functional groups are available (thus enabling faster degradation of the gel properties as a result of a similar degree of hydrolysis). Higher weight percentages of chitosan result in hydrogels that degrade slower, maintaining approximately half of their initial mass 12 days into the experiment.

Swelling results at pH 4 (mimicking vaginal pH), shown in Figure 3-9, show a slightly different trend.

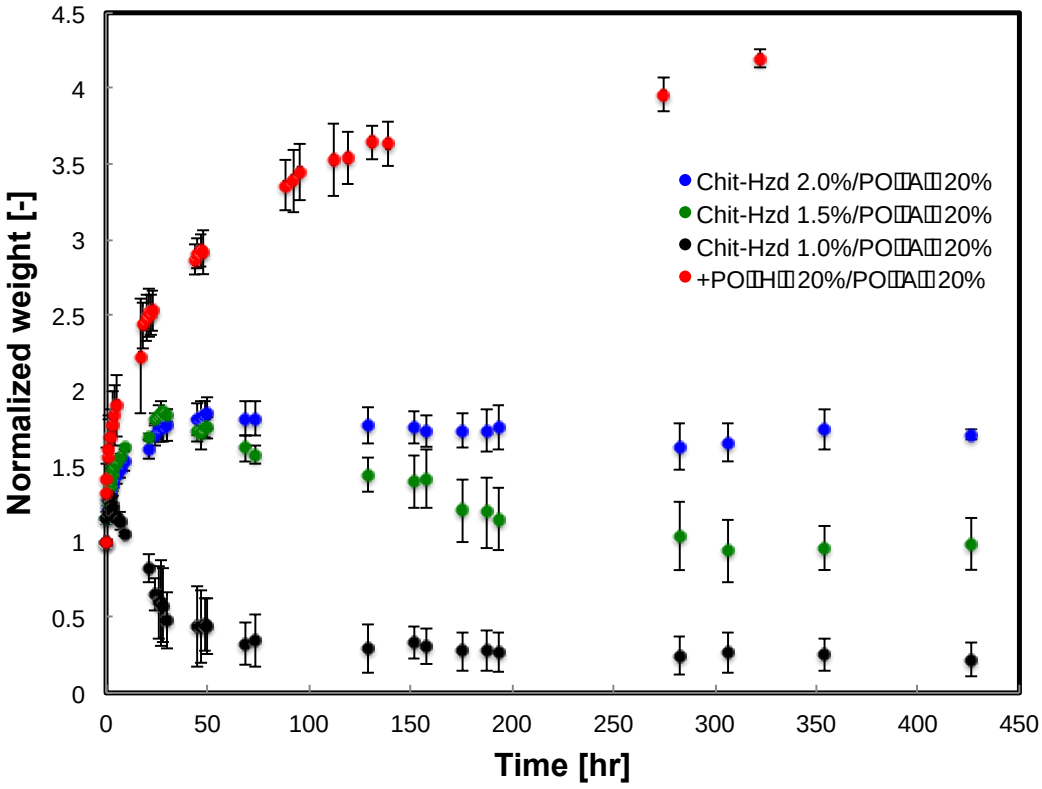

Figure 3-9: Swelling and degradation of POEGMA-POEGMA and chitosan-POEGMA hydrogels at pH 4 (n=4)

The POEGMA-POEGMA hydrogels again kept swelling throughout the whole test period (exceeding a normalized weight of 4 by day 12), Chit-Hzd 1.5%/$PO_{10}A_{30}$ 20% and Chit-Hzd 2.0%/$PO_{10}A_{30}$ 20% swelled initially to ~1.85 times their initial weight within 28 hours followed by slow degradation (with degradation faster at lower chitosan contents), and Chit-Hzd 1.0%/$PO_{10}A_{30}$ 20% swelled slightly over the first couple of hours followed by degradation to 0.58 of its normalized weight within 28 hours. All three Chit-Hzd data plots show the same trend: as the chitosan wt% decreases, the duration and magnitude of the initial swelling is reduced and degradation occurs faster.

Interestingly, the measured degradation times of the chitosan-POEGMA hydrogels are slightly longer at pH 4 relative to pH 5.5 despite the acid-labile nature of the hydrazone cross-link. This may be related to (1) the lower degree of initial hydrogel swelling observed at pH 4 relative to pH 5.5, resulting in slower diffusion of the aqueous buffer into the hydrogel or (2) protonation of at least some of the residual hydrazide residues at pH 4 that poses an electrostatic repulsion to the transport of H^+ ions inside the hydrogel.

The swelling results at normal physiological pH of 7.4 are shown in Figure 3-10.

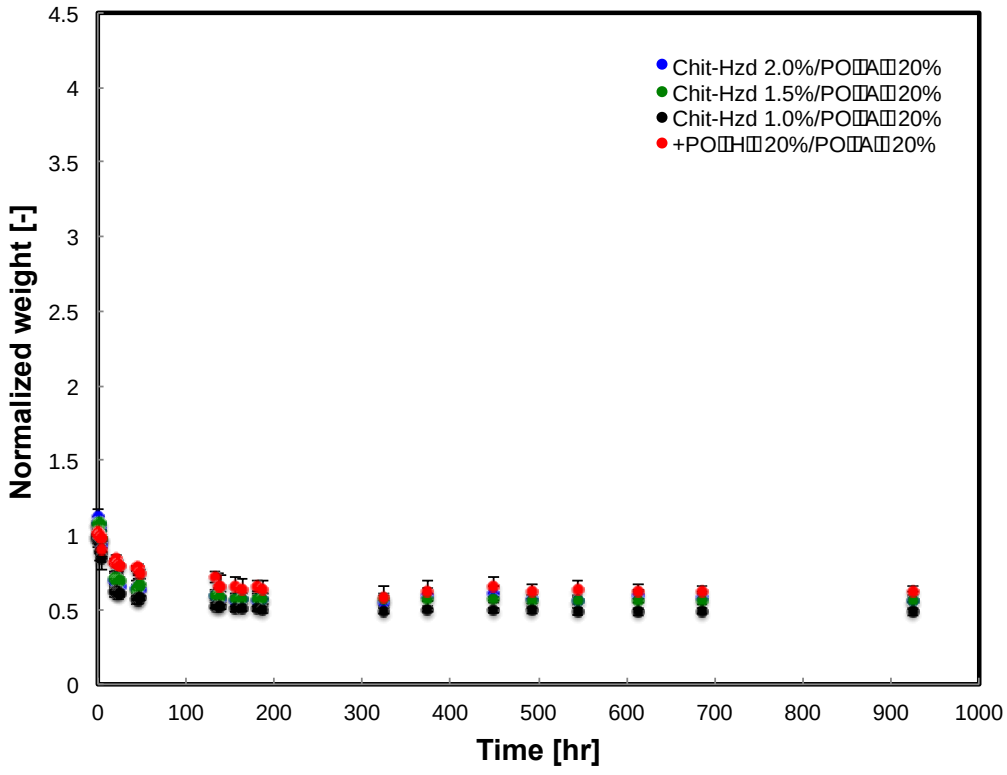

Figure 3-10: Swelling and degradation of POEGMA-POEGMA and chitosan-POEGMA hydrogels at pH 7.4 (n=4)

The swelling responses of each hydrogel at pH 7.4 are similar in that each gel swells slightly once incubated at 37°C followed by a collapse and a plateau at >100 hours out to the end of the test. $+PO_{10}H_{29}$ has the highest normalized weight over the plateau region followed by Chit-Hzd 2.0%/$PO_{10}A_{30}$ 20%, Chit-Hzd 1.5%/$PO_{10}A_{30}$ 20%, and finally Chit-Hzd 1.0%/$PO_{10}A_{30}$ 20%, directly correlated with the projected cross-link densities of each gel based on the aldehyde:hydrazide ratio. This result can be attributed to the phase transition properties of the $PO_{10}A_{30}$ polymer, which is thermosensitive (lower critical solution temperature ~53.6°C); the significantly lower charge density of chitosan at pH 7.4 relative to the acidic pH values tested allows the overall gel to demonstrate a phase transition whereas the higher charge densities at lower pH values combat this phase transition. In addition, the hydrolysis of the hydrazone cross-links is acid-catalyzed and thus would be quite slow at neutral pH. Of note, the Chit-Hzd 1.0%/$PO_{10}A_{30}$ 20% gels start losing their initial conformed shape and spread on the insert relatively quickly, potentially trapping water not part of the hydrogel matrix in the insert; this would result in an overestimation of the results for this hydrogel.

3.6. Water retention and loss of the hydrogels

For potential topical applications, the drying rate of the hydrogels under ambient humidity and temperature conditions is essential to understand. Figure 3-11 (a to d) shows the drying rate of the hydrogels tested at different relative humidity values, using a controlled humidity chamber for testing as well as the benchtop. All the humidity tests were done in multiples of three or four, with all weights (of actual gel without the insert) normalized to one (i.e. mass changes are expressed with respect to

the initial gel weights). Note that, based on the gel compositions tested, a "dry" sample for each of the recipes would correspond to the following normalized weights (denoted by a dashed line on each graph for reference):

1) Chit-Hzd 1.0%/$PO_{10}A_{30}$ 20%: 0.105 normalized weight
2) Chit-Hzd 1.5%/$PO_{10}A_{30}$ 20%: 0.1075 normalized weight
3) Chit-Hzd 2.0%/$PO_{10}A_{30}$ 20%: 0.11 normalized weight
4) +$PO_{10}H_{29}$ 20%/$PO_{10}A_{30}$ 20%: 0.2 normalized weight

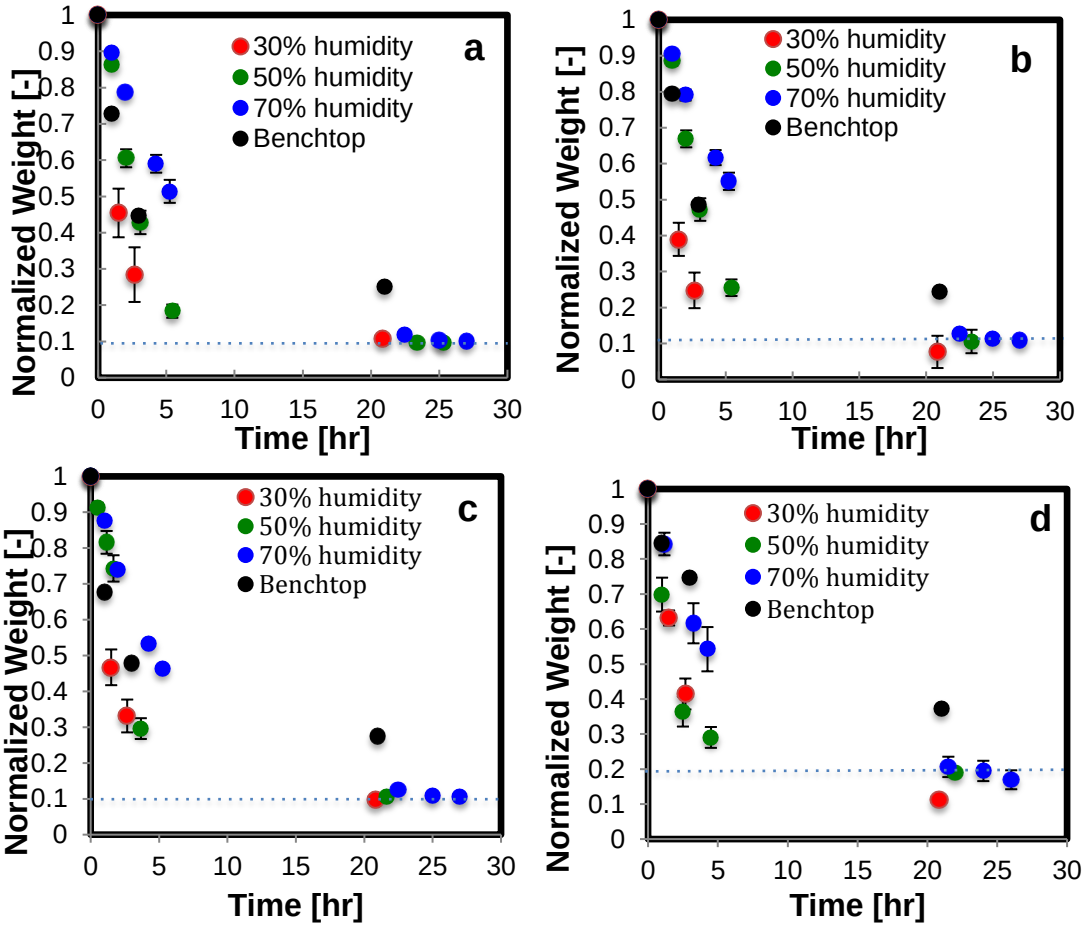

Figure 3-11: Evaporation-based mass loss of hydrogels inside a controlled humidity chamber and benchtop for (a) Chit-Hzd 1.0%/$PO_{10}A_{30}$ 20%, (b) Chit-Hzd 1.5%/$PO_{10}A_{30}$ 20%, (c) Chit-Hzd 2.0%/$PO_{10}A_{30}$ 20% and (d) +$PO_{10}H_{29}$ 20%/$PO_{10}A_{30}$ 20% (n=4)

At a relative humidity of 30%, the evaporation rate is rapid and all hydrogels reach 30% of their initial gel weight by the third hour. In comparison, hydrogels exposed to 50% relative humidity dropped to 30% of their normalized weight within the first 5 hours while at 75% relative humidity evaporation is again slower, with normalized weights of ~0.4 achieved only after six hours. Thus, not surprisingly, gels retained water for longer periods of time at higher relative humidities. However, relative to the benchtop evaporation experiment (~50% humidity on the day of the test), all the evaporation rates measured were significantly higher; all samples were fully dry within 24 hours for all experiments performed in the controlled humidity chamber, while under ambient conditions the normalized weights of the hydrogels remained in the range from 0.37 to 0.25, indicating significant water retention. We believe this observation is related to the significant air flow present in the humidity chamber, which enhances convective mass transfer versus normal, ambient conditions present in the benchtop test. The POEGMA-only hydrogels retained water somewhat shorter than the chitosan-containing hydrogels, when accounting for the dry hydrogel mass, although this effect was relatively small. Overall, for topical applications, the results suggest that water retention to some degree is possible over at least the targeted one-day period, depending on the relative humidity and convective conditions used in the test.

3.7. Rheological characterization

The storage modulus of the hydrogels, essential to understand for applying these hydrogels in potential wound healing or bioadhesive applications, is shown in

Figure 3-12 for each of the hydrogels tested as a function of frequency and plotted in terms of the average modulus value over the full frequency plateau in Table 3-6.

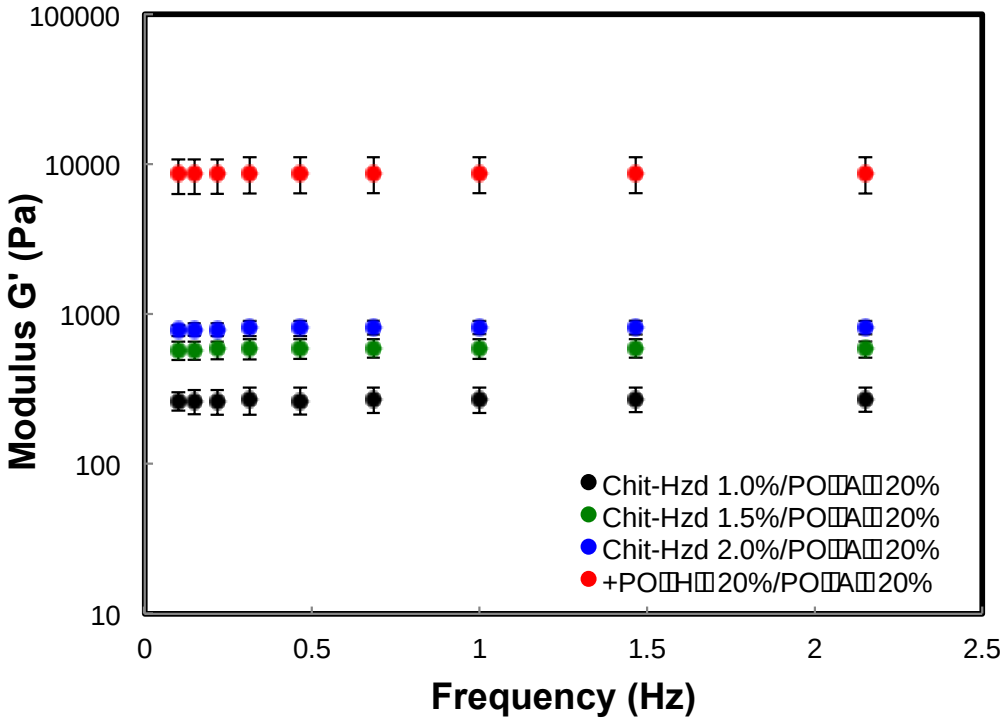

Figure 3-12: Elastic modulus (G') of all four hydrogels (n=4)

Table 3-6: Average elastic modulus for each hydrogel over the plateau region

Hydrogel (w/v)%	Average elastic modulus (Pa)
Chit-Hzd 1.0%/$PO_{10}A_{30}$ 20%	270 ± 50
Chit-Hzd 1.5%/ $PO_{10}A_{30}$ 20%	585 ± 84
Chit-Hzd 2.0%/ $PO_{10}A_{30}$ 20%	803 ± 82
+$PO_{10}H_{29}$ 20%/ $PO_{10}A_{30}$ 20%	8680 ± 2310

The POEGMA-POEGMA hydrogel has a significantly higher elastic modulus than the chitosan-POEGMA hydrogels; the +$PO_{10}H_{29}$ 20%/$PO_{10}A_{30}$ 20% hydrogel has an average elastic modulus of 8.7kPa, while the chitosan hydrogels are all lower than 1kPa (with higher moduli as the chitosan weight percentage increases). This result

was predicted based on the calculated aldehyde:hydrazide ratios of each hydrogel (Table 3-2), higher residual aldehydes results in fewer potential cross-links and thus a lower modulus value.

3.8. Chitosan-POEGMA hydrogel as a bioadhesive

3.8.1. 发 testing

Force versus displacement curves measured during the detachment process of the stainless steel testing probe (following a pre-compression step) from the tested hydrogels using the MACH-1 micromechanical tester are shown in Figure 3-13.

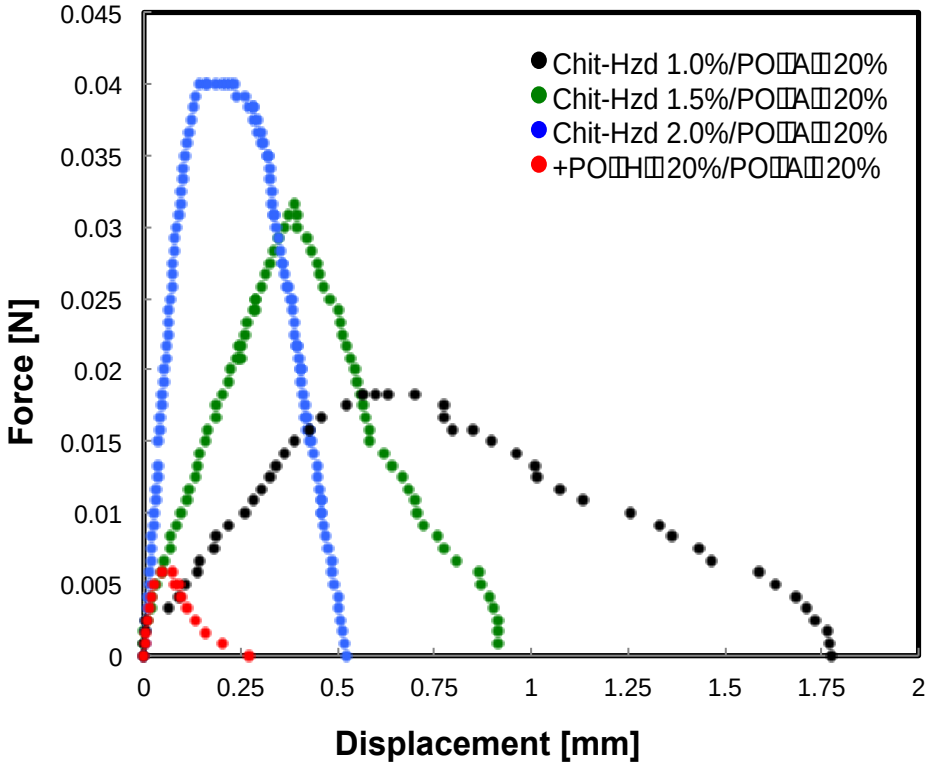

Figure 3-13: Tack detachment force of the tested hydrogels (n=3)

For the tack profiles, the two key parameters are of interest in a tack adhesion experiment are the peak force (i.e. the detachment force required to initiate

delamination) and the total area under the curve (related to the energy required to completely break the adhesive bond). By either measure the POEGMA-only hydrogels exhibited the least tack. For the chitosan hydrogels, gels prepared with lower chitosan levels have the lowest peak force but adhesive detachment over longer displacements, which can be clearly seen for Chit-Hzd 1.0%/$PO_{10}A_{30}$ 20% in Figure 3-12. In comparison, Chit-Hzd 1.5%/$PO_{10}A_{30}$ 20% has a higher delamination force but the detachment displacement (and hence time) was almost immediate (resulting in a significantly lower energy requirement to break the probe-sample interaction), and Chit-Hzd 2.0%/$PO_{10}A_{30}$ 20% had the highest delamination force with a clean and rapid delamination, as exhibited by the sharp slope of the curve. This data is consistent with the lower the cross-link density and thus increased "softness" of the hydrogels as the chitosan content is decreased, resulting in a more viscous and less elastic hydrogel that is tackier and sticks better to the surface; however, due to the lower crosslinking density, the force required to deform the hydrogel is lower. These combined properties result in a lower peak force but adhesion persisting over a longer displacement and time. However, the forces and energies associated with each tested hydrogels are very low relative to other materials, suggesting the gels all have minimal tack (as desirable for topical applications in particular).

3.8.2. Peel adhesion measurement of chitosan-POEGMA hydrogel

Table 3-7 shows the detachment force of hydrogels from porcine skin following the slow peeling of the polymer-skin interface until full detachment. Both

the peak load achieved and the average load measured in the plateau region is plotted for comparison. See Appendix A3 for representative peel curves for this system.

Table 3-7: Peel maximum and average force of detachment for the chitosan-POEGMA hydrogels (n=3)

Hydrogel (w/v)%	**Maximum force of detachment (N)**	**Average force of detachment (N)**
Chit-Hzd 1.0%/$PO_{10}A_{30}$ 20%	0.13 ± 0.02	0.09 ± 0.01
Chit-Hzd 1.5%/ $PO_{10}A_{30}$ 20%	0.15 ± 0.01	0.12 ± 0.01
Chit-Hzd 2.0%/ $PO_{10}A_{30}$ 20%	0.21 ± 0.07	0.18 ± 0.07

As the weight percentage of chitosan in the hydrogel is increased, enhancements in skin adhesion were observed. Chit-Hzd 1.0%/$PO_{10}A_{30}$ 20% (F=0.09N ± 0.01N) exhibited an average peel force of only one half of Chit-Hzd 2.0%/$PO_{10}A_{30}$ 20% (F=0.18N ± 0.07N), with Chit-Hzd 1.5%/$PO_{10}A_{30}$ 20% lying in between (F=0.12 ± 0.01N). However, likely due to the inherently high variation associated with peel tests [104], one-way ANOVA indicates that the change in the peel detachment force as the chitosan concentration was increased was not statistically significant at 95% confidence [F(2,6)=4.38]. Even so, given the lower number of residual aldehyde groups present as more chitosan-hydrazide is added to the gels; this observation suggests that the adhesion is not primarily attributed to Schiff base formation with amines on skin proteins but rather the chemical nature of the chitosan. Note that the failure mode during the peel experiment is adhesive detachment, with the hydrogel remaining completely attached to one of the skin pieces while the other is functionally detached from the hydrogel. The hydrogel itself, while stretching during the experiment, does not break apart, indicating strong cohesion. This mechanical profile is consistent with what would be favourable as a wound sealant.

3.8.3. Tensile bioadhesion measurement of chitosan-POEGMA hydrogel

Similar to the peel testing, tensile testing of the bioadhesive bond strength between porcine skin and the hydrogels indicate a positive correlation between the concentration of chitosan in the hydrogel matrix and the adhesive strength, as shown in Figure 3-14. Table 3-8 summarizes the maximum force of detachment and work of adhesion associated with each of the hydrogels.

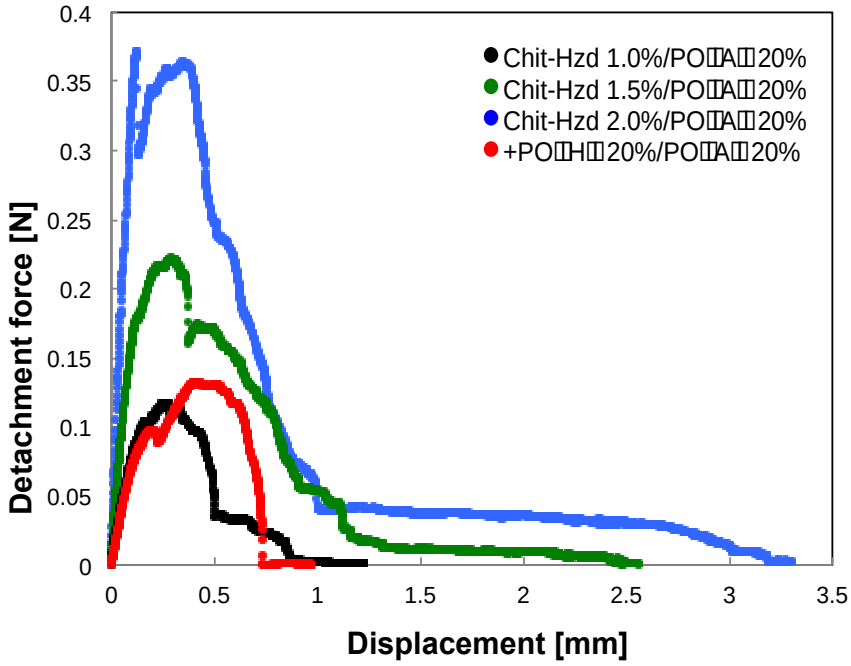

Figure 3-14: Representative tensile detachment profiles for all four hydrogels from porcine skin

Table 3-8: Maximum force of detachments and work of adhesion for each hydrogel (n=3)

Hydrogel (w/v)%	Maximum force of detachment (N)	Work of adhesion (N.mm)
Chit-Hzd 1.0%/$PO_{10}A_{30}$ 20%	0.13 ± 0.01	0.66 ± 0.16
Chit-Hzd 1.5%/ $PO_{10}A_{30}$ 20%	0.21 ± 0.01	1.83 ± 0.03
Chit-Hzd 2.0%/ $PO_{10}A_{30}$ 20%	0.32 ± 0.06	2.84 ± 0.89
+$PO_{10}H_{29}$ 20%/ $PO_{10}A_{30}$ 20%	0.13 ± 0.01	0.69 ± 0.41

The same roughly three-fold enhancement in bond strength between Chit-Hzd 1.0%/$PO_{10}A_{30}$ 20% and Chit-Hzd 2.0%/$PO_{10}A_{30}$ 20% observed in the peel experiment is again observed under tension, with the maximum tensile force increasing from 0.13N to 0.32N. A similar result is shown by integrating the area under the force versus distance curves, with the area under the curve (AUC, related to the work of adhesion of the polymer) also roughly tripling as the chitosan content of the gel is doubled. One-way ANOVA test confirms that there is a significant effect of increasing the chitosan concentration on the bioadhesive strength of the hydrogel at 95% confidence [$F(3,8)=27.48$]. These results indicate that chitosan significantly improves the bioadhesive capacity of the hydrogels via multiple mechanisms. In addition to charge, hydrogen bonding due to the presence of multiple functional groups (amines, residual carboxyl groups, and hydroxyl groups), as well as physical entanglement due to the high molecular weight of chitosan may also contribute to forming stronger adhesions between the tissue and hydrogel film. Also, pairwise t-tests for all other comparisons indicate that all other results are significantly different at a 95% confidence interval.

3.8.4. Mucoadhesion properties of chitosan precursor polymer

The mucoadhesive property of the functionalized chitosan polymer was characterized using rheological synergism. Figure 3-15 shows the storage modulus of Chit-Hzd 1.0% (Fig. 3-15a) and Chit-Hzd 1.5% (Fig. 3-15b) solutions, a 4wt% mucin solution, and a 1:1 volumetric ratio of the two solutions. Note that the final concentrations of Chit-Hzd in the mixture are lower than those used in the gel since

4wt% and 3wt% Chit-Hzd solutions could not be prepared; however, this result still gives insight into the fundamental polymer mucoadhesive properties.

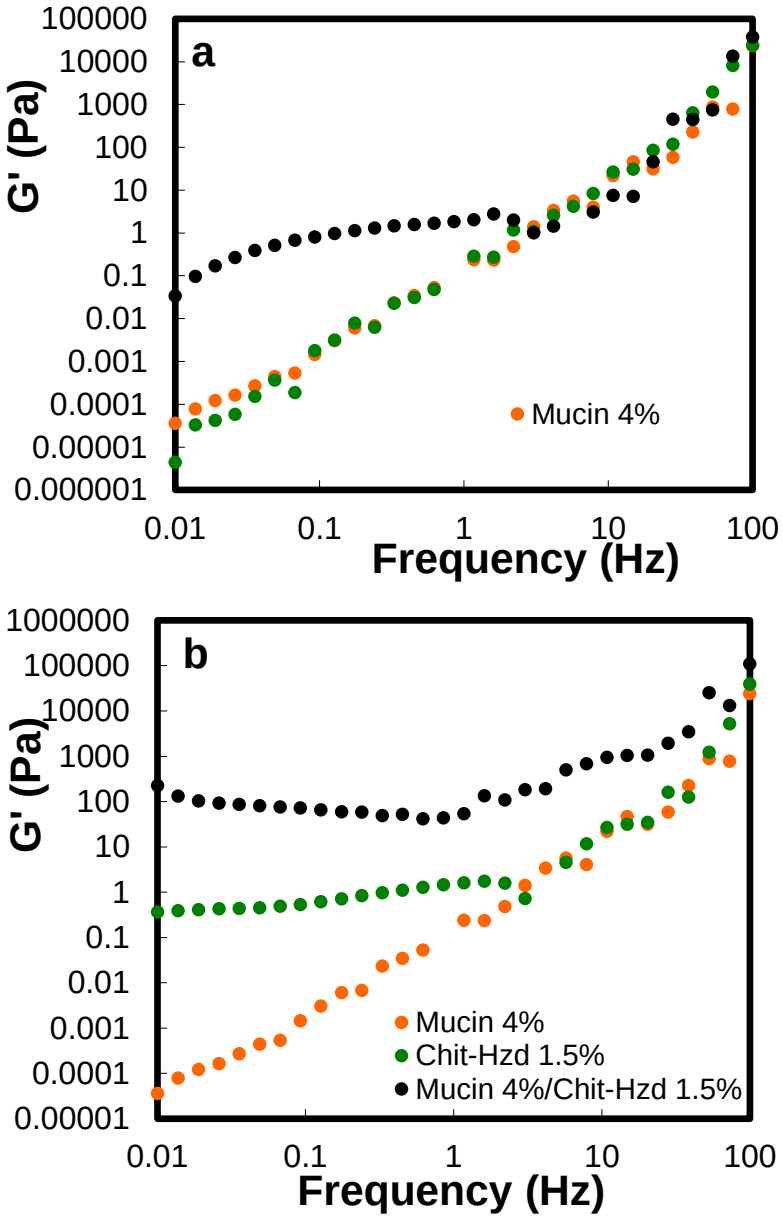

Figure 3-15: Dynamic storage modulus as a function of frequency for a) Chit-Hzd 1% and b) Chit-Hzd 1.5% with and without mucin

At the lower concentration (Chit-Hzd 1.0%), a significant excess modulus value ($\Delta G'$) was observed only at lower frequencies, suggesting a relatively weak

interaction. However, when the concentration was increased to 1.5wt%, the mucin-polymer mixture has an overall higher dynamic modulus and positive average excess modulus throughout the whole frequency range; an excess modulus value of ~2930Pa was observed over the whole frequency range (see Appendix A4 for a plot of excess modulus as a function of frequency). This result validates that functionalizing chitosan with carboxymethyl and then hydrazide groups did not eliminate its inherent mucoadhesive property, which is attributed to its positively charged free amino groups, hydrogen bonding, and also physical entanglement, which facilitate interactions with negatively charged sialic acid groups in the mucin structure.

3.8.5. Tensile mucoadhesion measurement of chitosan-POEGMA hydrogel

The same tack protocol for the rigid and biological tissue experiments was used for the quantification of the hydrogel's mucoadhesion, using mucin-soaked filter paper as a mucous layer mimic in place of the porcine skin. Table 3-9 shows that the same trend holds as would be implied from the rheological synergism results, with hydrogels containing higher chitosan concentrations also exhibiting stronger adhesion with the mucosal mimic.

Table 3-9: Work of adhesion of the hydrogels at two different mucin concentrations

Hydrogel (w/v%)	**75 mg/mL mucin Work of adhesion (N.mm)**	**100 mg/mL mucin Work of adhesion (N.mm)**
$+PO_{10}H_{29}$ 20%/$PO_{10}A_{30}$ 20%	0.034 ± 0.007	0.027 ± 0.007
Chit-Hzd 1.0%/$PO_{10}A_{30}$ 20%	0.062 ± 0.011	0.054 ± 0.011
Chit-Hzd 1.5%/$PO_{10}A_{30}$ 20%	0.107 ± 0.011	0.097 ± 0.011
Chit-Hzd 2.0%/$PO_{10}A_{30}$ 20%	0.164 ± 0.021	0.269 ± 0.038

As the concentration of chitosan in the hydrogel increases, the work of adhesion between the hydrogel and the mucosal mimic also increases, with Chit-Hzd 1.5%/$PO_{10}A_{30}$ 20% showing a work of adhesion almost double and Chit-Hzd 2.0%/$PO_{10}A_{30}$ 20% showing a work of adhesion roughly four-fold higher than that of the Chit-Hzd 1.0%/$PO_{10}A_{30}$ 20% hydrogels (Table 3-9). One-way ANOVA test confirms that the chitosan concentration has a significant effect on the mucoadhesion for both mucin concentrations tested at 95% confidence ([F(3,8)=30.69] at 75 mg/mL mucin and [F(3,8)=80.6] for 100 mg/mL mucin). This result is consistent with gels containing higher chitosan concentrations having more free amines present that allow for stronger interactions with the mucosal layer, thereby resulting in a stronger interfacial interaction and hence stronger adhesion and force of detachment. As the mucin concentration increases, there are more sialic acids present per surface area and hence a higher potential for interaction with each hydrogel, although this effect is only significant at the mucin concentrations tested in the case of the Chit-Hzd 2.0%/$PO_{10}A_{30}$ 20% hydrogel in which the overall potential for mucoadhesion (i.e. concentration of mucoadhesive chitosan repeat units) is significantly higher. Note also that the +$PO_{10}H_{29}$ 20%/$PO_{10}A_{30}$ 20% hydrogel shows significantly lower mucoadhesive bond strength than even the Chit-Hzd 1.0%/$PO_{10}A_{30}$ 20% hydrogel (95% confidence) despite its significantly higher (~9-fold) cationic charge density, again suggesting that the multi-faceted mucoadhesion-promoting properties of chitosan are critical to the performance of the chitosan-POEGMA hydrogels in this application.

3.9. Antibacterial properties

Based on the reported antibacterial properties of chitosan [29], [75], [78], [83], [96], several experiments were conducted to assess the antibacterial properties of both chitosan-Hzd and chitosan-POEGMA *in situ*-gelling hydrogels.

3.9.1. Minimum inhibitory concentration

After the carboxylation and subsequent hydrazide functionalization of chitosan, a MIC experiment was carried out to verify and then quantify the minimum chitosan precursor concentration needed to inhibit the bacterial growth when exposed to a bacterial suspension. Figure 3-16 shows the visual results of this experiment.

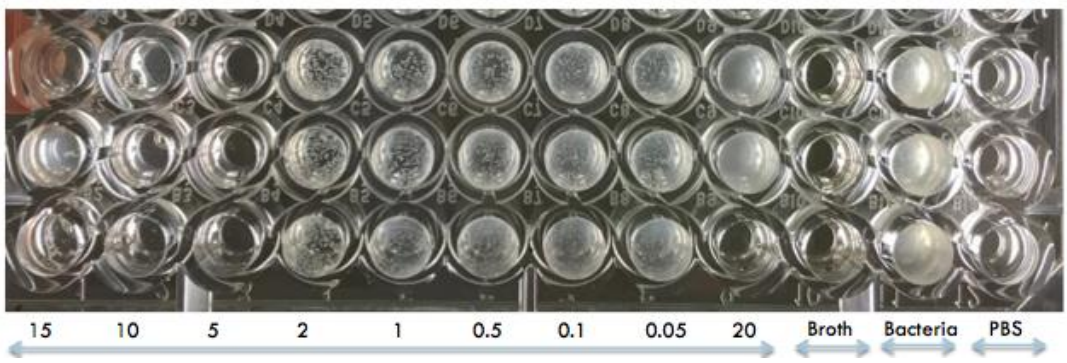

Figure 3-16: Minimum inhibitory concentration experiment with serial dilution of chitosan-hydrazide (mg/mL); 24-hour incubation period

The minimum inhibitory concentration of the hydrazide-functionalized chitosan clearly lies between 2mg/mL and 5mg/mL, with bacterial growth (indicated by spots and later extreme turbidity) apparent at concentrations 2mg/mL and less in the experiment. In comparison, the MIC of unmodified chitosan ranges from 0.02 to 1 mg/mL [78, 99]. This result is consistent with the consumption of a small (~20%) fraction of primary amine groups (primarily implicated in bacterial inhibition) following the carboxymethylation reaction [105]. However, the MIC value of 5

mg/mL is still below the final concentrations of chitosan-Hzd in the hydrogels, which for the tested gels lies between 10 and 20 mg/mL. Therefore, at the concentration used to form hydrogels, the hydrazide functionalized chitosan precursor polymer is verified to be antibacterial.

3.9.2. Topical antibacterial property of the chitosan-POEGMA hydrogel

To assess the contact antibacterial properties of the hydrogels, a LIVE/DEAD assay was used to image the bacteria deposited on the chitosan-POEGMA hydrogels. Figure 3-17 shows the result for the four different hydrogels (Chit-Hzd 1.0%/$PO_{10}A_{30}$ 20%, 1.5%/$PO_{10}A_{30}$ 20%, and 2.0%/$PO_{10}A_{30}$ 20%, and +$PO_{10}H_{29}$ 20%/$PO_{10}A_{30}$ 20%) as well as the polystyrene control. The images show an overlay of the green (live cell) and red (dead cell) fluorescence signals. The Chit-Hzd images are collected by streaking the gels across a microscope slide and subsequently imaging the streaked slide; this method has been demonstrated to provide lower background noise than imaging the gels directly and higher resolution relative to washing techniques for removing bacteria from the gels which inevitably dilute the bacterial suspension. The hydrogels were also imaged and the same results were witnessed; however due to the hydrogel's high fluorescence background during imaging, the images of the streaked method are reported.

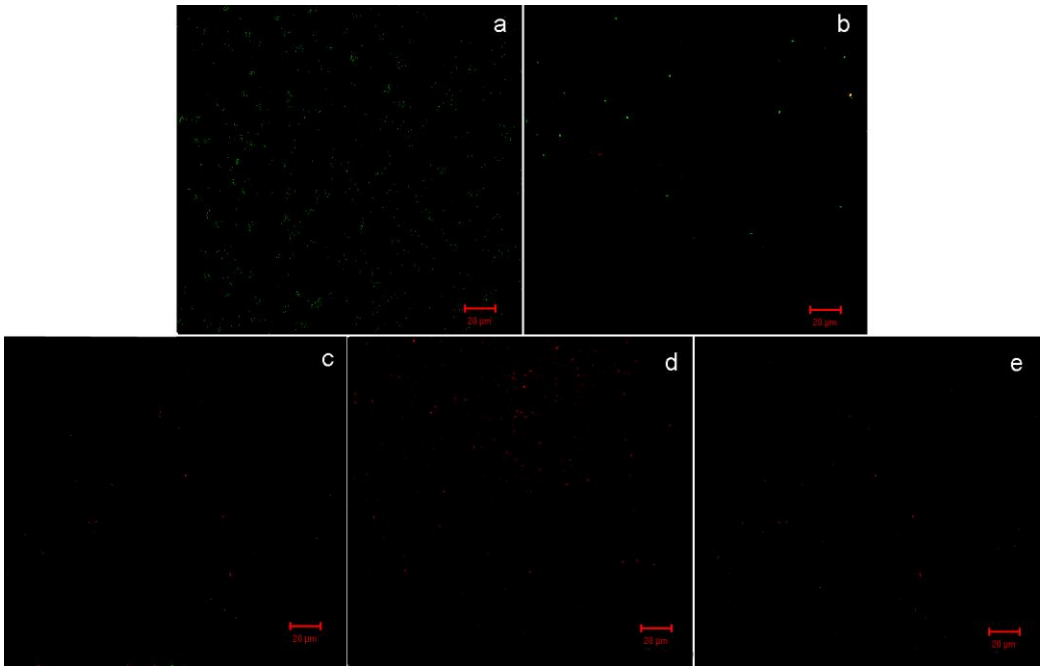

Figure 3-17: LIVE/DEAD assay response of E.coli incubated on the surface of the (a) Polystyrene control, (b) +$PO_{10}H_{29}$/$PO_{10}A_{30}$ 20%, (c) Chit-Hzd 1.0%/$PO_{10}A_{30}$ 20%, (d) Chit-Hzd 1.5%/$PO_{10}A_{30}$ 20%, and (e) Chit-Hzd 2.0%/$PO_{10}A_{30}$ 20% hydrogels

While the polystyrene control (Fig. 3-17a) as well as the +$PO_{10}H_{29}$ 20%/$PO_{10}A_{30}$ 20% containing hydrogels (Fig. 3-17b) maintained viable bacteria (i.e. all but a few of the cells stain green), almost all the bacteria appear red stained for the chitosan-based hydrogels, indicating that chitosan-POEGMA hydrogels have contact anti-microbial properties. This property is of potential utility in wound healing applications or in barrier applications in which the prevention of bacterial infection is critical (e.g. following peritoneal surgery) [106]. Again, given the viability of bacteria noted on the +$PO_{10}H_{29}$ 20%/$PO_{10}A_{30}$ 20% hydrogel, it is clear that the chitosan component in the hydrogel matrix is what gives it its antibacterial properties (i.e. anti-bacterial properties are not a simple charge effect).

3.9.3. Macro dilution method

To characterize the stability of the potential anti-bacterial properties of the chitosan-POEGMA hydrogel due to leaching (as well as the proposed contact mode of

bacterial killing), a macro dilution experiment was conducted to investigate the anti-bacterial properties of any leachates from the hydrogel. Figure 3-18 shows the concentration of *E. coli* bacteria in suspension before and after incubation with the chitosan-POEGMA and POEGMA+ hydrogels.

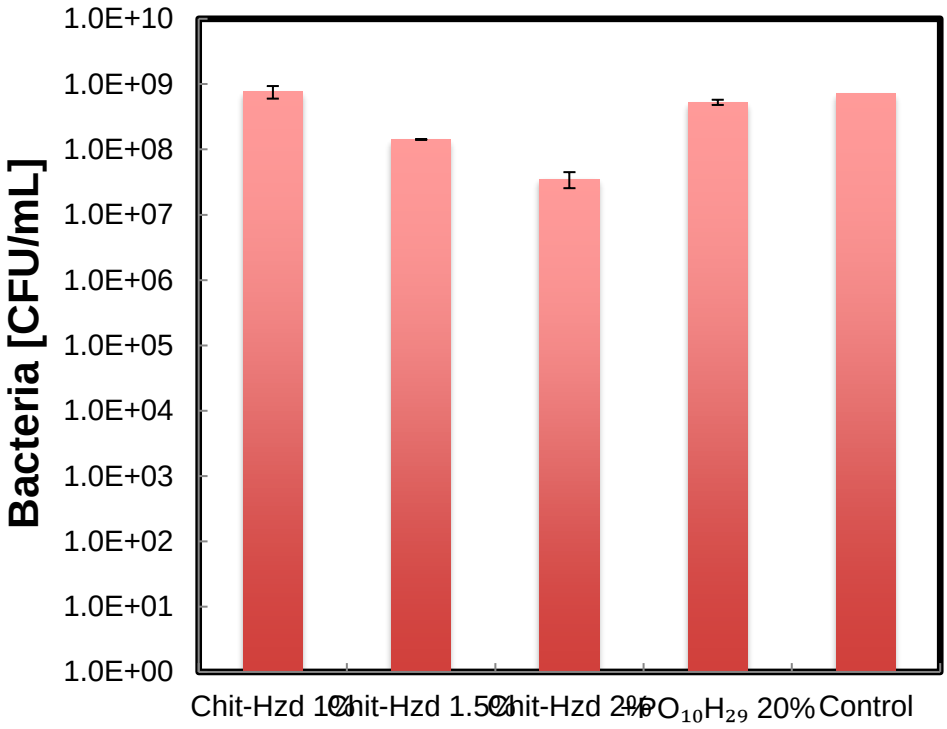

Figure 3-18: *E. coli* concentration after 24-hour incubation with and without the presence of the hydrogel

Overall, little to no decrease in *E. coli* concentration is observed after hydrogel incubation, with the slight decrease in *E.coli* concentration observed for Chit-Hzd 1.5%/$PO_{10}A_{30}$ 20% and Chit-Hzd 2.0%/$PO_{10}A_{30}$ 20% potentially attributable to the topical interaction between the hydrogel surface and bacteria that comes in contact with it.

3.9.4. Zone of Inhibition

A zone of inhibition test was also conducted to confirm that leachates, if present, are not at significant concentrations for the Chit-Hzd 1.0%, 1.5%, and 2% as well as $+PO_{10}H_{29}$ 20% with $PO_{10}A_{30}$ 20%. Figure 3-19 shows the typical zone of inhibition result for all the hydrogels tested.

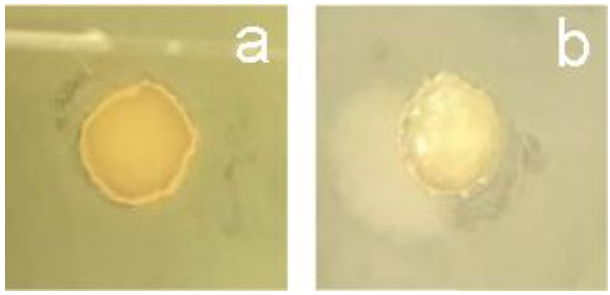

Figure 3-19: A zone of inhibition typical result for all the hydrogels

Qualitatively, due to the lack of a ring around the hydrogel, it is inferred that no significant leaching occurred, since leaching of chitosan-Hzd polymers from the hydrogel would induce killing in the area immediately around the gel. Note that the local concentration of any leached chitosan-Hzd immediately around the gel would be expected to be significantly higher in this experiment as opposed to the previous macro dilution experiment given the slow diffusibility of the chitosan in agar; the lack of apparent anti-bacterial activity further supports the absence of leachates from the hydrogels.

3.10. Cell viability

3.10.1. *In vitro* Polymer cytotoxicity

To ensure the hydrogel components are only antibacterial and not cytotoxic to mammalian cells, polymer cytotoxicity was measured against 3T3 mouse fibroblast cells using the resazurin assay. Figure 3-20 shows the cell viabilities in the presence of

various concentrations of the component prepolymers used to prepare the hydrogels studied.

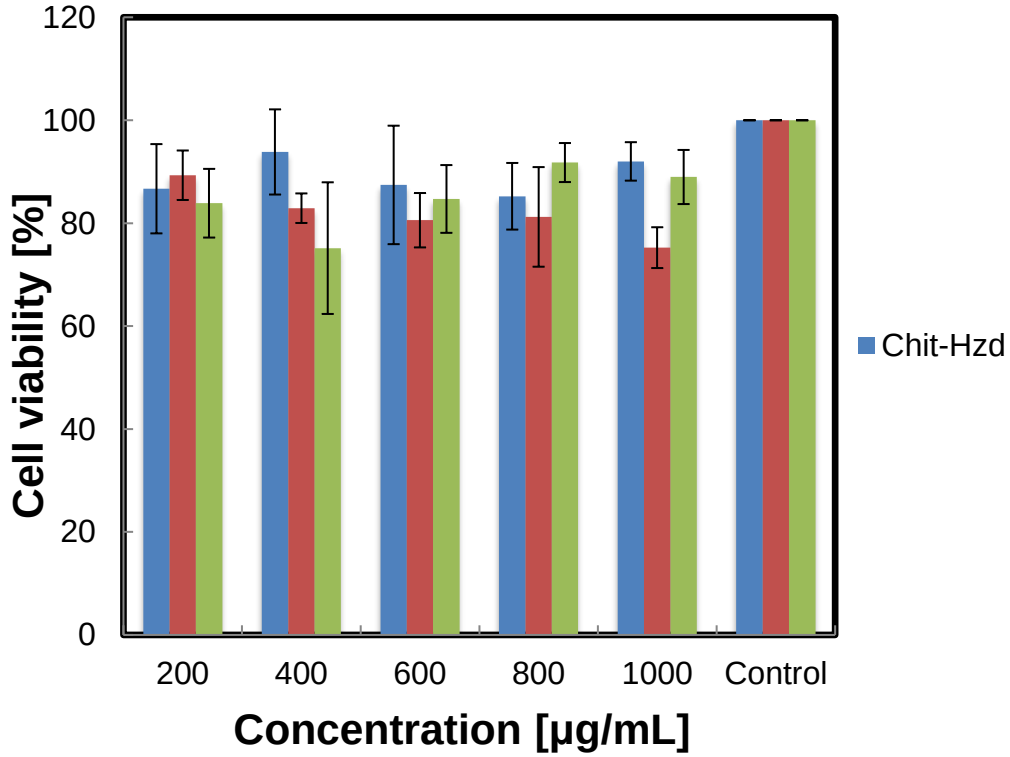

Figure 3-20: Cell viability (%, relative to cell-only control) of different concentration dilutions of chitosan-Hzd, $PO_{10}A_{30}$, and $+PO_{10}H_{29}$ polymers against 3T3 cells using the resazurin assay (n=4)

The data in Figure 3-20 shows that for any of the starting polymers, no cytotoxic effects against 3T3 cells were observed, suggesting that the polymers are not cytotoxic to mammalian cells.

3.10.2. Hydrogel cell adhesion

To further assess the cell compatibility of the hydrogels, a cell adhesion experiment was performed using a LIVE/DEAD assay to image the 3T3 fibroblast cells deposited on the hydrogels. Figure 3-21 shows the result for the four different

hydrogels (+$PO_{10}H_{29}$, Chit-Hzd 1%, 1.5%, and 2% with $PO_{10}A_{30}$ 20%) as well as the polystyrene control.

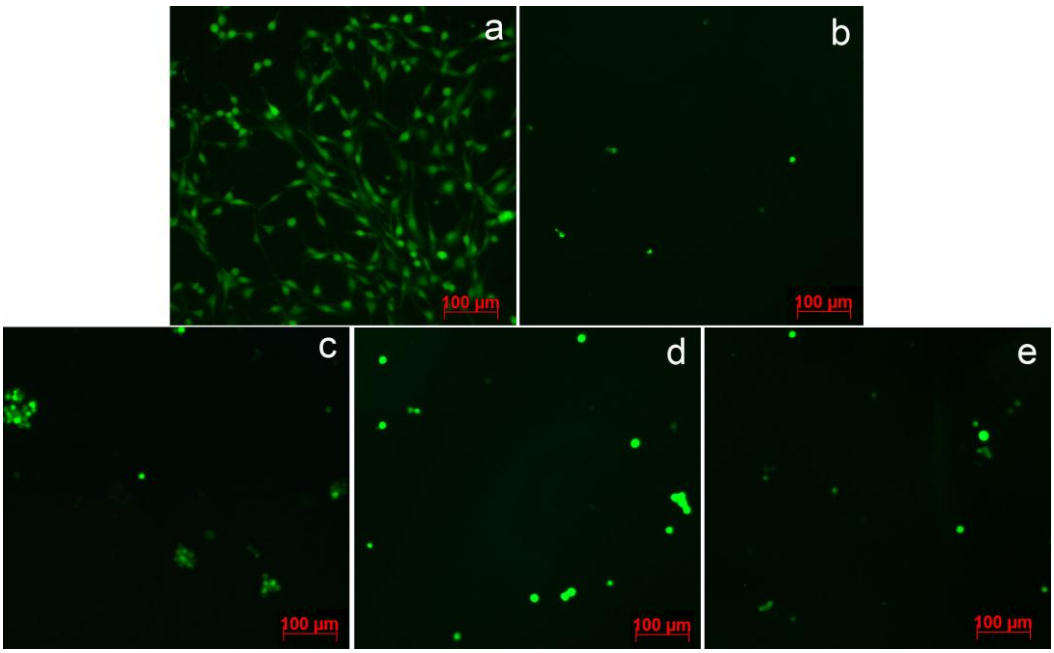

Figure 3-21: LIVE/DEAD assay response of 3T3 fibroblast cells incubated on the surface of the (a) Polystyrene control, (b) +$PO_{10}H_{29}$/$PO_{10}A_{30}$ 20%, (c) Chit-Hzd 1.0%/$PO_{10}A_{30}$ 20%, (d) Chit-Hzd 1.5%/$PO_{10}A_{30}$ 20%, and (e) Chit-Hzd 2.0%/$PO_{10}A_{30}$ 20% hydrogels

Both the cationic POEGMA hydrogel as well as all Chit-POEGMA hydrogels show apparent cell adhesion, although the degree of cell adhesion observed is less than that observed in the polystyrene control. This result is in contrast to previously reported uncharged POEGMA hydrogels [90], which exhibit virtually no cell adhesion; the cationic charge of these hydrogels can again be used to rationalize this result. However, while it is possible that the +$PO_{10}H_{29}$ 20%/$PO_{10}A_{30}$ 20% hydrogel results in adhesion with less cell clumping, there is no significant difference noted in the cell density adhered to any of the tested hydrogels. This result suggests that the gels are all moderately cell adhesive but also well tolerated by cells. Comparing this

result to the bacterial adhesion test (Fig. 3-17), it is clear that the chitosan-POEGMA hydrogels are effectively antibacterial but also well tolerated by mammalian cells, again ideal for use as an injectable antibacterial material.

3.11. Conclusion

The incorporation of chitosan in an *in situ* hydrogel matrix produced a hydrogel with both tissue and mucosal adhesive properties and topical antibacterial properties. The functionalization of chitosan with first carboxymethyl and then hydrazide groups did not eliminate chitosan's adhesive or antibacterial properties, resulting in a hydrogel matrix that can be potentially employed in multiple biomedical applications. Rheological synergism results indicate a significant synergistic interaction is present between the mucin and chitosan at chitosan concentrations as low as 0.75%. This was further validated through mechanical testing using porcine tissue as well as a mucin mimic substrate, where a 1% increase of chitosan in the hydrogel matrix results in a two to three fold increase in the detachment force as well as work of adhesion. As for the antibacterial properties, a minimum inhibitory concentration (MIC) of 5 mg/mL was measured, lower than the native chitosan MIC due to the 19% amine substitution with carboxyl groups but still within a relevant range for hydrogel antibacterial properties. This was further validated through the hydrogel's ability to inhibit and kill *E.coli* bacteria in contact with the hydrogel, as confirmed through the LIVE/DEAD assay images. The bioadhesive as well as antibacterial properties of this hydrogel combined with its potential for *in situ* gelation via either injection or spraying (via hydrazone bond chemistry) suggest particular

applications of these materials as wound sealants inside the body that have potential to reduce the need for invasive surgery and increase patient comfort.

4. Conclusions and Recommendations

4.1. Conclusions

- Soluble hydrazide functionalized chitosan was synthesized using a two step synthesis by initially carboxylating the chitosan and then performing an EDC/ADH reaction to attach the hydrazide functional groups via adipic acid dihydrazide conjugation.
- Different carboxymethylation recipes were pursued to generate the highest carboxymethylation percentage with the lowest degree of amine substitution. A 41% carboxymethyl substitution (with less than half of that functionalization occurring on the primary amine groups) was achieved, leading to a total of 305 hydrazide groups per chain for hydrazide chitosan.
- Gelation was achieved by mixing hydrazide-chitosan with aldehyde functionalized POEGMA in under 10 seconds. However, due to the relatively low (~2 wt%) upper limit of chitosan-hydrazide concentration required to maintain injectability and the resulting high aldehyde to hydrazide ratio in the resulting gels, the Chit-Hzd/$PO_{10}A_{30}$ gels are not as strong as cationic POEGMA gels; a maximum modulus of ~1kPa is achieved for the highest concentrated Chit-Hzd 2.0%/$PO_{10}A_{30}$ 20% hydrogel compared to the 8.5kPa for the +$PO_{10}H_{29}$ 20%/$PO_{10}A_{30}$ 20% hydrogel.
- The transparency of the hydrogel is not affected by the chitosan incorporation, with all samples exhibiting a transparency higher than 88% over the whole visible range.
- Water retention within the hydrogels can be achieved over 1-3 day periods, depending on the humidity and place of application

- Strong rheological synergism effects were observed between mucin and hydrazide-functionalized chitosan even at polymer concentrations of 0.75%, confirming the mucoadhesive property of the polymer post-functionalization
- Increasing the chitosan wt% in the hydrogel matrix results in stronger gels with higher bioadhesive and mucoadhesive strength.
- Both peel and tack testing between the hydrogel and porcine skin were used to mimic the potential external forces of a topical application; both tests showed similar detachment forces, with the vertical detachment mechanism requiring more force for detachment as compared to the peeling mechanism.
- The hydrazide functionalized chitosan polymer was shown to possess antibacterial properties through a minimum inhibitory concentration experiment, using *E.coli* as the model bacteria (albeit at somewhat higher concentrations than unfunctionalized chitosan). Given that no leaching of anti-bacterial polymers was detected via zone of inhibition tests, any antibacterial effects are inferred to be topically induced, a result validated through a LIVE/DEAD bacterial assay.
- Chit-Hzd 2.0%/$PO_{10}A_{30}$ 20% appears to be the most promising candidate as a bioadhesive, antibacterial gel due to its superior hydrogel strength and bioadhesive properties when compared to the lower chitosan content hydrogels.
- Chitosan's cationic property is not the dominant contributor to its bioadhesive and antibacterial properties but it is facilitated through multiple mechanisms.
- The properties of the hydrogel can be tuned to the application desired, with the elasticity, tack, degradation kinetics, and adhesion all adjustable based on the

chitosan content of the gel and/or the substitution of chitosan for cationic POEGMA.

- Cytotoxicity assessment using 3T3 fibroblast cells on the chitosan and POEGMA polymers indicated no significant cytotoxic effects.

4.2. Recommendations

- Synthesizing a more selectively carboxyl substituted chitosan in which carboxyl groups are incorporated solely on the primary hydroxyl group could potentially increase the adhesive strength of the hydrogel by maximizing the number of residual amine groups in the polymer.
- The aldehyde POEGMA concentration and/or the concentration of aldehyde functional groups should be decreased to reduce the aldehyde to hydrazide ratio and investigate the result of that ratio independent of the gel mechanics.
- Mixing cationic POEGMA-hydrazide with chitosan-hydrazide offers potential to maintain the desirable bioadhesive properties of chitosan-containing hydrogels while maintaining the strength of a POEGMA-POEGMA hydrogel
- Increasing the cationic co-monomer content of POEGMA to match that of the intermediate chitosan hydrogels would be beneficial to further confirm the role of charge density versus other chitosan properties on the bioadhesive and antibacterial properties of the hydrogels
- Antibacterial experiments for gram positive bacteria such as *Staphylococcus aureus* or *Staphylococcus epidermidis* should be conducted for a clear

understanding of the chitosan polymer as well as chitosan-POEGMA hydrogel's antibacterial properties

- Bacteria should be incubated on the surface of the hydrogel for 24-48 hours to assess the relative degree of colony formation as a log reduction in growth on the surfaces relative to a standard control well.
- An in vivo wound healing study of the adhesive properties of the hydrogel in rat models should be conducted to see the actual utility of these hydrogels in the proposed target applications.
- Functionalization of catechol groups on hydrazide functionalized chitosan offers potential for significantly enhanced adhesion properties in a wet tissue environment. Proof of principle of this concept has already been completed, with catechol-Chit-Hzd polymer successfully synthesized and gelled with an aldehyde POEGMA polymer.
- Quaternizing chitosan with quaternary amine groups offers potential for further enhancing the antibacterial properties of the chitosan-POEGMA hydrogel, although care must be taken to ensure the density of quarternization does not negatively influence the good mammalian cell compatibility observed with the present materials.
- Synthesizing a POEGMA control that matches the cationic charge as well as excess aldehyde to better understand chitosan's contribution to bioadhesion and as an antibacterial agent is recommended. In particular, reducing the $+PO_{10}H_{29}$ polymer concentration from 20wt% to 5wt% in the hydrogel formulations would result in a a gel with the same ~4.5:1 aldehyde:hydrazide ratio and ~0.75 mmol/mL charge density of the 2wt% Chit-Hzd-POEGMA

hydrogels, representing a significantly better control to isolate the effects of chitosan in the formulation.

- Gelling quaternized POEGMA-aldehyde polymers with catechol Chit-Hzd offers potential to form a hydrogel with high adhesive, antibacterial, and swelling properties for wound healing or topical mucosal drug delivery.
- Drug loading and release studies of an appropriate drug (e.g. an antibiotic for non-contact bacterial killing, an anti-fungal drug, or an anti-inflammatory drug) may be conducted to investigate the potential application of the chitosan-POEGMA hydrogel as a drug delivery system on mucosal and topical surfaces.

References

[1] J.D. Smart, "The basics and underlying mechanisms of mucoadhesion," *Advanced Drug Delivery Reviews,* vol. 57, pp. 1556-68, 2005.

[2] T.B. Reece, T.S. Maxey, and I. L. Kron, "A prospectus on tissue adhesives " *The American Journal of Surgery,* vol. 182, pp. S40-S44, 2001.

[3] A. Amit, S. Sharad, Ajazuddin, K. Junaid, and Swarna, "Theories and factors affecting mucoadhesive drug delivery systems: A review," *International Journal of of Research in Ayurveda & Pharmacy,* vol. 2, pp. 1155-1161, 2011.

[4] N.A. Peppas and J.J. Sahlin, "Hydrogels as mucoadhesive and bioadhesive materials: a review," *Biomaterials,* vol. 17, pp. 1553-1561, 1996.

[5] S.K. Roy and B. Prabhakar, "Bioadhesive polymeric platforms for transmucosal drug delivery systems - a review," *Tropical Journal of Pharmaceutical Research,* vol. 9, pp. 91-104, 2010.

[6] K. Kumar, N. Dhawan, H. Sharma, S. Vaidya, and B. Vaidya, "Bioadhesive polymers: novel tool for drug delivery," *Artificial Cells Nanomedicine and Biotechnology* vol. 42, pp. 274-83, 2014.

[7] K. Park and J. R. Robinson, "Bioadhesive polymers as platforms for oral-controlled drug delivery: method to study bioadhesion " *International Journal of Pharmaceutics* vol. 19, pp. 107-127, 1984.

[8] B. Idson, "Adsorption to skin and hair," *Journal Society of Cosmetic Chemists,* vol. 18, pp. 91-103, 1967.

[9] R.F. Donnelly, & A.D. Woolfson, "Bioadhesive drug delivery systems," in *Polymeric Biomaterials,* S. Dumitriu, & V. Popa, Ed(s), Boca Raton, FL, 2013, pp. 318-319.

[10] Z. Zhu, Y. Zhai, N. Zhang, D. Leng, and P. Ding, "The development of polycarbophil as a bioadhesive material in pharmacy," *Asian Journal of Pharmaceutical Sciences,* vol. 8, pp. 218-227, 2013.

[11] R.F. Donnelly, & A.D. Woolfson, "Bioadhesive systems for drug delivery," in *Bioadhesion and Biomimetics: From Nature to Applications,* H. Bianco-Peled, & N. Davidovich-Pinhas, Ed(s), Boca Raton, FL, 2015, pp. 235-265.

[12] M. Mehdizadeh and J. Yang, "Design strategies and applications of tissue bioadhesives," *Macromolecular Bioscience* vol. 13, pp. 271-88, 2013.

[13] G.P. Andrews, T.P. Laverty, and D.S. Jones, "Mucoadhesive polymeric platforms for controlled drug delivery," *European Journal of Pharmaceutics and Biopharmaceutics,* vol. 71, pp. 505-18, 2009.

[14] F.C. Carvalho, M.L. Bruschi, R.C. Evangelista, and M. Gremiao, "Mucoadhesive drug delivery systems," *Brazilian Journal of Pharmaceutical Sciences*, vol. 46, pp. 1-17, 2010.

[15] R.A.A. Muzzarelli, "Carboxymethylated Chitins and Chitosan," *Carbohydrate Polymers,* vol. 8, pp. 1-21, 1988.

[16] R.L. Srinivas, S. D. Johnson, and P. S. Doyle, "Oil-isolated hydrogel microstructures for sensitive bioassays on-chip," *Analytical Chemistry* vol. 85, pp. 12099-12107, 2013.

[17] C.C. Lin and K.S. Anseth, "Controlling Affinity Binding with Peptide-Functionalized Poly(ethylene glycol) Hydrogels," *Advanced Functional Materials,* vol. 19, p. 2325, 2009.

[18] Z. Zhu, C. Wu, H. Liu, Y. Zou, X. Zhang, H. Kang, *et al.*, "An aptamer cross-linked hydrogel as a colorimetric platform for visual detection," *Angewandte Chemie International Edition,* vol. 49, pp. 1052-6, 2010.

[19] T. Miyata, N. Asami, and T. Uragami, "A reversible antigen-responsive hydrogel," *Nature* vol. 399, pp. 766-768, 2013.

[20] S.P. Zustiak, Y. Wei, and J.B. Leach, "Protein-hydrogel interactions in tissue engineering: mechanisms and applications," *Tissue Engineering Part B: Reviews,* vol. 19, pp. 160-71, 2013.

[21] G. S. Longo and D. H. Thompson, "Ligand-receptor interactions between surfaces: The role of binary polymer spacers," *Langmuir,* vol. 24, pp. 10324-10333, 2008.

[22] K. Park, & H. Park, , "Test methods of bioadhesion," in *Bioadhesive Drug Delivery Systems,* V. Lenaerts, & R. Gurny, Ed(s), Boca Raton, FL, 1989, pp. 59.

[23] R. Asija, J.K. Kumawat, and D. Sharma, "Mucoadhesive drug delivery system: a review " *Journal of Drug Discovery and Therapeutics* vol. 1, pp. 1-8, 2013.

[24] X. Yang, K. Forier, L. Steukers, S. Van Vlierberghe, P. Dubruel, K. Braeckmans, *et al.*, "Immobilization of pseudorabies virus in porcine tracheal respiratory mucus revealed by single particle tracking," *PLoS One,* vol. 7, p. e51054, 2012.

[25] "Phases of wound healing," [online], available: http://www.clinimed.co.uk/wound-care/education/wound-essentials/phases-of-wound-healing.aspx, [accessed: July 10, 2015]

[26] J. H. Levy, "Hemostatic agents " *Transfusion,* vol. 44, pp. 58S-62S, 2004.

[27] I.P. Galankis, N. Vasdev, and N. Soomro, "A review of current hemostatic agents and tissue sealants used in laparoscopic partial nephrectomy " *Reviews in Urology*, vol. 11, pp. 131-138, 2011.

[28] K. Harding, & S. Enoch, "Wound bed preparation: The science behind the removal of barriers to healing [PART 1]," *Wounds*, vol.15, no.8, 2013.

[29] T. Dai, M. Tanaka, Y. Y. Huang, and M. R. Hamblin, "Chitosan preparations for wounds and burns: antimicrobial and wound-healing effects," *Expert Review Anti Infective Therapy* vol. 9, pp. 857-879, 2011.

[30] J.S. Boateng, K.H. Matthews, H.N. Stevens, and G.M. Eccleston, "Wound healing dressings and drug delivery systems: a review," *Journal of Pharmaceutical Science,* vol. 97, pp. 2892-2923, 2008.

[31] W.D. Spotnitz, "Fibrin Sealant: The Only Approved Hemostat, Sealant, and Adhesive-a Laboratory and Clinical Perspective," *ISRN Surgery* vol. 2014, p. 203943, 2014.

[32] W.D. Spotnitz, "Hemostats, sealants, and adhesives: A practical guide for the surgeon," *The American Surgeon* vol. 78, pp. 1305-1321, 2012.

[33] R. Kalimi, L.P. Faber, *Clinical Scenarios in Thoracic Surgery*, Lippincott Williams & Wilkins, PA, 2004, pp.220-221.

[34] S. Senel and S.J. McClure, "Potential applications of chitosan in veterinary medicine," *Advanced Drug Delivery Reviews,* vol. 56, pp. 1467-80, 2004.

[35] T. Yu, G.P. Andrews, and D.S. Jones, "Mucoadhesion and Characterization of Mucoadhesive Properties," in *Mucosal Delivery of Biopharmaceuticals*, ed. Springer, NY, 2014, pp. 35-58.

[36] W.M. Saltzmann, "Controlled drug delivery systems," in *Drug Delivery: Engineering Principles for Drug Therapy*, Oxford University Press, FL, 2001, pp. 235-259.

[37] C. Pegoraro, S. MacNeil, and G. Battaglia, "Transdermal drug delivery: from micro to nano," *Nanoscale,* vol. 4, pp. 1881-94, 2012.

[38] K.R. Vinod, R.T. Rohit, S. Sandhya, B. David, and R.B. Venkatram, "Critical review on mucoadhesive drug delivery systems," *Journal for Drugs and Medicines,* vol. 4, pp. 7-28, 2012.

[39] S. Turker, E. Onur, and Y. Ozer, "Nasal route and drug delivery systems," *Pharmaceutical World Science,* vol. 26, pp. 137-142, 2004.

[40] K. Thamizhvanan, R. Himabindu, K. Sarada, N. Hyundavi, and K. R. Lahari, "Current status and advanced approaches in ocular drug delivery systems," *International Journal of Current Pharmaceutical & Clinical Research,* vol. 2, pp. 77-86, 2012.

[41] B. Dhandayuthapani, Y. Yoshida, T. Maekawa, and D.S. Kumar, "Polymeric scaffolds in tissue engineering application: A review," *International Journal of Polymer Science,* vol. 2011, pp. 1-19, 2011.

[42] R. Langer and D. A. Tirrell, "Designing materials for biology and medicine " *Nature,* vol. 428, pp. 487-492, 2004.

[43] J. R. Fuchs, B. A. Nasseri, and J. P. Vacanti, "Tissue engineering: A 21st century solution to surgical reconstruction," *The Annals of Thoracic Surgery,* vol. 72, pp. 577-591, 2001.

[44] J. Zhu and R.E. Marchant, "Design properties of hydrogel tissue-engineering scaffolds," *Expert Review of Medical Devices,* vol. 8, pp. 607-26, 2011.

[45] B. Mahanta and R. Nigam, "An overview of various biomimetic scaffolds: Challenges and applications in tissue engineering," *Journal of Tissue Science & Engineering,* vol. 5, pp. 1-5, 2014.

[46] J. Elisseeff, "Structure starts to gel," *Nature,* vol. 7, pp. 271-273, 2008.

[47] E.M. Ahmed, "Hydrogel: Preparation, characterization, and applications: A review," *J Adv Res,* vol. 6, pp. 105-21, 2015.

[48] S. Gulrez, S. Al-Assaf, and G.O. Phillips, "Hydrogels: Methods of preparation, characterisation and applications," in *Analysis and Modeling to Technology Applications,* , A. Carpi, Ed., 2011, pp. 117-150.

[49] T. Hoare and D.S. Kohane, "Hydrogels in drug delivery: Progress and challenges," *Polymer,* vol. 49, pp. 1993-2007, 2008.

[50] O. Okay, "General Properties of Hydrogels," *Hydrogel Sensors and Actuators,* vol. 6, pp. 1-14, 2009.

[51] H. Tan, H. Li, J.P. Rubin, and K.G. Marra, "Controlled gelation and degradation rates of injectable hyaluronic acid-based hydrogels through a double crosslinking strategy," *Journal of Tissue Engineering and Regenerative Medicine,* vol. 5, pp. 790-7, 2011.

[52] M. Patenaude, N. Smeets, and T. Hoare, "Designing injectable, covalently cross-linked hydrogels for biomedical applications," *Macromolecular Rapid Communications* vol. 35, pp. 598-617, 2014.

[53] T.D. Johnson and K. L. Christman, "Injectable hydrogel therapies and their delivery strategies for treating myocardial infraction," *Expert Opinion on Drug Delivery,* vol. 10, pp. 59-72, 2013.

[54] J. Yang, J. Yeom, B.W. Hwang, A. Hoffman, and S.K. Hahn, "In situ-forming injectable hydrogels for regenerative medicine," *Progress in Polymer Science,* vol. 39, pp. 1973-1986, 2014.

[55] J. Maitra and V.K. Shukla, "Cross-linking in hydrogels - A review," *American Journal of Polymer Science,* vol. 4, pp. 25-31, 2014.

[56] S. D. Fitzpatrick, M. A. Mazumder, F. Lasowski, L. E. Fitzpatrick, and H. Sheardown, "PNIPAAm-Grafted-Collagen as an injectable, in situ gelling bioactive cell delivery scaffold," *Biomacromolecules,* vol. 11, pp. 2261-2267, 2010.

[57] P. Sheikholeslami, B. Muirhead, D.S. Baek, H. Wang, X. Zhao, D. Sivakumaran, *et al.*, "Hydrophobically-modified poly(vinyl pyrrolidone) as a physically-associative, shear-responsive ophthalmic hydrogel," *Experimental Eye Research,* vol. 137, pp. 18-31, 2015.

[58] S.Y. Choh, D. Cross, and C. Wang, "Facile synthesis and characterization of disulfide-cross-linked hyaluronic acid hydrogels for protein delivery and cell encapsulation," *Biomacromolecules,* vol. 12, pp. 1126-1136, 2011.

[59] Y. Li, J. Rodrigues, and H. Tomas, "Injectable and biodegradable hydrogels: gelation, biodegradation and biomedical applications," *Chemical Society Reviews,* vol. 41, pp. 2193-221, 2012.

[60] B.D. Mather, K. Viswanathan, K.M. Miller, and T.E. Long, "Michael addition reactions in macromolecular design for emerging technologies," *Progress in Polymer Science,* vol. 31, pp. 487-531, 2006.

[61] G.T. Hermanson, "Aldehyde and ketone reactions," in *Bioconjugate Techniques*, 3rd ed., Academic Press, San Diego, 2013, pp. 251-253

[62] "Carbonyl-reactive crosslinker chemistry", *Life Technologies*, [online], available: https://www.lifetechnologies.com/ca/en/home/life-science/protein-biology/protein-biology-learning-center/protein-biology-resource-library/pierce-protein-methods/carbonyl-reactive-crosslinker-chemistry.html, [accessed July 10, 2015].

[63] V. T. A. Kale, "Design, synthesis and characterization of pH-sensitive PEG-PE conjugates for stimuli-sensitive pharmaceutical nanocarries: The effect of substitutes at the hydrazone linkage on the pH stability of PEG-PE conjugates," *Bioconjugate Chemistry* vol. 18, pp. 363-370, 2007.

[64] H. Bidgoli, A. Zamani, and M.J. Taherzadeh, "Effect of carboxymethylation conditions on the water-binding capacity of chitosan-based superabsorbents," *Carbohydr Res,* vol. 345, pp. 2683-2689, 2010.

[65] J.M. Jeanette, "Preparation and characterization of gelatin and chitosan films," Honors thesis, Chemical and Biological Engineering, Tufts University, Massachusetts 2009.

[66] P.K. Dutta, J. Dutta, and V. S. Tripathi, "Chitin and chitosan: Chemistry, properties, and applications," *Journal of Scientific & Industrial Research,* vol. 63, pp. 20-31, 2004.

[67] A. Jimtaisong and N. Saewan, "Utilization of carboxymethyl chitosan in cosmetics," *International Journal of Cosmetic Science,* vol. 36, pp. 12-21, Feb 2014.
[68] D.P. Chattopadhyay and M.S. Inamdar, "Aqueous behaviour of chitosan," *International Journal of Polymer Science,* vol. 2010, pp. 1-7, 2010.

[69] C. Pillai, W. Paul, and C. Sharma, "Chitin and chitosan polymers: Chemistry, solubility and fiber formation," *Progress in Polymer Science,* vol. 34, pp. 641-678, 2009.

[70] F. Croisier and C. Jérôme, "Chitosan-based biomaterials for tissue engineering," *European Polymer Journal,* vol. 49, pp. 780-792, 2013.

[71] T. Muslim, M.H. Rahman, H.A. Begum, and M. A. Rahman, "Chitosan and carboxymethyl chitosan from fish scales of Labeo rohita," *Dhaka University Journal of Science,* vol. 61, pp. 145-148, 2013.

[72] A. DiPrato, "Mechanically robust multi-layered chitosan thin films," Masters of Science Materials Science and Engineering, Drexel University, 2010.

[73] H. Lin, H. Wang, C. Xue, and M. Ye, "Preparation of chitosan oligomers by immobilized papain," *Enzyme and Microbial Technology* vol. 31, pp. 588-592, 2002.
[74] J. Berger, M. Reist, J.M. Mayer, O. Felt, and R. Gurny, "Structure and interactions in chitosan hydrogels formed by complexation or aggregation for biomedical applications," *European Journal of Pharmaceutics and Biopharmaceutics,* vol. 57, pp. 35-52, 2004.

[75] M. Friedman and V. K. Juneja, "Review of antimicrobil and antioxidative activities of chitosans in food," *Journal of Food Protection* vol. 73, pp. 1737-1761, 2010.

[76] I. Kardas, M.H. Struszczyk, M. Kucharska, L. Van den Broek, J.. Van Dam, and D. Ciechan´ska, "Chitin and chitosan as funcitonal biopolymers for industrial applications," in *The European Polysaccharide Network of Excellence,* P. Navard, Ed., ed: Springer, 2013, pp. 329-373.

[77] J. Synowiecki and N. Al-Khateeb, "Production, properties, and some new applications of chitin and its derivatives," *Critical Reviews in Food Science and Nutrition,* vol. 43, pp. 145-171, 2003.

[78] M. Kong, X.G. Chen, K. Xing, and H.J. Park, "Antimicrobial properties of chitosan and mode of action: a state of the art review," *International Journal of Food Microbiology,* vol. 144, pp. 51-63, 2010.

[79] C. Caramella, MC. Bonferoni, S. Rossi, "Characterization of chitosan hydrochloride-mucin rheological interaction: influence of polymer concentration and polymer:mucin weight ratio," *Eur. J. Pharm. Sci.*, vol.12, no.4, pp.479-485, 2001.

[80] M. Chen, F. Mi, Z. Liao, & H. Sung, "Chitosan: Its applications in drug eluting devices," *Advances in Polymer Science,* vol. 243, pp. 185-230, 2011.

[81] S. Zaki, M. Ibrahim, & H. Katas, "Particle Size Affects Concentration-Dependent Cytotoxicity of Chitosan Nanoparticles towards Mouse Hematopoietic Stem Cells," *Journal of Nanotechnology*, vol.2015, 2015.

[82] B. Ha, T. L. Minh, To Nguyen, and D. Minh, "Naturally derived biomaterials: Preparation and application. ," in *Regenerative Medicine and Tissue Engineering*, ed, 2013, pp. 247-274.

[83] F. Wu, G. Meng, J. He, Y. Wu, F. Wu, and Z. Gu, "Antibiotic-loaded chitosan hydrogel with superior dual functions: antibacterial efficacy and osteoblastic cell responses," *ACS Applied Mater Interfaces,* vol. 6, pp. 10005-13, 2014.

[84] K. Tomihata and Y. Ikada, "In vitro and in vivo degradation of films of chitin and its deacetylated derivatives," *Biomaterials,* vol. 18, pp. 567-575, 1997.

[85] C. Lehr, J. A. Bouwstra, E. H. Schacht, and H.E. Junginger, "In vitro evaluation of mucoadhesive properties of chitosan and some other natural polymers," *International Journal of Pharmaceutics,* vol. 78, pp. 43-48, 1992.

[86] N. Alves and J. Mano, "Chitosan derivatives obtained by chemical modifications for biomedical and environmental applications," *Int J Biol Macromol,* vol. 43, pp. 401-14, 2008.

[87] H. Sashiwa, N. Kawasaki, A. Nakayama, E. Maruki, N. Yamamoto, and S. Alba, "Chemical modification of chitosan: Synthesis of water-soluble chitosan derivatives by simple acetylation," *Biomacromolecules,* vol. 3, pp. 1126-1128, 2002.

[88] K. Kurita, H. Ikeda, M. Shimojoh, and J. Yang, "N-Phthaloylated Chitosan as an Essential Precursor for Controlled Chemical Modifications of Chitosan: Synthesis and Evaluation," *Polymer Journal,* vol. 39, pp. 945-952, 2007.

[89] N. Smeets, M. Patenaude, D. Kinio, Y.F. Yavitt, E. Bakaic, F. Yang, *et al.*, "Injectable hydrogels with in situ-forming hydrophobic domains: oligo(d,l-lactide) modified poly(oligoethylene glycol methacrylate) hydrogels," *Polymer Chemistry,* vol. 5, pp. 6811-6823, 2014.

[90] E. Bakaic. N. Smeets, M. Patenaude, T. hoare, "Injectable and tunable poly(ethylene glycol) analogue hydrogels based on poly(oligoethylene glycol methacrylate)," *Chemical Communications,* vol. 50, pp. 3306-3309, 2014.

[91] E. Wischerhoff, K. Uhlig, A. Lankenau, H.G. Borner, A. Laschewsky, C. Duschl, *et al.*, "Controlled cell adhesion on PEG-based switchable surfaces," *Angewandte Chemie International Edition,* vol. 47, pp. 5666-8, 2008.

[92] "Healthcare-associated infections (HAIs)", [online], *Centers for Disease Control and Preventions,* available at: http://www.cdc.gov/HAI/surveillance/, [accessed: August 6, 2015].

[93] S. Joshi, "Surgical infections research," *Drexel University,* [online].

[94] M. Schweizer, "Surgical Site Infections Associated with Excess Costs at Veterans Affairs Hospitals," *The Jama Network,* [online].

[95] A. Anitha, S. Maya, N. Deepa, K.P. Chennazhi, S. S.V. Nair, H. Tamura, *et al.*, "Efficient water soluble O-carboxymethyl chitosan nanocarrier for the delivery of curcumin to cancer cells," *Carbohydrate Polymers,* vol. 83, pp. 452-461, 2011.

[96] X.F. Liu, Y.L. Guan, D.Z. Yang, Z. Li, and K.D. Yao, "Antibacterial action of chitosan and carboxymethylated chitosan," *Journal of Applied Polymer Science,* vol. 79, pp. 1324-1335, 2001.

[97] J. Li, L. Deng, & F. Yao, "Chitosan Derivatives," *Chitosan-based Hydrogels: Functions and Applications*, K. Yao, J. Li, F. Yao, & Y. Yin, Ed., Boca Raton, FL, 2012, pp.54.

[98] E. Bakaic, N. Smeets, and T. Hoare, "Injectable hydrogels based on poly(ethylene glycol) and derivatives as functional biomaterials," *RSC Advances,* vol. 5, pp. 35469-35486, 2015.

[99] M.S. Eldin, E.A. Soliman, A.I. Hashem, and T. M. Tamer, "Antibacterial activity of chitosan chemically modified with new technique," *Trends in Biomaterials and Artificial Organs,* vol. 22, pp. 125-137, 2008.

[100] R.A. Moravec, A. L. Niles, H. A. Benink, T.J. Worzella, L. Minor, D. Storts, *et al.*, "Cell Viability Assays," in *Promega Corporation*, ed.

[101] M. Patenaude and T. Hoare, "Injectable, mixed natural-synthetic polymer hydrogels with modular properties," *Biomacromolecules,* vol. 13, pp. 369-78, 2012.

[102] S.C. Chen, Y.C. Wu, F.L. Mi, Y.H. Lin, L.C. Yu, and H.W. Sung, "A novel pH-sensitive hydrogel composed of N,O-carboxymethyl chitosan and alginate cross-linked by genipin for protein drug delivery," *Journal of Control Release,* vol. 96, pp. 285-300, 2004.

[103] A.M. Carmona-Ribeiro and L.D. Carrasco, "Cationic antimicrobial polymers and their assemblies," *International Journal of Molecular Sciences*, vol. 14, pp. 9906-46, 2013.

[104] B. Zhao and R. Pelton, "Using peel as a measure of paper surface strength," *Tappi*, vol. 3, pp. 3-7, 2004.

[105] A.F. Martins, S.P. Facchi, H.D. Follmann, A.G. Pereira, A.F. Rubira, and E.C. Muniz, "Antimicrobial activity of chitosan derivatives containing N-quaternized moieties in its backbone: a review," *International Journal of Molecular Sciences*, vol. 15, pp. 20800-32, 2014.

[106] T. Hoare, Y. Yeo, E. Bellas, J.P. Bruggeman, and D.S. Kohane, "Prevention of peritoneal adhesions using polymeric rheological blends," *Acta Biomaterials*, vol. 10, pp. 1187-93, 2014.

Appendix A1

Potentiometric titration curve for (a) unmodified chitosan, (b) carboxymethylated chitosan, and (c) hydrazide functionalized chitosan to determine the pK_a of the amine as well as carboxyl groups (if present) through the ionization and pH derivative curves. For both the unmodified and hydrazide functionalized chitosan, only two maxima are present due to no carboxyl groups being present in the chitosan backbone. The pK_a is determined by initially finding the volume at the equivalence point (V_{eq}), which corresponds to the intersection between the pH and first derivative curves and finding the pH at the ½ V_{eq}. The same method applies for the carboxyl groups for the carboxymethylated chitosan.

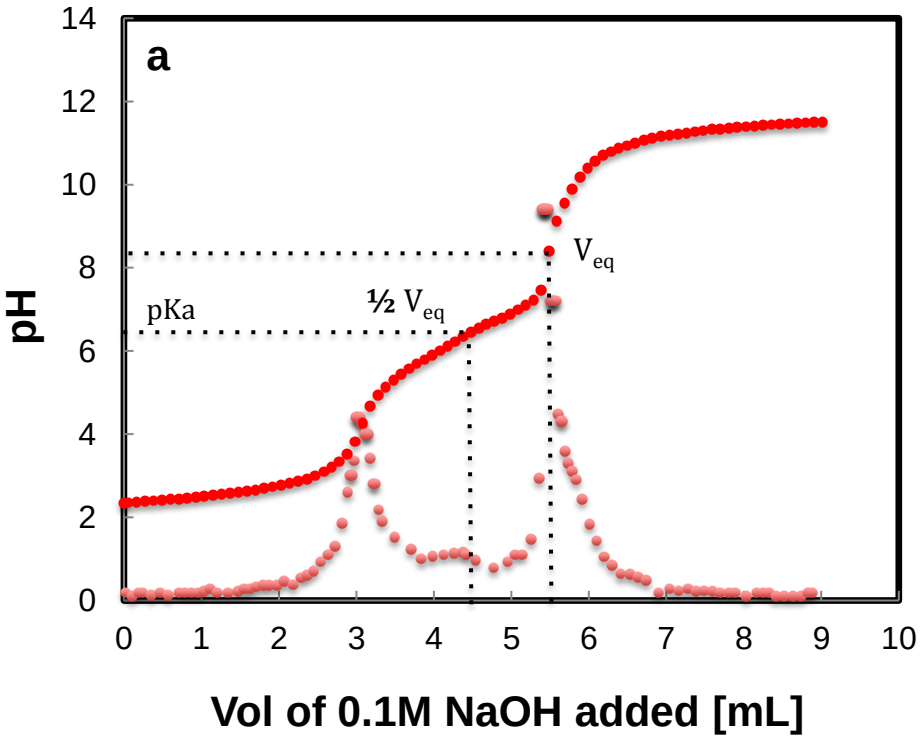

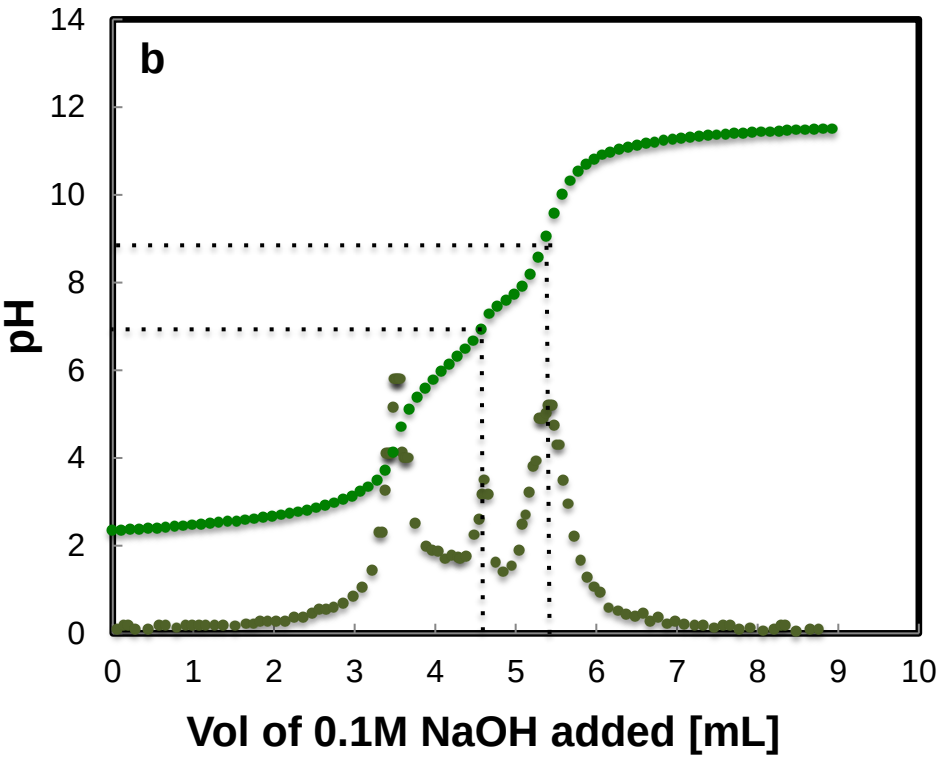
b
pH
Vol of 0.1M NaOH added [mL]
0
2
4
6
8
10
12
14
0
1
2
3
4
5
6
7
8
9
10

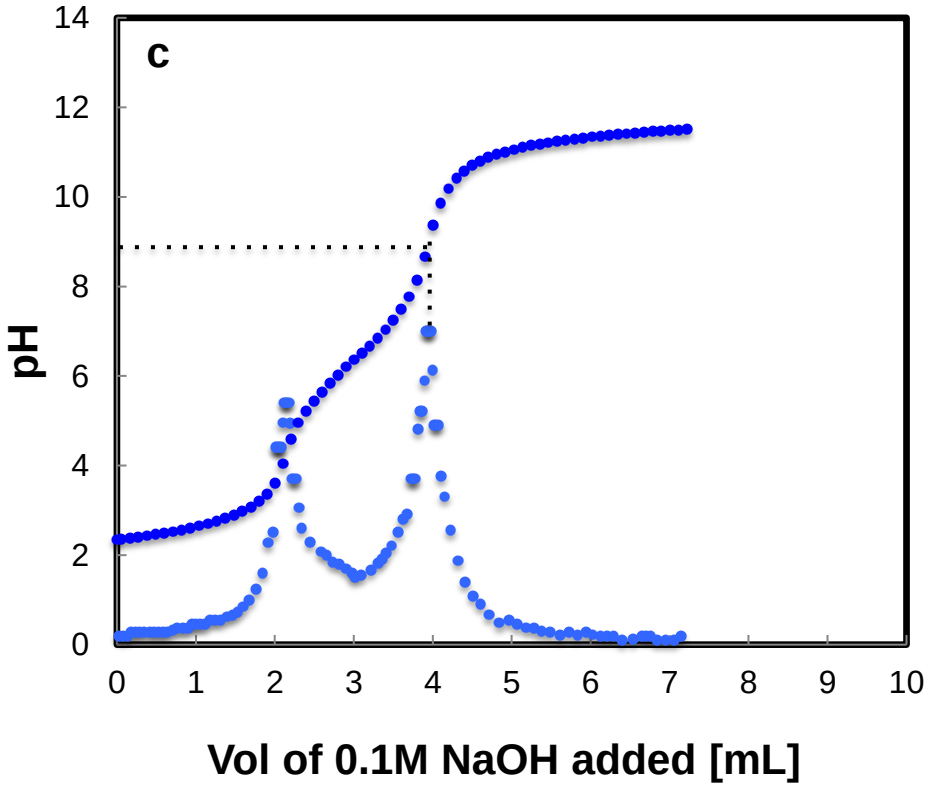
c
pH
Vol of 0.1M NaOH added [mL]
0
2
4
6
8
10
12
14
0
1
2
3
4
5
6
7
8
9
10

Appendix A2

Degree of Ionization vs. pH curves for titration data for (a) Unmodified chitosan, (b) Carboxylated chitosan, and (c) hydrazide functionalized chitosan

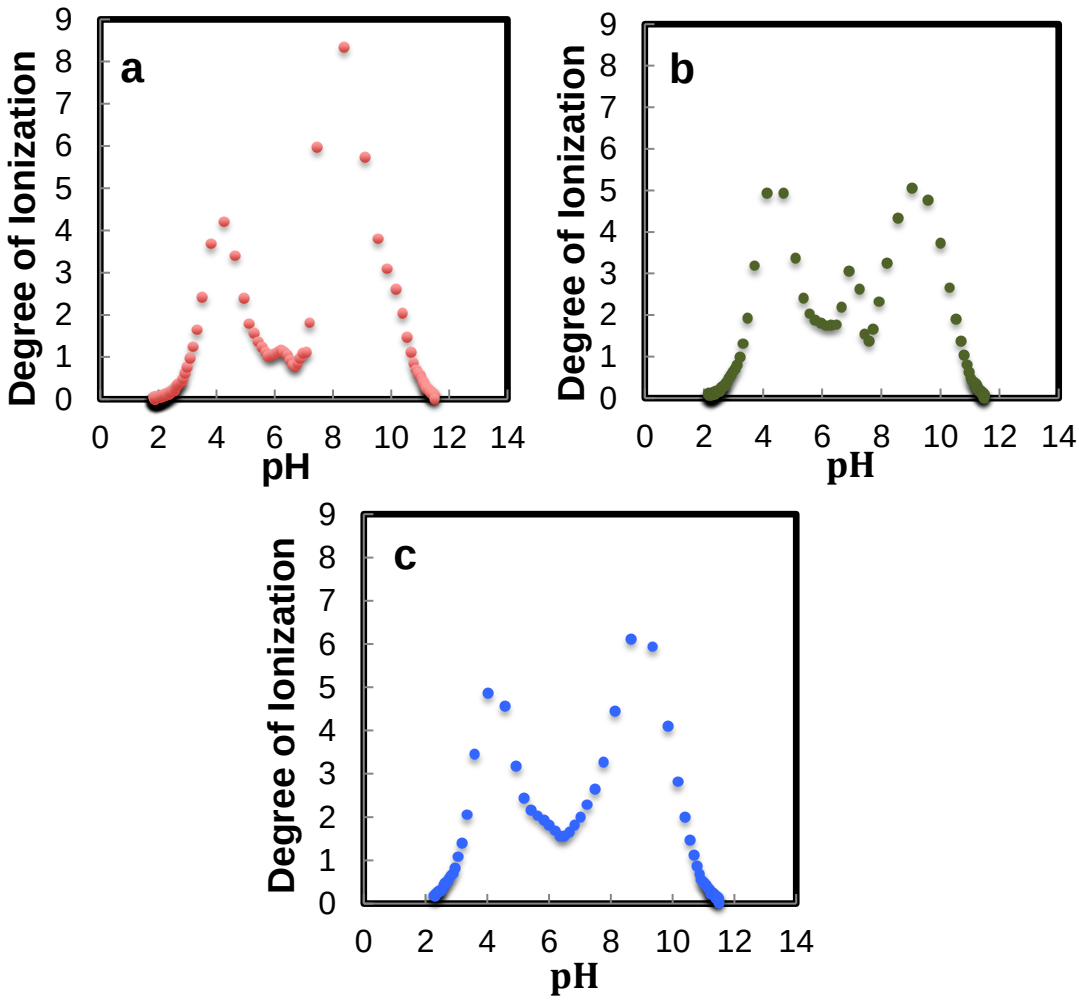

Appendix A3

Representative peel curves for (a) Chit-Hzd 1.0%/$PO_{10}A_{30}$ 20%, (b) Chit-Hzd 1.5%/$PO_{10}A_{30}$ 20%, (c) Chit-Hzd 2.0%/$PO_{10}A_{30}$ 20% are shown below.

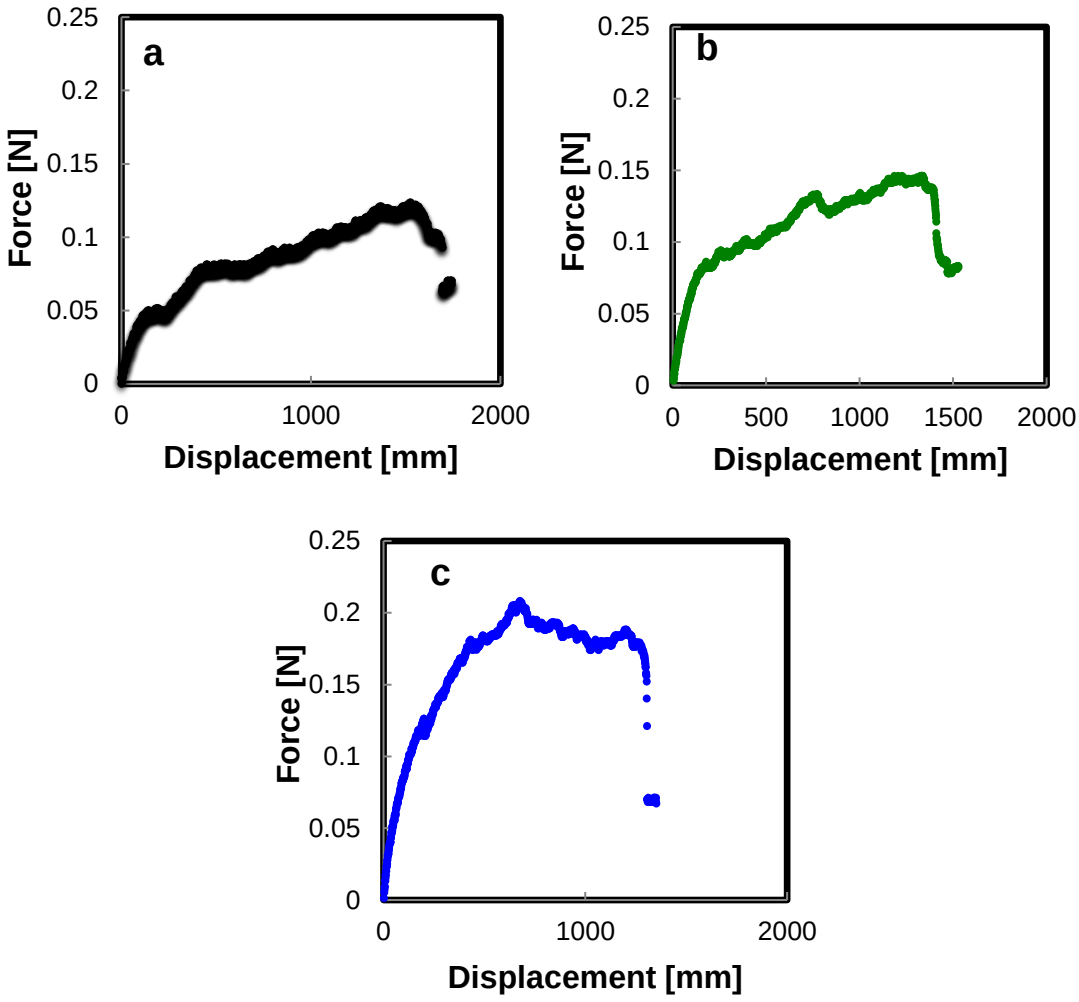

Appendix A4

The excess storage modulus (a) and the relative synergism parameter (b) for Chit-Hzd 1.5% was calculated and plotted on the curves below. Synergism is observed throughout the whole frequency range through positive ΔG' values and relative synergism values. Somewhat reduced synergism is observed at higher shear rates (Fig. b), consistent with the mucin-polymer interaction being physical in nature and thus susceptible to shear.